Ribosome profiling of selenoproteins *in vivo* reveals consequences of pathogenic Secisbp2 missense mutations

The establishment of translating ribosome affinity purification

Dissertation

zur Erlangung des Doktorgrades (PhD)

der Medizinischen Fakultät

der Rheinischen Friedrich-Wilhelms-Universität Bonn

Wenchao Zhao

aus Harbin, China

2020

Angefertigt mit der Genehmigung

der Medizinischen Fakultät der Universität Bonn

1. Gutachter: Prof. Dr. Ulrich Schweizer

2. Gutachter: Prof. Dr. Walter Witke

Tag der Mündlichen Prüfung: 27.10.2020

Institut für Biochemie und Molekularbiologie

Direktor: Prof. Dr. med. Volkmar Gieselmann

Index

List of abbreviations

Alb	albumin
CamK	calcium/calmodulin-dependent protein kinase II
CNS	central nervous system
DHPC	1,2-diheptanoyl-sn-glycero-3-phosphocholine
Dio	Iodothyronine Deiodinase
DNA	deoxyribonucleic acid
DTT	dithiothreitol
eEFsec	eukaryotic elongation factor for Sec
ER	Endoplasmic reticulum
GFP	green fluorescent protein
Gpx	glutathione peroxidase
i^6A	N^6-isopentenyladenosine
ISR	Integrated stress response
kDa	kilodalton
mRNA	message RNA
Neo	neomycin
NLS	nuclear localization sequence
NMD	non-sense mediated decay
NP-40	nonyl phenoxypolyethoxylethanol
PBS	phosphate-buffered saline
PCR	polymerase chain reaction
PFA	paraformaldehyde
RBD	RNA binding domain

RNA	ribonucleic acid
ROS	reactive oxygen species
RPF	ribosome protected mRNA fragments
rT3	reverse Triiodothyronine
SDS	sodium dodecyl sulfate
Se	selenium
Sec	selenocysteine
SECIS	selenocysteine insertion sequence
Secisbp2	selenocysteine insertion sequence binding protein 2
Selenof	selenoprotein F
Selenoi	selenoprotein I
Selenok	selenoprotein K
Selenom	selenoprotein M
Selenon	selenoprotein N
Selenon	selenoprotein N
Selenop	selenoprotein P
Selenos	selenoprotein S
Selenot	selenoprotein T
Selenow	selenoprotein w
Sephs2	selenophosphate synthetase 2
SEPN1-RM	SELENOPROTEIN N-related myopathy
SID	selenocysteine incorporation domain
SSMD	sedaghatian-type spondylometaphyseal dysplasia
T3	triiodothyronine

T4	thyroxine
TBS	tris-buffered saline
TRAP	translating ribosome affinity purification
Trit1	transfer RNA isopentenyltransferase 1
tRNA	transfer RNA
Trsp	transfer RNA Selenocysteine/Phosphoserine
TSH	thyrotropin releasing hormone
Txn	thioredoxin
Txnrd	thioredoxin reductase
URE	UGA recoding efficiency
UTR	untranslated region

1. Introduction

1.1 A brief introduction of Selenium

Selenium is an essential trace element which was discovered by the Swedish chemist Jöns Jacob Berzelius in 1817. "Selenium" was named after the Greek word for moon, selènè. In the early decades of selenium studies, selenium was always related to its toxic effect. It was reported that the livestock and insects were poisoned when they consumed selenium-accumulating plants (Moxon and Franke 1935; Hurd-Karrer 1936). This view of selenium toxicity was gradually shifted into selenium positive effect after 1954. Jane Pinsent first presented that selenite, an inorganic form of selenium, is essential for formic dehydrogenase synthesis in bacteria (Pinsent, 1954). Three years later, Klaus Schwarz and Calvin Foltz discovered that selenium deficiency in the diet caused liver necrosis in vitamin E-deficient rats. The condition was alleviated after selenium supplementation (Schwarz and Foltz 1957). This was the first time that selenium was recognized as an essential trace element in mammals. This remarkable finding guided people to investigate the beneficial effect of selenium. Shortly thereafter, Rahman discovered that selenium prevented exudative diathesis in chicken and poultry fed with a Vitamin E-deficient diet (Rahman et al. 1960). Subsequently, P.D Whanger demonstrated that selenium has a positive effect on protecting the lambs from developing white muscle disease (Whanger et al., 1969). These early selenium studies on livestock guided people to pay more attention on its biological function in the subsequent decades.

1.2 Selenoproteins and their biological functions

The main biological form of selenium is selenocysteine (Sec), the 21st proteinogenic amino acid, which is encoded by UGA codon (Labunskyy et al. 2014). Sec is co-translationally incorporated into selenoproteins. In the case of selenoproteins, in-frame UGA codon is decoded as Sec instead of recognizing as a canonical stop codon. This dedicated UGA recoding process required a complex and coordinated translational machinery, which will be explained in details in the next chapter. To date, there are 25 selenoprotein genes which were identified in human and 24 selenoproteins in mouse (Kryukov et al., 2003).

Almost all selenoproteins are recognized as oxidoreductases (Gpx family, Txnrd family, Selenow, Selenot etc.), which are mainly involved in maintaining redox homeostasis. However, individual selenoprotein serves diverse biological roles in different organs (Kasaikina et al. 2012). According to the known physiological functions of selenoproteins, selenoproteins are categorized into several families.

1.2.1 Glutathione Peroxidases (Gpx family)

Glutathione peroxidases are a group of critical antioxidant enzymes which are involved in the glutathione-dependent reduction of hydrogen peroxide and other hydroperoxides (Prabhakar et al. 2006). There are five identified Sec-containing GPXs (GPX1, GPX2, GPX3, GPX4, GPX6) in human and four in mice (Gpx1, Gpx2, Gpx3, Gpx4).

Gpx1 is the first identified mammalian selenoprotein by Flohe (Flohe et al. 1973) and Rotruck (Rotruck et al., 1973). This cytosolic enzyme catalyzes glutathione (GSH)-dependent reduction of hydroperoxides to water (Lubos et al. 2011). Gpx1 is the most abundant selenoprotein which is ubiquitously expressed in all cell types, particularly in the liver. Gpx1 expression is highly regulated by selenium status more than other selenoproteins (Sunde et al., 2009). Multiple Gpx1 knockout studies indicated that Gpx1 is dispensable for surviving, since *Gpx1* knockout mice were healthy and fertile. However, *Gpx1* knockout mice were more susceptible than wild types when exposed to oxidative stress (De Haan et al. 1998). Besides its antioxidant function, Gpx1 is also involved in insulin signaling. Both Gpx1 knockout and overexpression mouse model studies demonstrated that Gpx1 could interfere with insulin sensitivity by regulating intracellular reactive oxygen species (ROS) level (McClung et al. 2004 ; Loh et al. 2009).

Gpx2, the gastrointestinal form of glutathione peroxidases, is highly expressed in the mucosal epithelium of the gastrointestinal tract (Esworthy et al., 1998). Loss of Gpx2 in mice enhanced apoptosis in the intestinal epithelium (Florian et al., 2010). Furthermore, double knockout $Gpx1^{-/-}$ $Gpx2^{-/-}$ pups displayed a more severe phenotype in the ileum and the colon than $Gpx1^{-/-}$ $Gpx2^{+/-}$ pups under selenium depletion diet (Esworthy et al., 2005), indicating that Gpx2 is the predominate Gpx for the gastrointestinal tract.

Gpx3 is the only plasma glutathione peroxidase (Takahashi et al., 1987). Gpx3 is synthesized in the kidney epithelium and secreted into the plasma, where it plays an antioxidant role. The loss of Gpx3 in mice could interrupt the modulation of ROS, resulting in platelet activation and arterial thrombosis (Jin et al., 2011). Moreover, clinical studies indicated that a decreased level of plasma GPX3 has been associated with an increased risk of childhood stroke (Voetsch et al., 2007). The etiology of this disease was that the impaired modulation of ROS level, caused by the lack of plasma GPX3, reduced the bioavailability of nitric oxide (NO), resulting in abnormal platelet aggregation.

Gpx4 is an unique enzyme among the Gpx family due to its particular ability to reduce membrane-bound lipid hydroperoxides (Ursini et al. 1985). The Gpx4 family consists of three isoforms: the nuclear isoform (nGpx4), the mitochondrial isoform (mGpx4), and the cytosolic isoform (cGpx4). Nuclear isoform nGpx4 was found in a low abundance in the somatic cells as well as germ cells. Previous study showed that nGpx4 has been associated with chromatin compaction during spermiogenesis (Puglisi et al., 2012). Nuclear GPx4, together with protamine, facilitated disulfide bond formation resulting in the stability of sperm chromatin (Conrad et al., 2005). However, nGpx4 knockout mice did not show a significant defect in fertility and sperm maturation. Mitochondrial isoform mGpx4 is mainly expressed in the germ cells. Mitochondrial Gpx4 knockout mice showed infertility in males, demonstrating that mGpx4 is the major isoform in charge of spermatogenesis (Schneider et al., 2009). Cytosolic isoform cGpx4 is highly expressed in both somatic cells and germ cells. Cytosolic Gpx4 accounts for general Gpx4 function. Full knockout of Gpx4 resulted in embryonic lethality around postnatal 7.5 days (Yant et al., 2003), indicating a more vital function beyond maintaining the male fertility of mGpx4. Subsequent neuron-specific Gpx4 knockout mice showed movement disorders, neuronal degeneration and cortical astrogliosis (Seiler et al., 2008). The author also gave an explanation in this study that the loss of Gpx4 triggered apoptosis-inducing factor (AIF)-mediated cell death in neurons. Recently, a novel type of programmed cell death "Ferroptosis" has been associated with Gpx4 function (Angeli et al. 2014). Subsequently, Gpx4 was defined as a key regulator of ferroptosis (Ingold et al., 2018). Sec-containing Gpx4 could prevent ferroptosis by its resistance to overoxidation and irreversible inactivation in response to over exceeding ROS level. Apart from Gpx4 mouse studies,

patients with GPX4 mutations were identified with the symptom of Sedagathian disease (Smith et al., 2014). Sedaghatian-type spondylometaphyseal dysplasia (SSMD) is a lethal autosomal recessive disorder characterized by severe metaphyseal chondrodysplasia with mild limb shortening, platyspondyly, central nervous system abnormalities. This severe clinical phenotype of patients with mutant GPX4 emphasized the importance of GPX4.

1.2.2 Thioredoxin reductases (Txnrd family)

Thioredoxin reductases (Txnrds) together with thioredoxin (Txn) and nicotinamide adenine dinucleotide phosphate (NADPH) compose a thioredoxin system. The Txnrd family is involved in thiol-disulfide exchange reaction, which can regulate intracellular redox balance (Arnér, 2009). All three Txnrds (Txnrd1, Txnrd2, Txnrd3) are selenoproteins in mammals, which means the Txn system is selenium-dependent.

Txnrd1 is expressed in the cytosol as well as in the nucleus, while Txnrd2 is a mitochondria protein (Labunskyy et al., 2014). Patients with homozygous mutations in TXNRD1 displayed genetic generalized epilepsy. This severe neurological phenotype was ascribed to insufficient ROS detoxification caused by decreased TXNRD1 activity (Kudin et al., 2017). Mouse study also confirmed the importance of Txnrd1 by the fact that Txnrd1 knockout mice were embryonic lethal around E9 (Jakupoglu et al., 2005). Txnrd1 was also often reported in cancer research. Many studies manifested that Txnrd1 has strong correlation with carcinogenesis. Knockdown of Txnrd1 could inhibit tumor progression and metastases in a xenograft model (Yoo et al., 2006). The mitochondrial protein Txnrd2 is more related to cardiac function. Full Txnrd2 knockout mouse are embryonic lethal around E13 (Conrad et al. 2006). Subsequent heart specific Txnrd2 knockout mice showed a fatal dilated cardiomyopathy (Kiermayer et al., 2015). This phenotype was also identified in the patients carrying TXNRD2 missense mutations (Sibbing et al., 2011). Recently, another clinical study reported that a patient carrying a homozygous nonsense mutation in TXNRD2 showed severe neurodegenerative symptoms, indicating that TXNRD2 also plays an important role in neuronal maintenance (Holzerova et al., 2016). Txnrd3 was also named as thioredoxin/glutathione reductase, since it contains an N-terminal glutaredoxin

domain (not in Txnrd1 and Txnrd2) and a thioredoxin reductase domain (Sun et al., 2005). Txnrd3 has a low abundance in all tissues except in testis after puberty (Conrad et al., 2006). In testis, Txnrd3 catalyzes isomerization of protein and interprotein disulfide bonds during sperm maturation (Su et al., 2005).

1.2.3 Deiodinase family (Dio family)

Deiodinases family comprises three paralogous proteins (Dio1, Dio2, Dio3) in mammals. All of three deiodinases are involved in the regulation of thyroid hormone metabolism. Fig 1.1 below explicitly illustrates the thyroid axis and thyroid hormone metabolism.
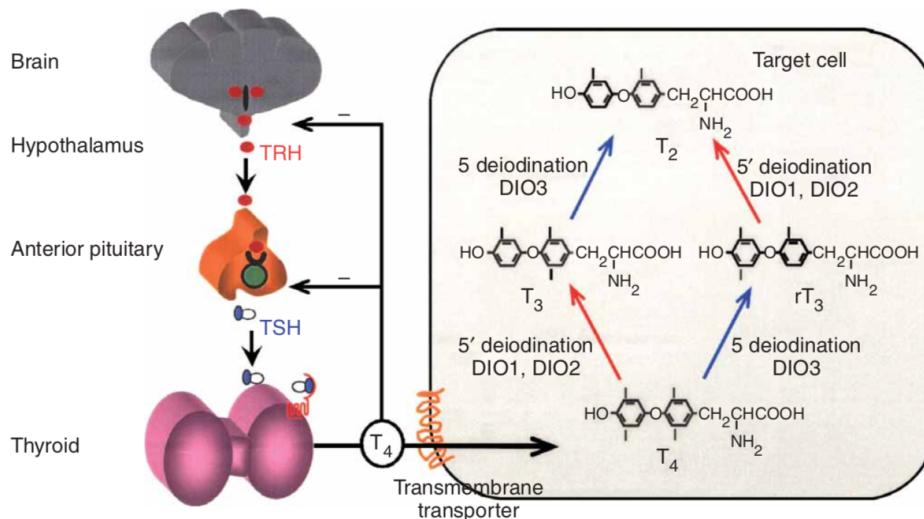
Fig 1.1 Thyroid axis (left) and thyroid hormone metabolism (right): Thyroxine (T4) is the main product of thyroid gland. Thyrotropin stimulating hormone (TSH) that is secreted by the anterior pituitary regulates the secretion of T4. TSH is also regulated by T4 through a negative feedback system. T4 has to be converted into biologically active T3. This process is catalyzed by Dio1 and Dio2. Conversely, Dio3 inactivates T4 and T3 to form rT3 or T2, respectively. To be noticed, Dio1 is capable of both enzymatic functions: it can activate T4 to T3 and inactivate T4 to rT3 (not shown in figure). T4 and TSH level are vital indexes of thyroid function test in clinical research (Dumitrescu et al., 2005).

Dio2 is mainly expressed in pituitary and brown fat tissue, while Dio1 is highly expressed in liver and kidney. Dio1 and Dio2 are both able to convert T4 to active T3, but with a different enzymatic efficiency (Luongo et al. 2019). Although both enzymes play important

roles in regulating thyroid hormone metabolism, Dio1, Dio2 single and double knockout mice were seemingly healthy (Schneider et al., 2001, 2006; Galton et al., 2009). The thyroid hormone test on Dio1 KO mice showed unaltered T3, TSH level and elevated T4, rT3 level, while unaltered T3, rT3 level and elevated T4, TSH level in Dio2 KO mice. Dio1/Dio2 double knockout mice presented a sum of the thyroid phenotype of Dio1 knockout and Dio2 knockout mice. On one hand, active T3 level was unaltered in the lack of both enzymes, indicating that Dio1 and Dio2 are not essential for maintaining active T3 level. On the other hand, the dysregulation of T4, rT3 and TSH level in the lack of both enzymes evidenced that Dio1 and Dio2 play an essential role in thyroid hormone homeostasis. Conversely, Dio3 catalyzes the conversion from T4 to rT3. Elevated active T3 level was the main consequence of the deficiency of Dio3. The loss of Dio3 in mice results in hyperactivity and central hypothyroidism (Hernandez et al., 2010).

The first patient carrying SECISBP2 (Selenocysteine insertion sequence element binding protein 2) mutation was identified due to abnormal thyroid hormone metabolism. (Dumitrescu et al., 2005). Thyroid function test showed elevated TSH and T4 levels, while active T3 level was decreased. This syndrome of thyroid hormone resistance (RTH) will be explicitly introduced in Secisbp2 chapter (see the details in 1.3.5).

1.2.4 Other selenoproteins

Apart from the three mentioned selenoprotein families, there are still dozen of selenoproteins under explored.

Selenoprotein P (Selenop) is a unique selenoprotein which contains multiple UGA/Sec codons in its open reading frame and two SECIS elements in the 3' UTR (Hill et al., 2003). The function of Selenop is related to this unusual Sec-rich structure, since Selenop functions as a plasma selenium transport protein. Genetic targeting of Selenop interrupted selenium transport to multiple organs, including the brain (Schomburg et al., 2003). Further hepatocyte-specific Selenop knockout mouse studies revealed that plasma Selenop was mainly by synthesized in the liver and secreted from the liver (Streckfuß et al., 2005).

Selenophosphate synthetase 2 (Sephs2) is another special selenoprotein, which is the only selenoprotein involved in selenocysteine biosynthesis. In eukaryotes, Sephs2 catalyzes the formation of active selenium donor, selenophosphate ($H_2SePO_3^-$) (Xu et al., 2007). Knockdown of Sephs2 in mice downregulated the expression of several selenoprotein which corroborates its role in selenoprotein biosynthesis (Xu et al., 2007).

The selenoproteins (Selenok, Selenos, Selenot, Selenon, Selenom and Selenof) were identified as resident selenoproteins in endoplasmic reticulum (ER) (Shchedrina et al., 2010). The ER serves many important functions in eukaryotic cells, including protein folding, protein misfolding quality control, phospholipids and steroids biosynthesis, protein transportation, synthesis of secretory proteins and regulation of the cellular calcium ion signal (Shchedrina et al., 2010). This specific location (ER) might designate the function of these six selenoproteins which are involved in ER-related processes. Selenok research was always related to immune system. Calcium flux in immune cells was impaired by the lack of Selenok, which consequently resulted in the loss of immune cell functions like cell migration, proliferation (Verma et al., 2011). Selenos has been studied along with Selenok due to their overlapping roles. Both Selenos and Selenok are involved in ER-associated degradation of glycosylated misfolded protein (Shchedrina et al., 2011). Apart from its essential role in ER, Selenos also plays an important role in the inflammatory pathway. Polymorphisms in the SELENOS gene leads to higher levels of inflammatory markers – cytokines, suggesting that SELENOS functions as a mediator of inflammatory response (Curran et al., 2005). Selenot is a thioredoxin-like enzyme which is abundantly expressed in different organs. *In vitro* studies confirmed that recombinant Selenot displays a thioredoxin reductase-like activity. Selenot knockout mice were early embryonic lethal which suggests a pivotal role of Selenot during embryogenesis (Boukhzar et al., 2016). Subsequent brain specific Selenot knockout mouse study demonstrated that the loss of Selenot leads to dopaminergic neuronal degeneration and motor dysfunction via induced oxidative stress (Boukhzar et al., 2016). Malfunction of Selenon is always related to muscle diseases. Patients carrying homozygous or compound heterozygous SELENON mutations suffered from SELENON-related myopathy (SEPN1-RM), a novel muscle disorder. The clinical phenotype of SEPN1-RM includes weakness of the neck and trunk muscles in patients which leads to respiratory insufficiency (Moghadaszadeh et al., 2001).

Further studies showed that SEPN1-RM is caused by oxidative stress and abnormal calcium ion flux which were both triggered by the loss of SELENON (Arbogast et al., 2009). Selenom is highly expressed in the brain and plays a protective role in neurons against oxidative stress (Reeves et al. 2010). Moreover, Selenom knockout mice displayed increased body weight, elevated white adipose tissue deposition and higher serum leptin level (Pitts et al., 2013), indicating its potential role in regulating energy metabolism.

Not all selenoproteins are mentioned above, while the function of some selenoproteins still remain unclear. However, some of not well-studied selenoproteins are probably not essential in humans, since homozygous inactivating alleles of these selenoproteins have been found in completely sequenced human genomes (Santesmasses et al. 2020). With current knowledge of well-studied selenoproteins, these selenoproteins are vital and indispensable for human health by exerting diverse and significant physiological functions.

1.3 Selenoprotein biosynthesis

The core event of selenoprotein biosynthesis is selenocysteine insertion (UGA recoding). In mammals, this essential process is facilitated by a complex translational machinery which requires several trans-factors and cis-factors, like selenocysteine tRNA$^{[Ser]Sec}$ (tRNAsec), Secisbp2, eukaryotic elongation factor for Sec (eEFsec), in-frame UGA/Sec codon, selenocysteine insertion sequence (SECIS element) and other non-essential SECIS binding proteins (eIf4a3, L30, nucleolin) (Labunskyy et al., 2014). The Fig 1.2 below illustrates this complex selenoprotein biosynthesis machinery.
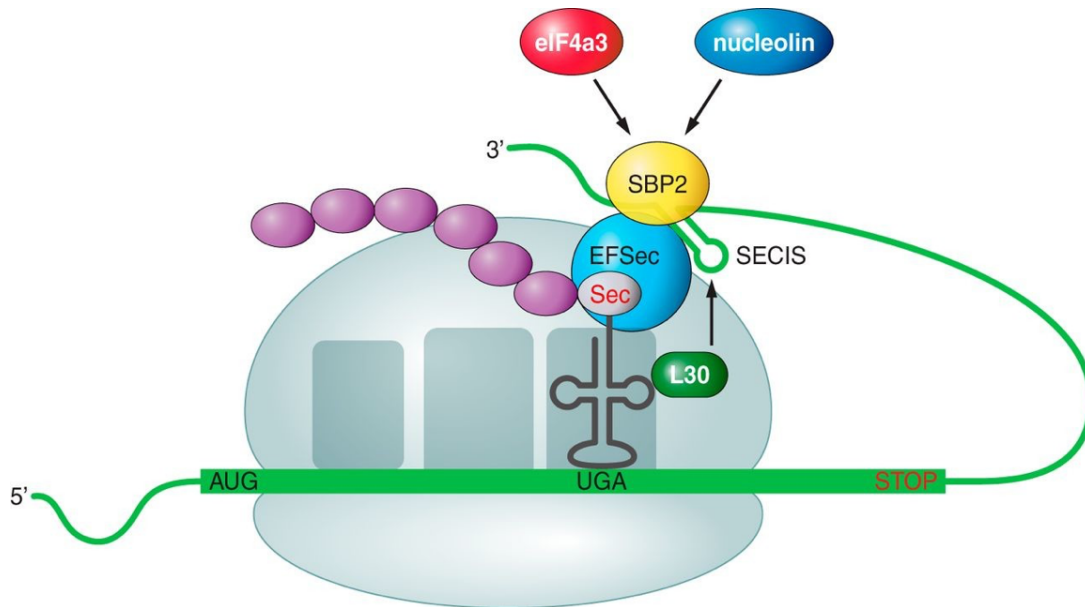
Fig 1.2 Selenoprotein biosynthesis machinery: This figure displays all the essential and non-essential factors which are required for Sec incorporation in response to in-frame UGA codon (Labunskyy et al., 2014). (See the text for details)

1.3.1 Selenocysteine tRNA[Ser]Sec

Selenocysteine (Sec) is a unique amino acid due to two aspects. One aspect is that Sec is encoded by a UGA codon, which was generally designated as a terminal codon (Russell, 2003). Another aspect is that Sec biosynthesis occurs on its own tRNA, tRNA[Ser]Sec (Jing Yuan 2006). In eukaryotes, Sec biosynthesis on tRNA[Ser]Sec goes through several steps. Transfer RNA[Ser]Sec is initially aminoacylated with serine by seryl-tRNA synthetase (SERS). Then the charged serine-tRNA[Ser]Sec is phosphorylated by phosphoseryl-tRNA[Ser]Sec kinase (PSTK) to form O-phosphoseryl-tRNA[Ser]Sec (pSer-tRNA[Ser]Sec). Inorganic selenium form is converted into active selenium donor (selenophosphate) by the presence of Sephs2. The final step is the production of Sec-tRNA[Ser]Sec by using selenophosphate as selenium donor. This reaction is catalyzed by an enzyme, Sep (O-phosphoserine) tRNA:Sec (selenocysteine) tRNA synthase (Sepsecs) (Xu et al., 2007).
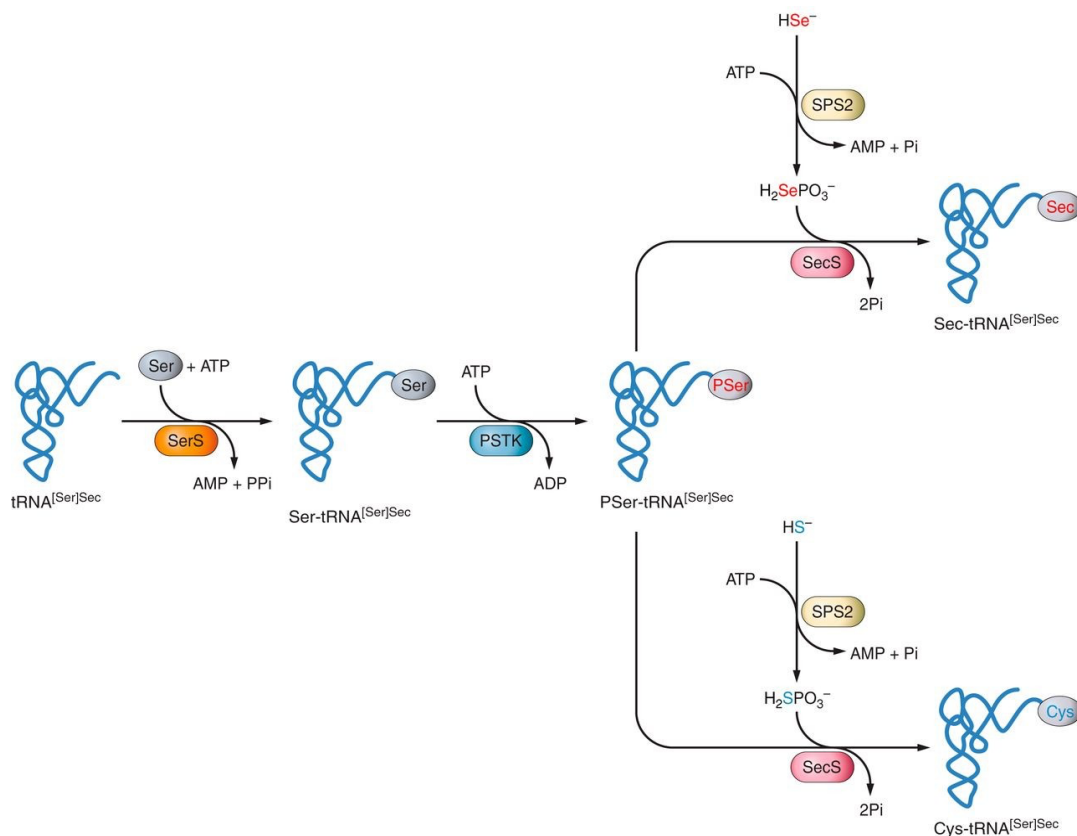
Fig 1.3 The biosynthesis of Sec-tRNA[Ser]Sec: The de novo synthesis of Sec (top right) and Cys (bottom right) in eukaryotes are shown (Labunskyy et al., 2014). (see the text for details)

Transfer RNA[Ser]Sec is encoded by transfer RNA Selenocysteine/Phosphoserine (Trsp). Since tRNA[Ser]Sec has been described as one of the central components of selenoprotein biosynthesis machinery (Gladyshev and Hatfield, 1999), Trsp knockout studies were widely applied to elucidate selenoproteome function in individual tissue or cell type. The first Trsp full knockout mouse study demonstrated the vital role of selenoproteins for survival of the organism and the importance of Trsp for selenoprotein biosynthesis (Bösl et al., 1997). Further conditional Trsp knockout mouse studies illustrated that selenoproteins are involved in maintaining the healthy status of many organs, cells and systems, like liver (Carlson et al., 2004), heart (Shrimali et al., 2007), brain (Wirth et al., 2010), skin (Sengupta et al., 2010), thyroid (Chiu-Ugalde et al., 2012), prostate (Luchman et al., 2014) and immune system (Downey et al., 2009). Recently, a patient with a mutation

in tRNA[Ser]Sec has been identified (Schoenmakers et al., 2016). The patient displayed a variety of symptoms, including abdominal pain, fatigue, muscle weakness, and low plasma levels of selenium. The clinical phenotype of this patient resembles patients with SECISBP2 mutations.

1.3.2 Selenocysteine (Sec)-Specific Eukaryotic Elongation Factor (eEFSec)

Literally, eEFSec is an elongation factor that exclusively delivers Sec-tRNA[Ser]Sec to the empty A site of the ribosome in response to an in-frame UGA/Sec codon. Unlike the general elongation factor (eEF1A), eEFSec is only able to interact with Sec-tRNA[Ser]Sec (Tujebajeva et al., 2000). Recently, the crystal structure of human eEFSec was resolved. eEFSec has four domains which are formed in a chalice like structure. Apart from domain I,II,III similar to eEF1A, eEFSec contains a unique domain IV (Dobosz-Bartoszek et al., 2016). This unique domain IV is the key site for Sec-tRNA[Ser]Sec and Secisbp2 binding (Dubey et al. 2016).

1.3.3 Selenocysteine insertion sequence (SECIS element)

As mentioned before, in order to ensure that in-frame UGA codon in selenoprotein mRNA is decoded as Sec, a stem-loop structure (SECIS element) located in the 3' UTR of selenoprotein mRNA (Berry et al., 1993) and its particular binding protein Secisbp2, are required (Copeland et al., 2000).

The eukaryotic SECIS element consists of two helices, an internal loop, an apical loop and a GA Quartet (Grundner-Culemann et al., 1999). The GA Quartet is conserved among all species (Mariotti et al., 2013). It is composed of four tandem non-Watson-Crick base pairs which form a kink-turn motif. This particular kink turn motif is highly flexible, allowing the variable conformation of the SECIS element during the interaction with SECIS binding proteins (Fletcher et al., 2001). Mutations in GA Quartet lead to impaired Secisbp2 binding and a lower efficiency of UGA recoding (Copeland et al., 2000). Apart from conserved GA Quartet, the apical loop is relatively variable among the species. In general, SECIS

element can be classified into two types by the presence of a bulge in the apical loop (Grundner-Culemann et al., 1999).
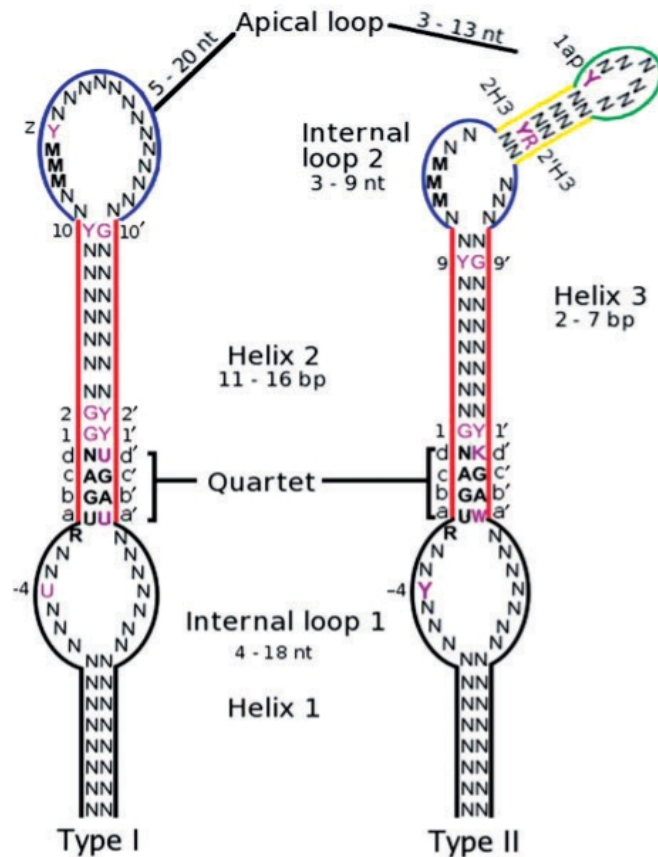
Fig 1.4 Type 1 and Type 2 of SECIS element: The structure of two types SECIS element are illustrated (Chapple et al. 2009). (See the text for the details)

1.3.4 SECIS binding protein 2 (Secisbp2)

Secisbp2 was identified and purified by anion exchange and RNA affinity chromatography (Copeland and Driscoll, 1999). Within this publication, the authors also discovered a 500 kDa band in activity gel filtration chromatography of Secisbp2 (120 kDa), indicating that Secisbp2 might interact with other proteins forming a protein-protein complex. Since then, the scientists tried to figure out Secisbp2 function and the mechanism of selenoprotein translation. After one year, the same group revealed the dependency of Secisbp2 for Sec incorporation both *in vivo* and *in vitro* (Copeland et al., 2000). Apart from binding with

SECIS element, Secisbp2 was also shown to interact with eEFSec and the ribosomes (Kinzy et al., 2005). Secisbp2 was identified as a limiting factor of Sec incorporation (Low et al., 2000). Subsequently, three distinct domains of Secisbp2 were identified by using site-specific mutagenesis: N-terminal domain (1-399) and C-terminal domain (399-784). And C-terminal domain contains Sec incorporation domain (SID) and RNA binding domain (RBD) (Allmang et al., 2002; Caban et al., 2007). The C-terminal domain of Secisbp2 accounts for full function of Secisbp2: SECIS element binding, interaction with eEFSec and ribosome binding. In details, RBD domain contains a conserved L7Ae domain (Allmang et al., 2002). Previous studies revealed that this L7Ae domain could specifically interacts with the kink-turn of the SECIS. The mutagenesis of RBD domain resulted in impaired SECIS binding (Fletcher et al., 2001). RBD domain is indispensable but not sufficient for Sec incorporation. SID domain is also involved in Sec incorporation. Although SID domain does not interact with SECIS element directly, SID domain can enhance the affinity between SECIS element and RBD domain (Donovan and Copeland, 2009).

The function of the Secisbp2 N-terminal domain still remains unclear, since SID and RBD are sufficient for Sec incorporation *in vitro* (Copeland et al., 2000). The N-terminal domain contains a lysine-rich nuclear localization sequence (NLS). Previous studies showed that oxidative stress induced nuclear accumulation of Secisbp2 by NLS motif regulation (Papp et al., 2006). Additionally, the N-terminal of Secisbp2 underwent several splicing events. Some of the splicing events altered the open reading frame which lead to a premature stop codon. However, these splicing forms could be initiated from down-stream ATG start codons (Met 233, Met 300 etc.). Interestingly, all of these splicing isoforms contain the NLS motif (Papp et al., 2008). Although the N-terminal domain does not play a role in Sec incorporation, it might be involved in Secisbp2 translocation and Secisbp2 function in the nucleus.

1.3.5 Human SECISBP2 mutations

Clinical studies corroborated the importance of SECISBP2 and gave us some hints about SECISBP2 functions. To date, 13 individuals with either homozygous or compound heterozygous mutations in 11 families have been identified. In general, the clinical

phenotypes of patients carrying SECISBP2 mutations are relatively modest but variable (Schoenmakers and Chatterjee, 2020).

The first family carrying homozygous SECISBP2 mutation (R540Q), which locates in SID domain, was identified in 2005. The patient displayed the short stature and delayed bone age. Therefore, patient was under thyroid hormone test. The thyroid hormone test showed the elevated TSH, T4 and rT3 levels and reduced active T3 level. Further test confirmed that the defect of the conversion from T4 to active T3 was caused by DIO2 deficiency. Apart from DIO2 deficiency, GPX activity and serum SELENOP were also grossly reduced in the patients (Dumitrescu et al., 2005).

Another patient carrying missense compound heterozygous mutations (C691R, fs65X and fs76X), locates in RBD domain, was identified in 2010. The child patient presented a global development delay, muscle weakness and mild bilateral high-frequency hearing loss. Subsequently, the thyroid hormone test showed elevated T4 level, normal active T3 level and normal TSH level in the patient. The serum selenium level was reduced together with plasma GPX3 and selenium transporter SELENOP. Muscle phenotype was similar to SELENON-related myopathy which leads the author to measure SELENON level. Reduced SELENON level is comparable to a case carrying SELENON mutation(Arbogast et al., 2009). *In vitro*, the antioxidative capacity of patient's fibroblast was decreased due to a general reduction of selenoproteins (Schoenmakers et al., 2010).

Both mutant SECISBP2 lead to a general selenoprotein deficiency, but with distinct clinical outcomes. Therefore, the correlation between phenotype and genotype on molecular basis need to be elucidated by generating mutant Secisbp2 mouse models.

1.3.6 Secisbp2 mouse model

The first full Secisbp2 knockout mouse model was generated by my former colleague Sandra Seeher. However, the homozygous Secisbp2 knockout mice were embryonic lethal around E 7.5 (Seeher et al., 2014). To overcome this embryonic lethality, tamoxifen-inducible and tissue specific Secisbp2 conditional knockout mouse models were

generated subsequently (Fu et al., 2017; Seeher et al., 2014). The tamoxifen-inducible full Secisbp2 knockout mouse model replicated the abnormal thyroid phenotype of patients carrying SECISBP2 mutation, as the elevated T4, rT3 level, as well as reduced deiodinases activity. However, active T3 level was unaltered in Secisbp2 knockout mice resembling Dio1 and Dio2 double knockout mice, while active T3 level was decreased in SECISBP2 patients. Not surprisingly, a global reduction of selenoproteins was also observed in this mouse model. In order to investigate tissue-specific effect, our group generated hepatocyte (Alb-Cre) and neuron (Camk-Cre) specific Secisbp2 knockout mouse models (Seeher et al., 2014). Hepatocyte specific Secisbp2 knockout mice did not show any obvious phenotype. Alanine-aminotransferase and aspartate-aminotransferase activities were not significantly increased, suggesting that there was no overt liver damage in the lack of Secisbp2 (Seeher et al., 2014). Selenoprotein mRNA and protein levels were generally reduced. However, the reduction of individual selenoproteins were quantitatively different. Several selenoprotein mRNAs are the canonical targets of non-sense mediated decay (NMD) when in frame UGA/Sec codon cannot be recoded. Accordingly, potential NMD targets, as *Gpx1* and *Dio1*, were grossly reduced. Non-NMD targets, as *Txnrd1* and *Selenoi*, remained unchanged. It was proposed that apart from its function in Sec incorporation, Secisbp2 also plays a role in stabilizing selenoprotein mRNA by preventing mRNA degradation. In contrast to the mild phenotype found in hepatocyte-specific Secisbp2 knockout mice, neuron-specific knockout mice showed lower body weight and body length, movement disorders and rarely survived over 21 days. A loss of GABAergic parvalbumin positive interneurons in primary somatosensory cortex and striatum was detected as well as massive astrogliosis in the deeper cortical layers (Seeher et al, 2014). Accordingly, selenoprotein mRNA and protein levels were reduced in neuron specific Secisbp2 knockout mouse cortex. However, the effect of Secisbp2 deficiency on individual selenoprotein is variable. The mRNA and protein levels of Gpx1 and Selenow were grossly reduced. While *Gpx4* mRNA was unaltered, Gpx4 protein level was remarkable decreased. Therefore, a systematic and detailed research on individual selenoprotein was required.

Ribosome profiling is a novel and robust methodology which provides a deep and detailed insight into translational process (Ingolia 2014). This technique is a perfect tool to

investigate the mechanism of selenoprotein biosynthesis from the side of translation. The information obtained from deep sequencing of ribosome protected mRNA fragments (RPFs) could reveal ribosome stalling, the speed of elongation, identifying the alternative initiation sites and frameshift as well as evaluation of UGA recoding in selenoprotein translation.
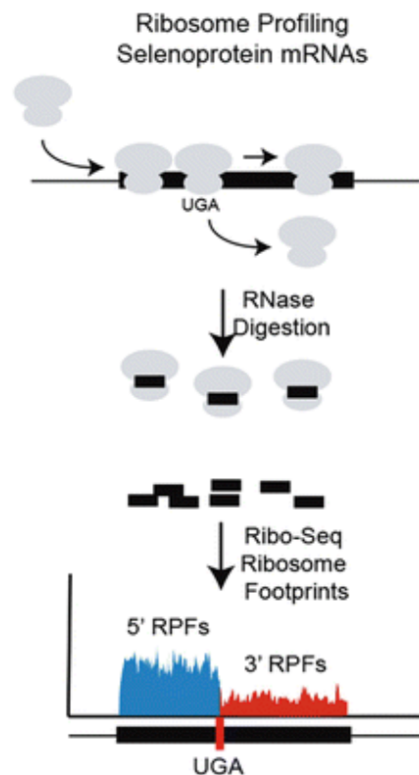
Fig 1.5 The workflow of ribosome profiling on selenoprotein mRNAs: The Schematic of ribosome profiling. Monosomes are isolated by digesting polysomes with RNase. After full digestion of monosomes, RPFs are obtained and subsequently sequenced. Then RPFs are mapped to the transcripts which indicates the location of translating ribosomes. (Fradejas-Villar et al., 2017)

The second study on the hepatocyte-specific Secisbp2 knockout mouse model used ribosome profiling for exploring Secisbp2 functions on individual selenoprotein biosynthesis (Fradejas-Villar et al., 2017). The profiling data showed that there was an

80 % reduction of selenoprotein 3'RPF in the Secisbp2 knockout mouse liver, indicating that the lack of Secisbp2 highly affected UGA recoding. RNA-seq data was also performed in order to normalize RPFs by the amount of mRNA. By combining two datasets, selenoprotein was classified into three categories due to the loss of Secisbp2: (1) those selenoprotein levels were significantly reduced due to degradation of selenoprotein mRNAs like Gpx1, Selenow, Selenop, Dio1. (2) those selenoprotein levels were grossly reduced (3'RPFs), but their mRNA levels remained unchanged, like Gpx4, Selenof. (3) those selenoprotein mRNA and protein levels were both unaltered, like Txnrd1, Selenos. However, by integrating all the parameters and information (NMD rule, the type of SECIS element, the position of UGA/Sec codon), no overall mechanism was found to account for this selenoprotein expression pattern. Therefore, the authors suspected a gene-specific response to the loss of Secisbp2 according to their individual role in specific tissues.

Although a global selenoprotein deficiency was observed in the patients with SECISBP2 mutation, mutant SECISBP2 differentially affect selenoprotein expression. Therefore, by using ribosome profiling, a systematic study on how the mutant Secisbp2 affect individual selenoprotein translation was necessary.

1.4 Translating ribosome affinity purification (TRAP)

The cellular diversity of heterogeneous tissue obstructs gene-function studies in a specific cell type, such as neurons in the mammalian central nervous system (CNS). A novel methodology, translating ribosome affinity purification (TRAP), is one way to address this challenge (Doyle et al., 2008). Single cell RNA-Seq represents an alternative way, however, it cannot give information on translational level (Shapiro et al. 2013). The strategy of TRAP is that firstly genetically modified ribosomal protein (Rpl10, large ribosome subunit protein 10) is tagged with an enhanced green fluorescent protein (EGFP) under a Cre-loxp system (Zhou et al., 2013). Rpl10-EGFP is exclusively expressed in the specific cell type, depending on the specificity of Cre recombinase, such as Alb-Cre for hepatocytes in liver or CamK-Cre for neurons in brain. Then cell-specific translating polysomes are pulled down by GFP antibodies attached to magnetic beads. Eventually,

translating mRNA in specific cell type can be purified by RNA extraction kits and further analyzed by qPCR, Northern blot or RNA-Seq.

The first application of TRAP was to identify cell-specific enriched transcripts for 24 CNS cell populations (Doyle et al., 2008). Thousands of cell-specific mRNAs, which were not detected in whole-tissue studies, were identified. Since EGFP is exclusively expressed in the cell of interest, EGFP fluorescence could be also utilized to localize the cell of interest. Therefore, a cellular taxonomy in the CNS was also well-defined by performing TRAP. Subsequently, TRAP has been widely used for either identifying the markers of specific cell type or discovering gene regulation of specific cell type under physiological perturbations, as identifying candidate markers in preoptic sleep neurons (Chung et al., 2017) and Purkinje cells (Kratz et al., 2014), the pattern of excitatory neuronal gene expression in long term potential (Chen et al., 2017), cholinergic-neuronal gene regulation in neurodegenerative disease (McKeever et al., 2017). After being validated by numerous studies, TRAP has become a solid, promising method for the study of cell-specific transcripts in complex tissue. However, TRAP has more potential applications by coupling with other methods. Recently, TRAP was coupled with ribosome profiling protocol (Sapkota et al., 2019). Instead of completely digestion after pulling-down polysomes by TRAP, RNaseI was applied to pulling-down polysomes for digesting only unprotected mRNA fragment. As described in ribosome profiling before, RPFs of cell of interest were captured. Eventually, RPFs were deep sequenced (Sapkota et al., 2019). This combination (TRAP-RP) could provide translational information of a specific cell type in a codon resolution, which breaks the limitation of both methods.

In order to establish and validate this robust TRAP in our lab, one of our mouse models (CamK-Cre Trit1 knockout) has been used as a trial. Transfer RNA isopentenyltransferase 1 (Trit1) accounts for tRNA modification N^6-isopentenyladenosine (i^6A37) in several tRNAs (Fradejas et al., 2013). The lack of i^6A37 modification leads to translational infidelity. Differential analysis of RNA-seq datasets of CamK-Cre Trit1 mice and wild types showed that a bunch of upregulated genes were involved in integrated stress response (ISR), and a bunch of downregulated genes were cytoskeleton-related in CamK-Trit1 KO mouse cortex. More detailed information about CamK-Cre Trit1 knockout mouse model can be

obtained from Dr. Simon Bohleber's doctoral thesis (Einfluss der tRNA Modifikation i6A37 auf die Translation in Säugern und deren Mitochondrien). Instead of collecting the information from the transcripts of all the cell types in the cortex, neuronal transcripts will be particularly captured and analyzed by performing TRAP. The validation of TRAP on CamK-Trit1 KO mice will be multifaceted.

2. Material and Methods

2.1 Material

2.1.1 Chemicals and disposable materials

All the used chemicals in the lab were purchased from the manufacturers below: Sigma-Aldrich, Merck, Applichem, Thermo Fisher Scientific, Qiagen and Roche. The disposable materials in the lab were purchased from the manufacturers below: Eppendorf, Sarstedt, Bio-Rad, Medltrade.

2.1.2 Commercial Kits

Table 2.1: Commercial Kits

Commercial Kit	Manufacturer	Accession Number
Absolute qPCR SYBR Green Fluorescein Mix	ThermoFisher	AB-1219/B
iScript cDNA Synthesis	Bio-Rad	1708891
Pierce BCA Protein	ThermoFisher	23225
SuperSignal^{TM} West Dura	ThermoFisher	34095
TRIzol	ThermoFisher	15596026

2.1.3 Equipment

Table 2.2: Equipment

Equipment	Manufacturer
Nanodrop 2000	Thermo Fisher Scientific
Plate reader Infinite 200 Pro	Tecan
Zeiss Axioplan 2	Carl Zeiss
Centrifuge 5471C	Eppendorf
Centrifuge 5417R	Eppendorf
Centrifuge 5810R	Eppendorf
Thermomixer comfort	Eppendorf
Vortex IKA VF2	Janke & Kunkel
Pipettes (0.1-2.5 µl, 0.5-10 µl, 10-100 µl, 100-1000µl)	Eppendorf
Mastercycler Nexus GSX1	Eppendorf
Mastercycle EPgradients	Eppendorf
Classic Gel documentation	Intas
Cryosection CM 3050S	Leica
Vibratome VT 1000S	Leica
Electrophoresis Powersupply E802	Consort
Balance BP2100S	Sartorius
pH-Meter 761 Calimatic	Knick
Rotarod	Jones & Roberts
Electrophoresis System	BioRad
Tapestation 2000	Agilent
Incubator	Heraeus
Fusion Solo imaging system	Vilber Lourmat
Shaker #3016	GFL

2.1.4 Software

Table 2.3: Software

Software	Manufacturer
Mendeley v1.19.4	Elsevier
Axiovision 4.1	Carl Zeiss
ImageJ 1.48	NIH
GraphPad Prism 7	GraphPad Prism Software
Microsoft Office 2016 16.16.9	Microsoft (Germany)
Adobe photoshop CS6	Adobe (Germany)

2.1.5 The approval of mouse study

Mouse studies were approved by the authorities in Berlin and Nordrhein-Westfalen: approval numbers G0468/09 and T0458/09 and approval number 84-02.04.2012.A146. The generation of the mice was performed by my former colleague Sandra Seeher. The mice were bred and matured in the animal facility of Haus für Experimentelle Therapie (HET) at University of Bonn.

2.2 Method

2.2.1 Genotyping of CamK-RQ, CamK-CR, Alb-RQ and Alb-CR mice

The ear punches from mice were collected in 1.5 ml reaction tubes. The tissue was lysed in 100 µl Alkaline buffer (25 mM NaOH, 0.2 mM EDTA, PH 12) in the thermomixer at 95 °C for 1 h. Subsequently, one hundred microliter Neutral Buffer (0.04 mM Tris-HCl, 22 mM HCl PH 6) was added for neutralization. One microliter of the resulting lysate was applied for PCR reaction. PCR protocols are given in table 2-4, 2-5, 2-6, 2-7 and 2-8. The used primers are available in table 2-9. At the meantime, a 2% Agarose gel (2g Agarose powder in 100 ml 1x TBE Buffer (0.1M Tris, 0.1M Boric acid, 2 mM Na_2EDTA) with 3 µl HD Green Plus DNA Stain. The agarose gel was prepared by overheating in the microwave and cooling to room temperature. Twenty-five microliter PCR product from each sample was mixed with 5 µl 6x Loading Buffer (0.25 % Bromophenol blue, 30 % Glycerol). After loading of the total sample amount and 7 µl DNA ladder (Thermo Fisher), 125 V where applied for 40 minutes onto the gel. Afterwards, the bands were visualized by UV light.

Table 2.4: Genotyping reaction of Alb-Cre

PCR Component		PCR Program		
dH$_2$O	22.3 µl			
10x Buffer	3 µl	94 °C	5 min	
5 mM dNTPs	1.5 µl			
10 µM Alb-Cre fwd	1 µl	94 °C	30 sec	
10 µM Alb-Cre rv	1 µl	57 °C	30 sec	35 cycles
5 U/µl Taq Polymerase	1 µl	72 °C	45 sec	
Genomic DNA	1 µl			
Total	30 µl	72 °C	3 min	

Table 2.5: Genotyping reaction of CamK-Cre

PCR Component		PCR Program		
dH$_2$O	22.3 µl			
10x Buffer	3 µl	94 °C	5 min	
5 mM dNTPs	1.5 µl			
10 µM CamK-Cre fwd	1 µl	94 °C	30 sec	
10 µM CamK-Cre rv1	1 µl	57 °C	30 sec	35 cycles
10 µM CamK-Cre rv2	1 µl	72 °C	45 sec	
5 U/µl Taq Polymerase	0.2 µl			
Genomic DNA	1 µl	72 °C	3 min	
Total	30 µl			

Table 2.6: Genotyping reaction of Secisbp2 floxed

PCR Component		PCR Program		
dH$_2$O	21.38 µl			
10x Buffer	3 µl	94 °C	5 min	
5 mM dNTPs	1.5 µl			
50 mM MgCl$_2$	1 µl	94 °C	30 sec	
10 µM Secisbp2 floxed fwd	1 µl	60 °C	45 sec	35 cycles
10 µM Secisbp2 floxed rv	1 µl	72 °C	45 sec	
5 U/µl Taq Polymerase	0.125 µl			
Genomic DNA	1 µl	72 °C	3 min	
Total	30 µl			

Table 2.7: Genotyping reaction of Secisbp2 R543Q

PCR Component		PCR Program		
dH$_2$O	21.3 µl			
10x Buffer	3 µl	95 °C	3 min	
5 mM dNTPs	1.5 µl			
50 mM MgCl$_2$	1 µl	95 °C	30 sec	
10 µM Secisbp2 R543Q fwd	1 µl	58 °C	45 sec	35 cycles
10 µM Secisbp2 R543Q rv	1 µl	72 °C	1 min	
5 U/µl Taq Polymerase	0.2 µl			
Genomic DNA	1 µl	72 °C	3 min	
Total	30 µl			

Table 2.8: Genotyping reaction of Secisbp2 C696R

PCR Component		PCR Program		
dH$_2$O	21.3 µl			
10x Buffer	3 µl	95 °C	3 min	
5 mM dNTPs	1.5 µl			
50 mM MgCl$_2$	1 µl	95 °C	45 sec	
10 µM Secisbp2 C696R fwd	1 µl	60 °C	45 sec	35 cycles
10 µM Secisbp2 C696R rv	1 µl	72 °C	1 min	
5 U/µl Taq Polymerase	0.2 µl			
Genomic DNA	1 µl	72 °C	3 min	
Total	30 µl			

Table 2.9: Genotyping primer list

Gene	Sequence
Alb-Cre fwd	ACCTGAAGATGTTCGCGATTATCT
Alb-Cre rv	ACCGTCAGTACGTGAGATATCTT
CamK-Cre fwd	GGTTCTCCGTTTGCACTCAGGA
CamK-Cre rv1	CCTGTTGTTCAGCTTGCACCAG
CamK-Cre rv2	CTGCATGCACGGGACAGCTCT
Secisbp2 floxed fwd	TGTTTCTATTCTCATCTACTCTGCTCA
Secisbp2 floxed rv	TAACTCCCCCTTTCCATCTG
Secisbp2 R543Q fwd	GTTCTGGTTTGATGTTTTGGTTCC
Secisbp2 R543Q rv	AGGCCACAGTCCTATGGTTG
Secisbp2 C696R fwd	TGCAGCCAGATGCTTAGTAAAG
Secisbp2 C696R rv	AGGTCAGGCTAACTGCTGGA

2.2.2 Sample preparation and storage

The mice were killed in accordance with the guidelines of the Animal Welfare. The mice were anesthetized by carbon dioxide inhalation and then decapitated. Brain and liver were removed after sacrifice. The tissue was then snap-frozen in liquid nitrogen and stored at - 80 °C if not used immediately. The samples were used for RNA isolation, Western blot, RNA-seq, 3'RNA-seq.

For immunohistochemistry, the mice were anesthetized by carbon dioxide inhalation and then transcardially perfused by 1x phosphate-buffered saline (PBS) and 4% paraformaldehyde (PFA). Then the intact brain was removed and fixed in 4% PFA overnight at 4 °C. Eventually, the brain was gently washed with 1x PBS to remove 4% PFA. Fixed brain was stored in 1x PBS at 4 °C and ready for sectioning by the vibratome.

2.2.3 Real-time Polymerase Chain Reaction (RT-PCR)

2.2.3.1 RNA isolation

Fifty micrograms of each sample were used for RNA isolation. The samples were homogenized in 1 ml TRIzol with a hand homogenizer. The well-homogenized samples were incubated for 5 minutes for completely dissociation. After addition of 200 µl chloroform, the samples were mixed and incubated for 2 minutes at room temperature. Afterwards the samples were centrifuged for 15 minutes at 12000 x g at 4 °C. The aqueous phase was transferred to a new 1.5 ml tube and 500 µl (1.5 volumes) of isopropanol was added. The samples were incubated for 10 minutes at room temperature and centrifuged for 10 minutes at 12000 x g at 4 °C. The supernatant was discarded with a tiny pipette. The pellet was resuspended by adding 1 ml 75% ethanol and then centrifuged for 5 minutes at 7500 x g at 4 °C. The supernatant was discarded again with a pipette. The pellet was air-dried for 10 minutes, resuspended by adding 30 µl RNase-free water and then incubated at 55 °C for 15 minutes. Total RNA concentration was determined by Nanodrop.

2.2.3.2 cDNA synthesis

cDNA synthesis was performed by following by the iScript cDNA Synthesis Kit protocol. The composition of the reaction as well as the temperature program is available in Table 2-10. After reaction, the samples were diluted 1:10 with dH_2O and stored at -20 °C.

Table 2.10: cDNA synthesis reaction mix and program

Reaction components		Program	
iScript Reaction Buffer	4 µl	25 °C	5 min
Reverse Transcriptase	1 µl	46 °C	20 min
RNA	1 µg	95 °C	1 min
dH_2O	ad 20 µl		

2.2.3.3 RT-PCR

The RT-PCR was followed by SYBR Green Fluorescein Mix protocol. The reaction mix and RT-PCR program are available in Table 2-11. The primer sequences were listed in Table 2-12. To be noticed, the cDNA templates from previous step were diluted 1:10 with RNase-free water.

Table 2.11: RT-PCR reaction mix and program

PCR Component		PCR Programm		
SYBR Green Mix	12.5 µl			
10 µM Primer fwd	0.25 µl	95 °C	15 min	
10 µM Primer rv	0.25 µl			
cDNA template (1:10)	5 µl	95 °C	30 sec	
RNase-Free Water	7 µl	60 °C	45 sec	40 cycles
Total	25 µl	72 °C	30 sec	
		72 °C	3 min	

Table 2.12: RT-PCR Primer list

Gene	Sequence (5' to 3')
Gpx1 fwd	ATCAGTTCGGACACCAGGAG
Gpx1 rev	CATTCCGCAGGAAGGTAAAG
Gpx4 fwd	ATGCCATCAAATGGAACTTTAC
Gpx4 rev1	GTGTAGGGGCACACACTTGTA
Selenop fwd	GTTGAAGAAGCCATTAAGATCG
Selenop rev	ATTCTCTGAAGGCTTACTGCTG
Selenow fwd	CAGCTCAAGGAGAAGCTAGAAC
Selenow rev	
	GGAACTTGCTCTCTGTATCCAC
Selenot fwd	GGCTTAATAATTGTTGGCAAAG
Selenot rev	TATCTCAAATGCACCTGTTGAC
Sephs2 fwd	TAGCTTGTGCCAATGTGCTC
Sephs2 rev	TAATCCACGGGTTGACCACT
18s rRNA fwd	TTGACGGAAGGGCACCACCAG
18s rRNA rev	GCACCACCACCCACGGAATCG
Actb fwd	AGTGTGACGTTGACATCCGT
Actb rev	TGCTAGGAGCCAGAGCAGTA

2.2.4 Western Blot

2.2.4.1 Sample preparation

Two hundred microliter RIPA lysis buffer (50 mM Tris-HCl (pH7.5), 150 mM NaCl, 1% NP-40, 0.5 % deoxycholate, 0.1 % SDS, 1x protease inhibitors cocktail, 1 mM DTT) was added into each tube for the lysis of the samples. The samples were well homogenised by a homogenizer on ice and then centrifuged for 10 minutes at 15000 x g at 4 °C. The supernatant was transferred to a new pre-chilled tube on ice.

2.2.4.2 Protein quantification

Protein quantification was performed following the BCA Protein Assay Kit protocol. The standards were prepared in following concentrations: 2.0, 1.5, 1.3, 1.0, 0.75, 0.5, 0.375, 0.25, 0.1875, 0.125, 0.0625 and 0.0 µg/µl BSA in 1.5 ml tubes. 10 µl of each standard, 2 µl of each sample and blank (RIPA lysis buffer) were added into 240 µl (for samples) and 248 µl (for standards) pre-mixed solution A and B in the kit, respectively. 220 µl of each standard and sample was incubated at 37 °C for 30 minutes and then transferred onto 96 wells plate. The absorbance was measured at 562 nm on the Tecan plate reader. Protein concentration was calculated by the standard curve formula. The working dilution of samples (2 µg/µl) was prepared with 4x Laemmli buffer (8 % SDS, 40 % glycerol, 0.01 % Bromophenol Blue, 0.2572 M Tris-HCl (pH 6.8), dH$_2$O) according to calculated protein concentration. The samples were stored at -20 °C if not used immediately.

2.2.4.3 Sodium dodecyl sulfate polyacrylamide gel electrophoresis (SDS Page)

SDS page is a technique used to separate the proteins according to their sizes. The effect of different shapes and charges of proteins can be eliminated by adding Dithiothreitol (DTT) and SDS. The proteins can be separated depending on the individual mobility in a polyacrylamide gel. The Bio-Rad gel caster system was used for the SDS pages. The recipes of stacking gel and resolving gel were available in Table 2-13.

Table 2.13: The component of SDS PAGE gel

Component	12 % Resolving Gel (40ml)	5% Stacking Gel (18ml)
H_2O	17.4 ml	11 ml
1.5 M Tris-Cl pH 8.8	10 ml	4.5 ml
40% acrylamide	12 ml	2.25 ml
20% SDS	200 µl	90 µl
10% APS	400 µl	180 µl
TEMED	40 µl	18 µl

Prior loading, the samples were incubated in a thermal block at 95 °C for 10 minutes and pulse centrifuged. 50 µg liver protein and 100 µg brain protein were applied for gel electrophoresis, respectively. 7 µl protein marker was loaded as an indicator of protein size. The polyacrylamide gel was running in running buffer (25 mM Tris-HCl, 190mM glycine, 0.1% SDS) under 90 V until the front bromophenol blue line reached the resolving gel and then under 120 V until the front line reached the bottom.

2.2.4.4 Membrane transfer and immunoblot

After gel electrophoresis, the stacking gel was cut and discarded. The remaining resolving gel was rinsed in the transfer buffer (25 mM Tris-HCl, 290 mM glycine, 20 % methanol) together with whatman paper and 0.2 µm nitrocellulose membrane. The semi-dry transfer system was running under 23 V for 1 h. After the transfer, the membrane was rinsed in ponceau red solution (0.1% Ponceau in 5 % acetic acid) for checking the quality of transfer. Then the membrane was incubated in blocking solution (5 % milk powder in TBST) at room temperature for 1 h and then with diluted primary antibody solution at 4 °C overnight (table 2-14). On the following day, the primary antibody solution was removed and recycled. The membrane was washed 3 times 10 minutes each with TBST (20 mM Tris-HCl, 150 mM NaCl, 0.1 % Triton x100) and then incubated with corresponding secondary antibody solution (1 % milk powder in TBST) on a shaker at room temperature for 1 h. Again, the membrane was washed 3 times 10 minutes each with TBST. Eventually, the detection was performed by Fusion Solo imaging system using Supersignal West Dura.

Table 2.14: The list of Western Blot Antibodies

Antibody	Dilution	Manufacturer
Primary Antibody:		
Anti-Gpx1 (rabbit)	1:1000	Abcam
Anti-Gpx4 (rabbit)	1:1000	Abcam
Anti-Txnrd1 (rabbit)	1:1000	Abcam
Anti-Selenot (rabbit)	1:250	Sigma Aldrich
Anti-Selenom (rabbit)	1:1000	Sigma Aldrich
Anti-Sephs2 (mouse)	1:1000	Rockland
Anti-Selenow (mouse)	1:2000	Rockland
Anti-Selenos (rabbit)	1:1000	Sigma Aldrich
Anti-Secisbp2(rabbit)	1:1000	Proteintech
Anti-β-actin (mouse)	1:25000	Sigma Aldrich
Secondary Antibody:		
HRP goat anti-mouse	1:15000	Jackson Immunotech
HRP goat anti-rabbit	1:15000	Jackson Immunotech

2.2.5 Immunohistochemistry

The mice were transcardially perfused with 1x PBS and then 4% Paraformaldehyde (PFA). After rapid dissection, brains were post-fixed in 4% PFA overnight and then washed three times with 1 x PBS for 10 minutes at room temperature. Seventy micrometer brain slices were cut by vibratome and placed in 1 x PBS in 24 well plate. Then the brain slices were washed 3 times for 5 minutes with 1 x PBST and soft shaking. Two percent BSA (Bovine serum albumin) in 1 x PBST was used as blocking solution for 1 h incubation. The brain slices were incubated with primary antibodies at 4 °C overnight and washed 3 times for 5 minutes by 1 x PBST with soft shaking. The corresponding secondary antibodies were applied and incubated for 1 h. After incubation, the brain slices were washed 3 times 5 minutes by 1 x PBS and then placed on the glass slides. The glass slides were mounted by Mowiol and then covered by coverslips. The images were captured by Zeiss Axioplan 2 microscope and operated by Axiovision software. The cell counting was performed by using ImageJ.

Table 2.15: The list of Immunohistology Antibodies

Antibody	Dilution	Manufacturer
Primary Antibody:		
Anti-Parvalbumin (rabbit)	1:5000	Swant
Anti-GFAP (mouse)	1:1000	Sigma Aldrich
Anti-Iba1 (rabbit)	1:1000	Wako
Secondary Antibody:		
Alexa 488 goat anti-rabbit	1:1000	Jackson Immunotech
Dylight 488 donkey anti-mouse	1:1000	ThermoFish Scientific
Cy3 donkey anti rabbit	1:1000	Jackson Immunotech

2.2.6 High throughput sequencing (3' mRNA Sequencing, RNA Sequencing, Ribosome Profiling)

RNA sequencing is widely used for analyzing differential gene expression between control and experimental group. RNA from mouse cortex was isolated by following RNeasy Mini Kit protocol. The RNA-Seq library was prepared by following NEBNext Small RNA Library Prep Set Guide. Subsequently, the samples were sequenced by using Illumina HiSeq 2000. The sample preparation was performed by my colleagues Dr. Noelia Fradejas Villar and Dr. Simon Bohleber. Sequencing was performed by Dr. Brian Dalley in the University of Utah.

Three prime RNA sequencing is a newly developed RNA sequencing technology. The dataset produced by 3' mRNA sequencing is highly overlapping with RNA sequencing dataset and reproducible between biological replicates (Ma et al., 2019). Compared to the conventional RNA sequencing, 3' mRNA sequencing has relatively lower cost and simpler library preparation protocol. Total RNA was isolated by following TRIzol protocol. The 3' mRNA sequencing library was prepared by following QuantSeq 3'mRNASeq Library Prep Kit Guide by our university intern core facility. Subsequently, the samples were sequenced by using Illumina HiSeq 2500. The sequencing was performed by Dr. André Heimbach in the Next Generation Sequencing Faculty of University of Bonn.

Ribosome profiling is a robust method to detect the location of translating ribosomes on mRNAs and assess the translational process (Ingolia 2014). For ribosome profiling, 50 mg mouse cortex was homogenized in the 1 ml lysis buffer (10 mM Tris-HCl (pH 7.5), 300 mM KCl, 10 mM $MgCl_2$, 200 µg/ml cycloheximide, 1 mM DTT and 1% Triton X-100). After centrifugation at 12000 x g at 4 °C, the supernatant was transferred to a new pre-chilled 1.5 ml reaction tube on ice. Ten microliter RNase1 (1000 U) was added into tissue lysate and incubated for 20 minutes on a shaker at room temperature for proper digestion to monosomes. After incubation, the reaction was blocked by adding 10 µl SUPERase Inhibitor. Subsequently, 220 µl of the lysate was placed on top of a 50% sucrose buffer and centrifuged for 3 h at 85.000 rpm on a Beckman-Coulter ultracentrifuge with the TLA110 rotor. The supernatant was removed and the pellets were resuspended in Qiazol

and the mRNA fragments with attached ribosomes were isolated by following miRNeasy kit guide. The RNA concentration was determined by Nanodrop 2000. Further RPF purification was done by the sequencing core facility of the university of Utah by Dr. Brian Danley via Pippin Prep on 15 % TBE-Urea Gel. Indicating by the size marker, 17-34 nucleotides region was excised and gel purification was performed afterwards. The ribosome profiling library was constructed by following TruSeq Small RNA Sample Prep kit Guide. Then the samples were sequencing by Illumina HiSeq 2000.

All the high-throughput sequencing data analysis were performed by my colleague Dr. Simon Bohleber, institut für Biochemie und Molekularbiologie, Rheinische Friedrich-Wilhelms Universität Bonn. The raw sequencing data of CamK-RQ is available in the NCBI GEO repository entry GSE119681. The scripts for data analysis of CamK-Trit1 KO can be tracked in Dr. Simon Bohleber doctoral thesis (Einfluss der tRNA Modifikation i^6A37 auf die Translation in Säugern und deren Mitochondrien).

2.2.7 Translating ribosome affinity purification (TRAP)

The Rosa26^{fsTRAP} mice were obtained from Jackson laboratory (Stock No.022367). ROSA26, locates on mouse chromosome 6, is a locus widely used for both constitutive and conditional gene expression in mice. The structure of constructed Rosa26^{fsTRAP} allele is displayed in Fig 2-1. The Rosa26 locus consists of a strong CAG promoter followed by a floxed-neomycin (Neo) resistance cassette, a polyA sequence, GFP-L10 cDNA, 2xHA (hemagglutinin) tagged bacterial birA (biotin ligase) and a polyA sequence. GFP was fused with large 60s ribosomal subunit L10. In the absence of Cre, the expression of GFP-L10 is prevented by the stop signal.

Fig 2-1 The structure of Rosa26^{fsTRAP} allele (Zhou et al., 2013)

Further, the Rosa26^{fsTRAP} mice were interbred with CamK-Cre Trit1 knockout mice. After removal of the loxP-flanked Neo-polyA cassette via CamK-Cre-mediated recombination, activated GFP-L10a is expressed exclusively in the ribosomes of the neurons (Zhou et al., 2013).

TRAP was performed based on Heiman's work (Heiman et al., 2014), but with some subtle modifications. The materials and recipes of solutions are listed in Table 2-16 and 2-17. The top priority of the experiment is to avoid RNase contamination. Before starting the experiment, it is thus important to set up an RNase-free work zone. RNase decontaminating reagents RNase-Zap was used to decontaminate working surface and equipment. Certified RNase-free plasticware and reagents, as well as aerosol resistant tips, were also used.

Table 2.16: Materials used for TRAP

Reagent and Chemicals	Manufacturer	Accession Number
Absolutely RNA Nanoprep kit	Agilent	400753
Biotinylated Protein L	Fisher Scientific	PI-29997
IgG and protease-free Bovine Serum	Jackson	001-000-162
Cycloheximide	Sigma	C7698
Dl-Dithiothreitol	Sigma	D9779
Ethanol	Sigma	E7023
Glucose	Sigma	G7528
Hank's Balanced Salt Solution	Invitrogen	14065-056
HEPES	Affymetrix	16924
1M $MgCl_2$ Solution	Applied Biosystems	AM9530G
Methanol	Sigma	322415
NP-40	AG Scientific	P1505
2M KCl Solution	Applied Biosystems	AM9640G
Protease inhibitor tablets	Roche	11836170001
RNase Zap Wipes	Applied Biosystems	AM9786
RNasin	Promega	N2515
$NaHCO_3$	Sigma	S6297
Streptavidin MyOne T1 Dynabeads	Invitrogen	65601
Sulfolane	Sigma	400753
Superasin	Applied Biosystems	AM2694

Table 2.17: The recipe of solutions for TRAP

Solution	Component (final concentration)
Dissection Buffer	1 x HBSS
	2.5 mM HEPES
	35 mM Glucose
	4 mM NaHCO$_3$
	100 µg/ml Cycloheximide
	RNase-free water
Tissue lysis Buffer	20 mM HEPES
	10 mM MgCl$_2$
	150 mM KCl
	0.5 mM DTT
	1 tablet Protease Inhibitor
	100 µg/ml Cycloheximide
	40 U/ml RNasin
	40 U/ml Superasin
	RNase-free water
Low Salt Buffer	20 mM HEPES
	10 mM MgCl$_2$
	150 mM KCl
	0.5 mM DTT
	100 µg/ml Cycloheximide
	1% NP-40
	RNase-free water
High Salt Buffer	20 mM HEPES
	10 mM MgCl$_2$
	350 mM KCl
	100 µg/ml Cycloheximide
	1% NP-40
	RNase-free water

2.2.7.1 Preparation of the affinity matrix

Each affinity matrix for 40 mg mouse cortex requires: 150 μl Streptavidin MyOne T1 Dynabeads, 60 μl Biotinylated Protein L (1 μg / μl in 1x PBS), and 25 μg each of GFP antibodies 19C8 and 19F7. The GFP antibodies were purchased from Memorial-Sloan Kettering Monoclonal Antibody Facility. One hundred and fifty microliter magnetic beads were transferred from the well-mixed original bottle to a new 1.5 ml reaction tube. Then the beads were washed by 1 x PBS and then incubated with 60 μl biotinylated Protein L in 1 x PBS for 35 minutes at room temperature by using a tube rotator. The Protein L-coated beads were collected on the magnet and then washed 5 times with 3% BSA in 1 x PBS. Afterwards, the beads were incubated with GFP antibodies (19C8 and 19F7) for 1 h at room temperature. After 1 h incubation, the beads were washed 3 times with low salt buffer. Eventually, the beads were resuspended and kept in 200 μl low salt buffer.

2.2.7.2 The preparation of mouse cortex lysate

Rapid hand dissection of mouse brain was performed. Forty milligram fresh mouse cortex was weighted and placed into pre-chilled dissection buffer. After quickly wash with dissection buffer, the tissue was transferred into a pre-chilled 1,5ml Ep tube and homogenized with 1 ml tissue lysis buffer on ice. Then the supernatant was collected after 2000 x g centrifugation at 4°C for 10 minutes. 111 μl 10% nonyl phenoxypolyethoxylethanol (NP-40) and 123.5 μl 300 mM 1,2-diheptanoyl-sn-glycero-3-phosphocholine (DHPC) were added into the supernatant and then mixed gently. Eventually, the supernatant was collected after 20000 x g centrifugation at 4°C for 10 minutes.

2.2.7.3 Immunopurification and RNA isolation

200 μl pre-prepared affinity matrix was added into the supernatant above and incubated at 4 °C for 16 h in a tube rotator. After incubation, the beads were collected with a magnet on ice and subsequently washed with high salt buffer three times. After removing all washing buffer, the beads were placed at room temperature for 5 minutes. Then the beads

were resuspended in 100 µl Nanoprep Lysis Buffer (Absolutely RNA Nanoprep Kit) with 0.7 µl β-mercaptoethanol and incubated for 10 minutes at room temperature. The RNA-containing supernatant was seperated from the beads with a magnet and ready for RNA isolation.

The RNA isolation was performed by following Absolutely RNA Nanoprep Kit Guide. All the reagents mentioned below are available in the kit. 100 µl 80% sulfolane was added into the supernatant above and mixed well. The mixture was transferred into a seated nano-spin cup and centrifuged at 12000 x g for 1 minute. The filtrate was discarded and the nano-spin cup was retained. After two times washing with high-salt buffer, 15 µl DNase solution was added directly onto the fiber matrix of the spin cup and incubated at 37 °C for 15 minutes. Again, after two times washing low-salt buffer, 10 µl elution buffer was added directly onto the fiber matrix and incubated at 60 °C for 2 minutes. Then the nano-cups were spun twice at 12000 x g for 5 minutes. The filtrate was transferred into a new reaction tube. The quality of RNA was tested by Tapestation 2000. Further, RNA samples were sequenced by following the 3' mRNA sequencing protocol.

3. Results

3.1 Hepatocyte-specific Secisbp2 R543Q and C696R mice are indistinguishable from Secisbp2 knockout mice

3.1.1 The generation of hepatocyte-specific Secisbp2 R543Q and C696R mice

Mouse studies were approved by the authorities in Berlin and Nordrhein-Westfalen: approval numbers G0468/09 and T0458/09 and approval number 84-02.04.2012. A146, respectively. The original idea was to reproduce patients' pathological mutations in the mouse models. Unexpectedly, homozygous Secisbp2 R543Q and C696R mice were embryonic lethal around E7, resembling Secisbp2 knockout mice (Table 3.1). Therefore, conditional Secisbp2 mutant mice were required for the further study due to the embryonic lethality of full homozygous Secisbp2 mutant mice. Conditional Secisbp2 mutant mice were generated by combining a missense mutant allele with a conditional Secisbp2 knockout allele. On the Secisbp2 knockout allele, the deletion of Secisbp2 was caused by the activation of Cre/loxP system. Here, the Cre recombinase expressed under the control of a hepatocyte-specific albumin promoter (Alb-Cre) (Seeher et al., 2014). Thus, the only translated Secisbp2 mRNA was produced by the missense Secisbp2 allele in hepatocytes (Alb-Cre *Secisbp2* $^{fl/R543Q}$, Alb-Cre *Secisbp2* $^{fl/C696R}$). Moreover, hepatocyte-specific Secisbp2 knockout mice (Alb-Cre *Secisbp2* $^{fl/fl}$) was included in most analyses for the comparison (Seeher et al, 2014). In order to simplify the terms, Alb-RQ, Alb-CR, Alb-KO will be mentioned below.

Table 3.1: Number of mice born from heterozygous Secisbp2 mutations

Genotype	Number
Heterozygous Secisbp2 R543Q/+ cross-breeding	
Secisbp2 +/+	43
Secisbp2 R543Q/+	66
Secisbp2 R543Q/R543Q	0
Heterozygous Secisbp2 C696R/+ cross-breeding	
Secisbp2 +/+	30
Secisbp2 C696R/+	80
Secisbp2 C696R/C696R	0

3.1.2 Undetectable Secisbp2 expression in Alb-RQ and Alb-CR mouse livers resembling Alb-KO

Western blot analysis (Fig 3.1) showed that both mutant Secisbp2 proteins were virtually undetectable like full KO in the liver.
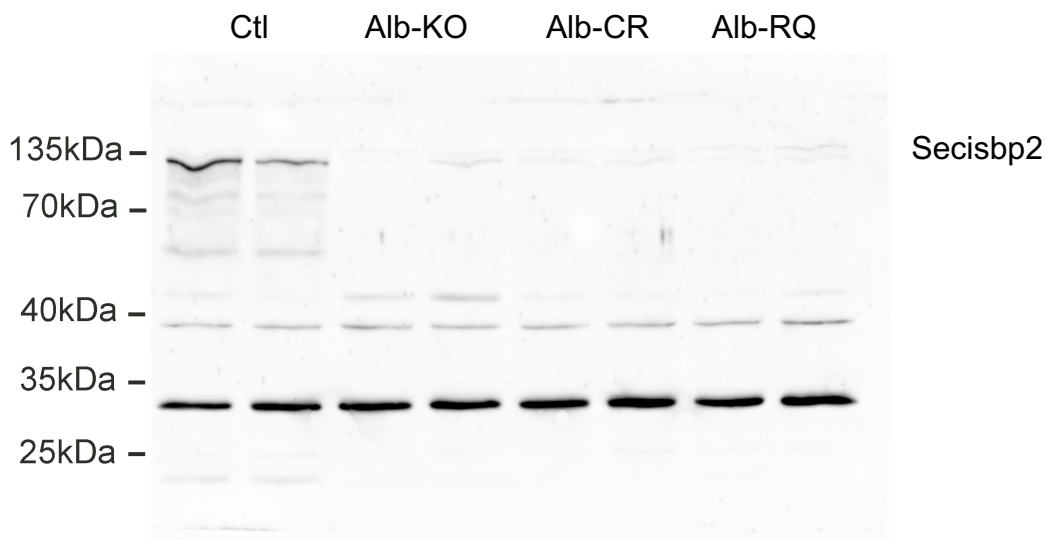
Fig 3.1 Secisbp2 expression in hepatocyte-specific Secisbp2 mutant mice assessed by western blot. Wildtype mice (Ctl) were compared with Alb-KO, Alb-CR, Alb-RQ. The non-specific bands indicate equal loading.

3.1.3 Reduced selenoprotein expression in Alb-RQ and Alb-CR mouse liver

Previous study suggested that Secisbp2 is indispensable for selenoprotein translation (Copeland et al., 2000). Apart from facilitating selenoprotein translation, Secisbp2 also plays a role in stabilizing selenoprotein mRNA (Fradejas-Villar et al., 2017). Selenoprotein contains one or multiple in-frame UGA codons on its mRNA, which might cause selenoprotein mRNA being degraded by nonsense-mediated decay (NMD) in response to the inactivation of Secisbp2 (Seeher et al., 2014). In order to probe the impact of both mutant Secisbp2 on selenoprotein expression in the liver, selenoprotein mRNA and protein expression were measured by RT-RCR and western blot, respectively. RT-RCR analysis (Fig 3.2) revealed that all selected selenoprotein mRNA levels were significantly reduced in Alb-RQ and Alb-CR resembling Alb-KO. *Gpx1* and *Selenop* mRNA, two most abundant selenoproteins in the liver, were virtually undetectable in Alb-CR and Alb-RQ mouse livers. *Selenow* and *Sephs2* mRNA also presented a gross reduction in Alb-Cre CR and RQ mouse livers. In contrast, *Gpx4* and *Selenot* mRNA displayed a relatively moderate reduction. To be noticed, all selected selenoprotein mRNAs showed no obvious difference between Alb-RQ and Alb-CR.
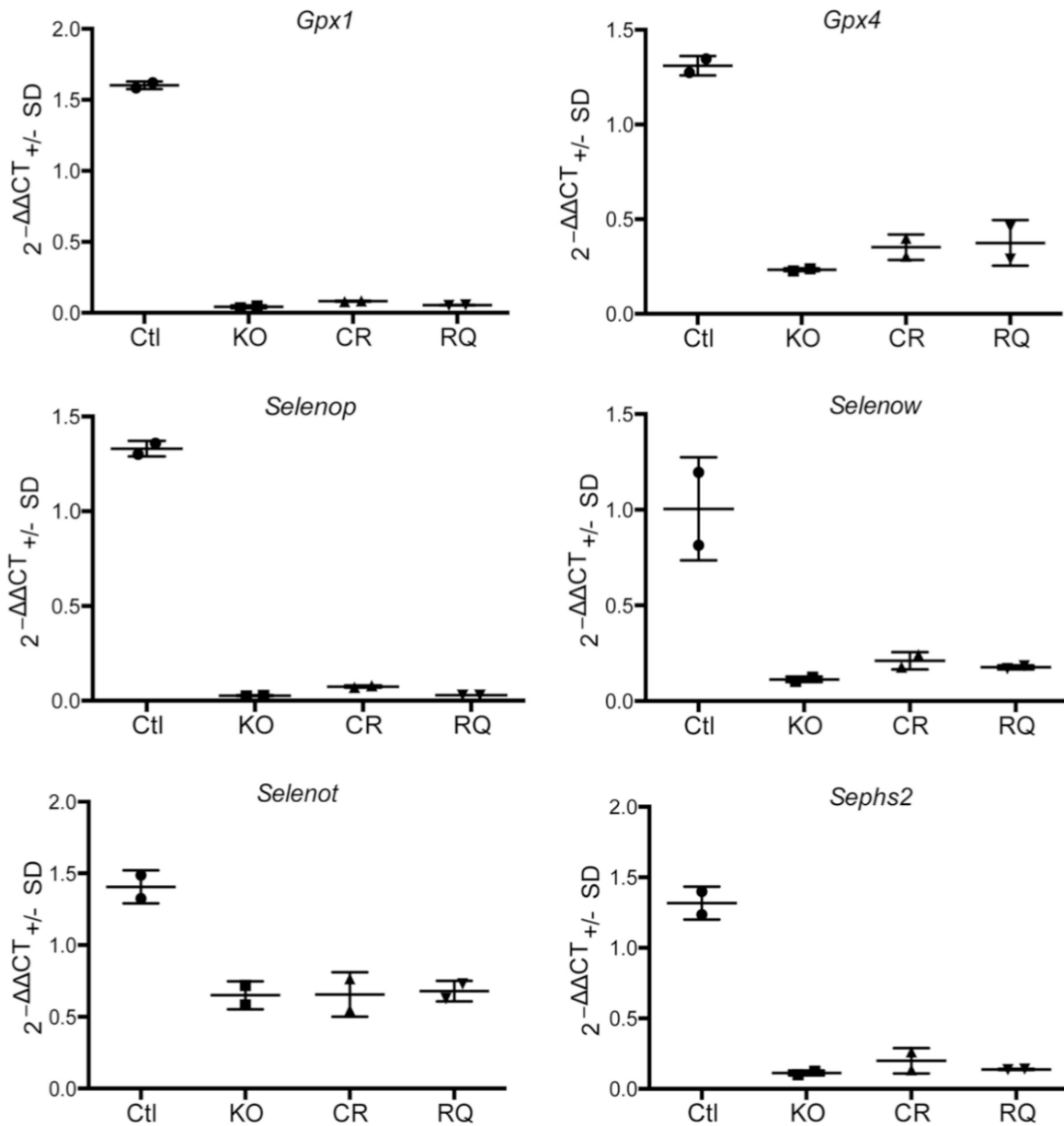
Fig 3.2 Reduced Selenoprotein mRNA in hepatocyte-specific Secisbp2 mutant mouse livers. Wildtype mice (Ctl) were compared with Alb-KO, Alb-CR and Alb-RQ. RT-PCR analysis was applied for selected selenoproteins. Calculated ΔΔCT values are normalized to 18S rRNA as housekeeping gene. Means are given ± S.D. n=2 (per genotype).

Meanwhile, Gpx1, Gpx4, Selenot and Sephs2 protein levels were accordingly reduced in Alb-CR and Alb-RQ resembling Alb-KO (Fig 3.3). Based on the condition of non-overexposure of wildtype bands, Gpx1, Selenot and Sephs2 protein were virtually undetectable, while subtle bands were remaining in Alb-CR and Alb-RQ on the Gpx4 blot. Txnrd1 protein level was unaltered in all groups. Again, all selected selenoproteins showed no obvious difference between Alb-RQ and Alb-CR.
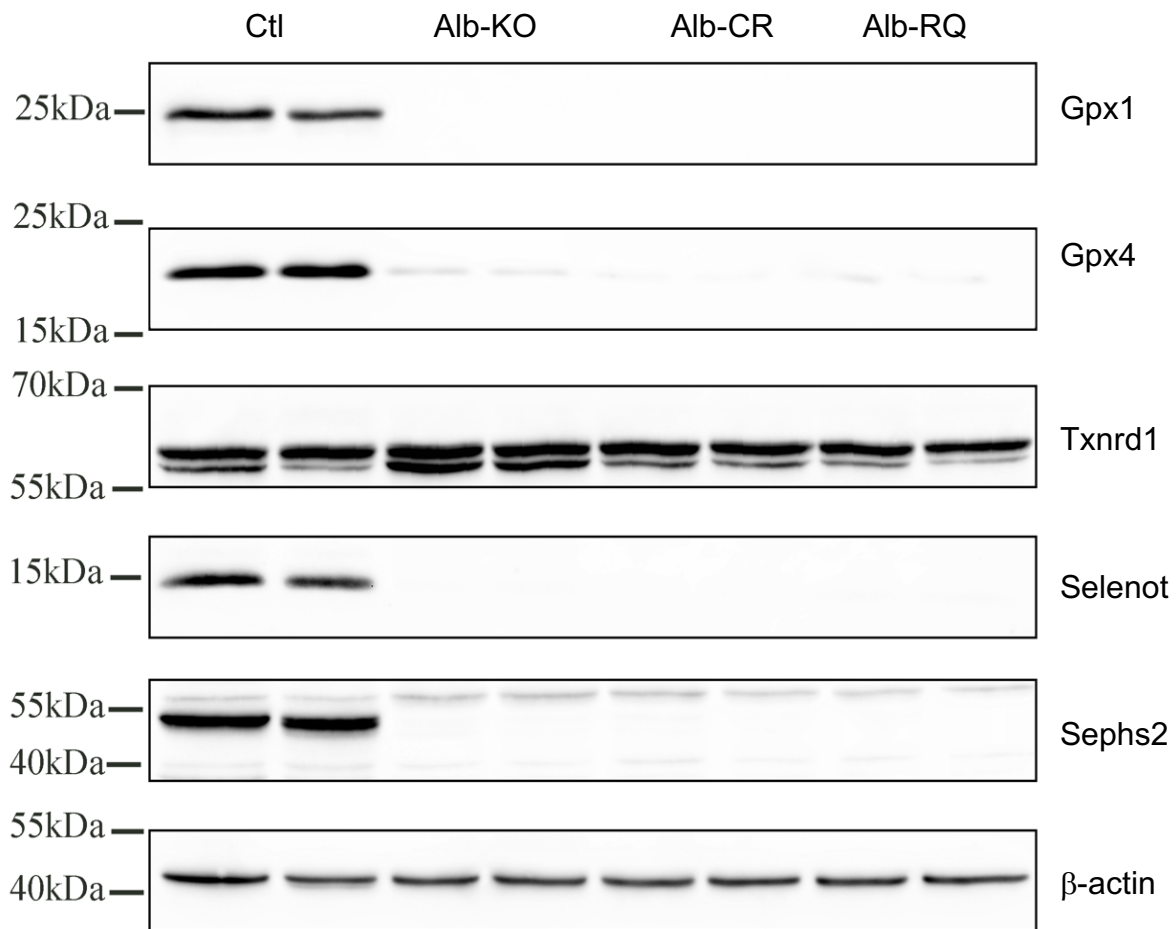
Fig 3.3 Reduced selenoprotein in hepatocyte-specific Secisbp2 mutant mouse livers assessed by western blot. Two individual liver extracts were analyzed for each genotype. Housekeeping protein β-actin indicates equal loading.

3.2 Neuron specific Secisbp2 R543Q is partial functional and Secisbp2 C696R is function null in the cortex

As mentioned in 3.1, both homozygous Secisbp2 mutant mice were embryonic lethal. Additionally, patients carrying SECISBP2 mutations and other single or global selenoprotein knockout mouse models showed a diverse spectrum of neurological phenotypes (Schoenmakers & Chatterjee, 2020; Pitts et al., 2014). Therefore, neuron is another desired cell type in Secisbp2 mutation studies. Neuron-specific Secisbp2 mutant mice were generated by using a Cre recombinase expressed under the control of the calcium/calmodulin-dependent protein kinase II (CamK) promoter (Seeher et al, 2014). The only translated Secisbp2 mRNA was produced by the missense mutant Secisbp2 allele in neurons, while a deletion of the other allele was caused by Cre/loxP system (CamK-Cre Secisbp2 $^{fl/R543Q}$, CamK-Cre Secisbp2 $^{fl/C696R}$). Moreover, neuron-specific Secisbp2 knockout mice (CamK-Cre Secisbp2 $^{fl/fl}$) was included in most analyses for the comparison (Seeher et al. 2014). In order to simplify the terms, CamK-CR, CamK-RQ and CamK-KO will be mentioned subsequently.

3.2.1 CamK-CR mice presented a neurological phenotype resembling CamK-KO

Compared to wild types, CamK-CR mice displayed smaller stature and died before weaning (Fig 3.4). On P16-18, the mean body masses were 7.27 ± 0.56 g and 3.82 g ± 0.60 g for the wild types and CamK-CR, respectively. CamK-CR mice showed a dystonic gait in the cages. Moreover, CamK-CR mice gripped their forelegs when handling, while hardly recovered the balance after handling. This neurological phenotype was similar to CamK-KO mice. Subsequently, based on previous CamK-KO mouse study (Seeher et al. 2014), the presence of astrogliosis and the loss of parvalbumin positive interneurons was tested in CamK-CR mice in the next step.

Ctl   CamK-CR
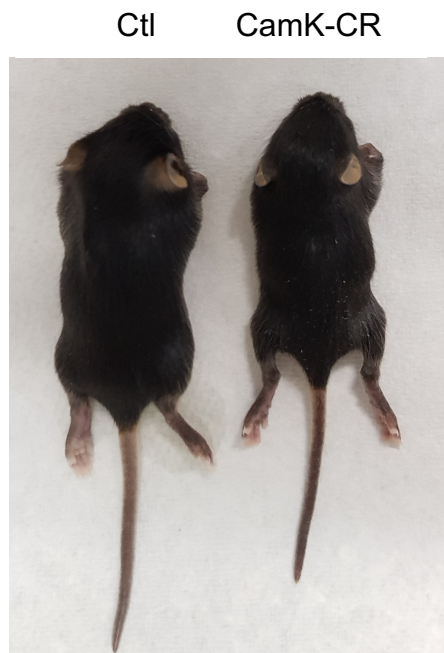
Fig 3.4 Size comparison of wild type mice and CamK-CR mice. Compared to wild type mice, CamK-CR mice presented a smaller stature. The picture was captured at 16 days of age.

3.2.2 Astrogliosis and the loss of parvalbumin positive interneurons in CamK-CR mouse somatosensory cortex

Astrogliosis is a spectrum of molecular and cellular changes in astrocytes in response to CNS insults, such as chronic neurodegenerative disease and traumatic brain injury (Sofroniew 2015). Fig 3.5 shows that the occurrence of astrogliosis in the lower cortical layer of somatosensory cortex were observed, when Gfap immunohistochemistry was performed at P16. Additionally, the location of astrogliosis was consistent to Gfap staining in the somatosensory cortex of CamK-KO mice (Seeher et al, 2014), which further confirmed the consistence between CamK-CR and CamK-KO mice.

| | |
| Ctl | CamK-CR |
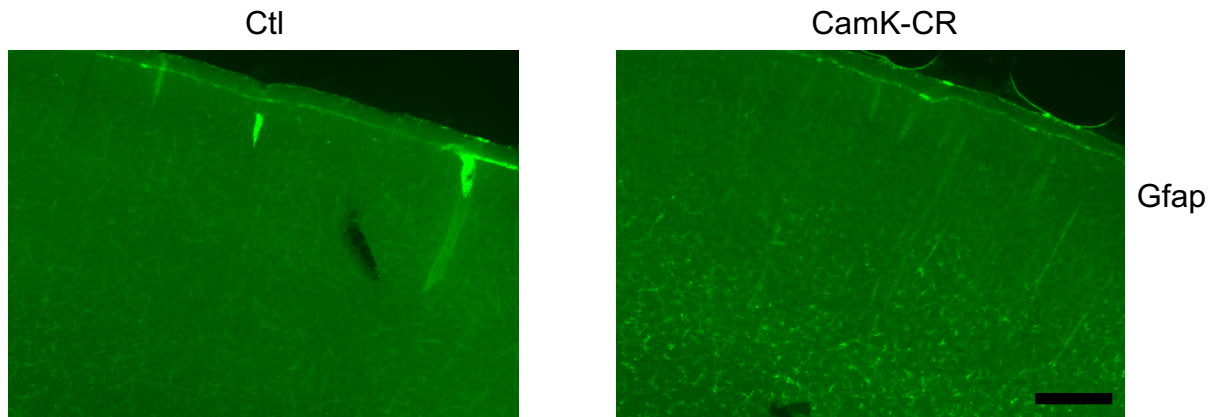
Gfap

Fig 3.5 Astrogliosis in the somatosensory cortex of CamK-CR assessed by GFAP staining (P16). Astrogliosis in CamK-CR mouse cortex was visualized with antibody against astrocyte marker Gfap (green). Gfap immunoreactivity was increased in the lower cortical layer of somatosensory cortex. The brain slices were sectioning for 70 μm by the vibratome. The images are the representative of results obtained from 2 animals per genotype. Scale bar (black bar), 100 μm.

Parvalbumin positive interneurons (PV+) are a subgroup of GABAergic inhibitory interneurons. The loss of parvalbumin positive interneurons was a common phenotype in many mouse models with single or global selenoprotein deficiency (neuron-specific Gpx4, Secisbp2 knockout) (Seeher et al, 2014; Wirth et al., 2010). A loss of parvalbumin positive interneurons in the somatosensory cortex of CamK-CR mice was also observed (Fig 3.6). Counting by ImageJ, the mean amount of PV+ interneurons per mm^2 were 107 ± 9 and 75 ± 11 in wild types and CamK-CR, respectively. Taken together, the neurological phenotype of CamK-CR is comparable to CamK-KO, displaying a similar neurodegeneration.
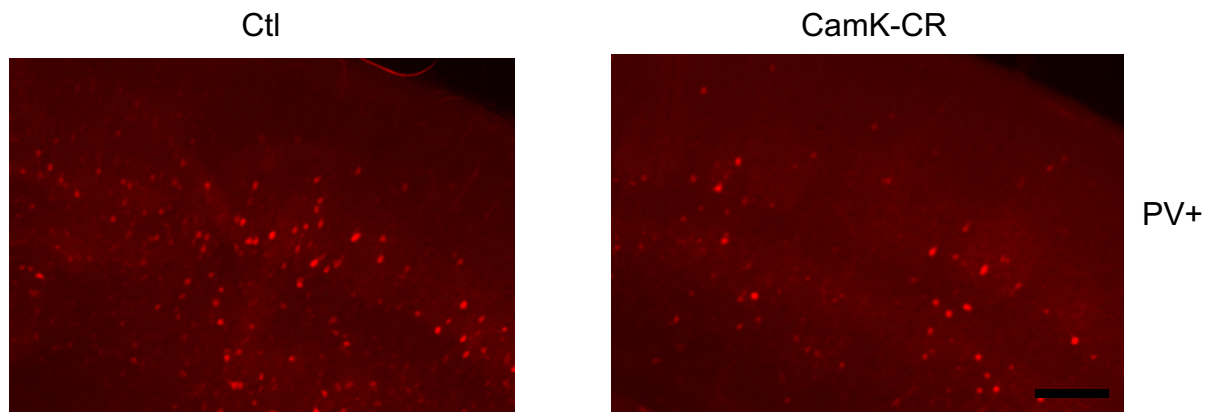
Fig 3.6 The loss of parvalbumin positive interneurons in CamK-CR somatosensory cortex (P16). Parvalbumin positive interneurons was visualized with antibody against parvalbumin (red). The brain slices were sectioning for 70 μm by the vibratome. The images are the representative of results obtained from 3 animals per genotype. Scale bar (black bar), 100 μm.

3.2.3 A global selenoprotein reduction in CamK-CR mouse cortex

Again, the evaluation of selenoprotein expression is essential to probe mutant Secisbp2 function. As shown in Fig 3.7 A, sensitive selenoprotein mRNAs (*Gpx1*, *Selenow*) were reduced, while *Gpx4* and *Selenot* mRNAs were unaltered between the genotypes. But both Gpx4 and Selenot protein level were remarkable reduced in CamK-CR (Fig 3.7 B). Except Txnrd1, overall selenoprotein protein levels were reduced in CamK-CR somatosensory cortex. Because in-frame UGA/Sec codon in *Txnrd1* mRNA locates at the penultimate codon closed to C-terminus. Selenos also did not show a remarkable reduction since its selenocysteine also locates closed to C-terminus. But unlike undetectable selenoprotein expression in mutant Secisbp2 liver samples, selenoproteins remained partial expression in CamK-CR mouse cortex.

A
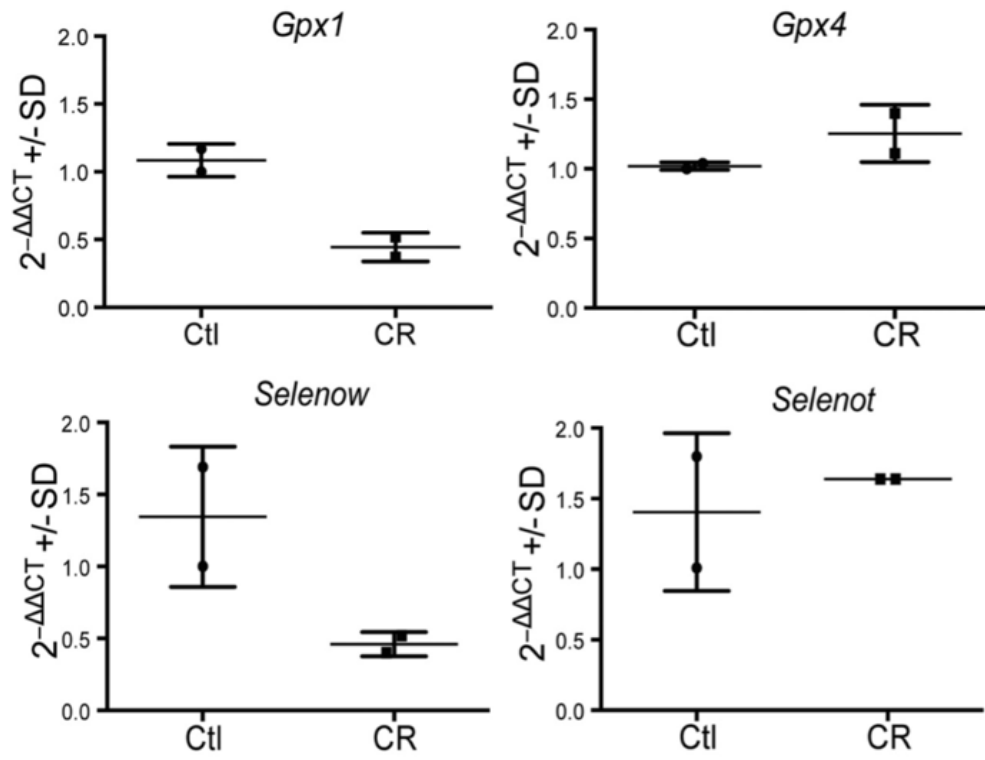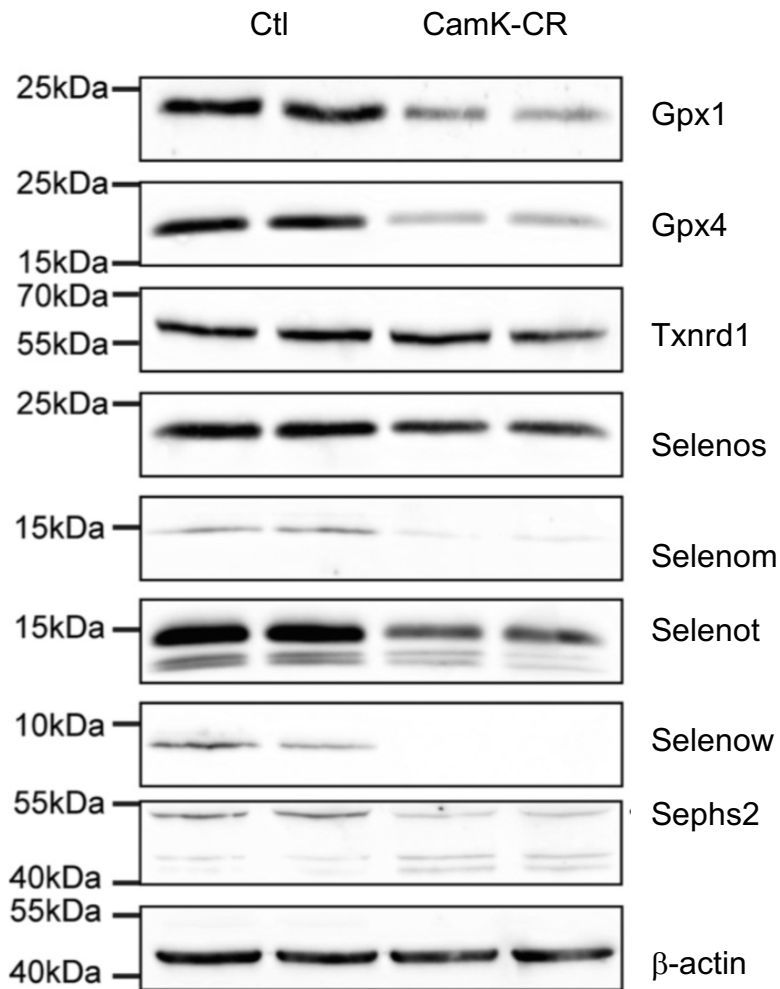
Fig 3.7 General reduced Selenoprotein expression in CamK-CR mouse cortex. A, RT-PCR analysis were applied for selected selenoprotein mRNA. Calculated $\Delta\Delta$CT values are normalized to 18S rRNA as housekeeping gene. Means are given $\pm$ S.D. n=2 (per genotype). B, Selenoprotein protein level in wild type (Ctl) and CamK-CR mouse cortex assessed by western blot. Two individual cortex extracts were analyzed for each group. Housekeeping protein β-actin indicates equal loading.

3.2.4 Unlike CamK-CR, no behavioral abnormalities in CamK-RQ mice

CamK-RQ mice behaved indistinguishable from wild types. Unlike CamK-CR and CamK-KO, the body weight and length of CamK-RQ mice were comparable to wild types. Additionally, CamK-RQ did not show any obvious neurological phenotype. Based on previous experiment on CamK-CR, parvalbumin immunohistology was also applied for the somatosensory cortex of CamK-RQ. As in Fig 3.8 shown, expectedly, no remarkable reduction of parvalbumin positive interneurons was observed in the somatosensory cortex of wild types and CamK-RQ (P35). Counting by ImageJ, the mean amounts of PV+ interneurons per mm^2 were 197 ± 18 and 215 ± 9 in wildtype and CamK-RQ, respectively.
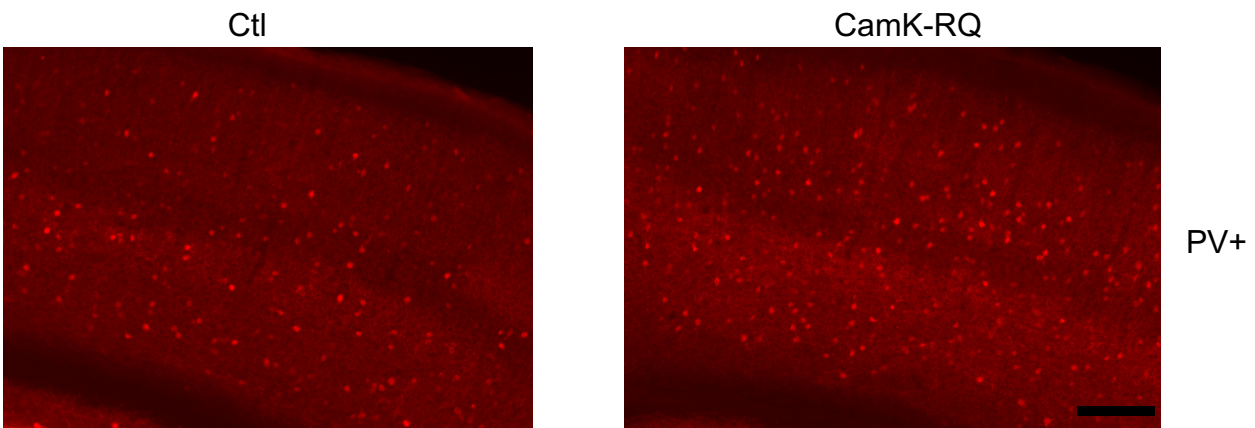
Fig 3.8 Unaltered parvalbumin positive interneuron density in the somatosensory cortex of CamK-RQ mice (P35). Immunohistology for Parvalbumin positive interneurons (red). The brain slices were sectioning for 70 µm by the vibratome. The images are the representative of results obtained from 4 animals per genotype. Scale bar (black bar), 100 µM.

3.2.5 Reduced but retained mutant Secisbp2 in CamK-RQ mouse cortex

As in Fig 3.9 shown, Secisbp2 expression were reduced in the cortex of CamK-RQ and CamK-CR mice, but not above the retaining level in CamK-KO samples. Moreover, unlike undetectable mutant Secisbp2 expression in the liver samples, mutant Secisbp2 was retaining in the cortex samples.
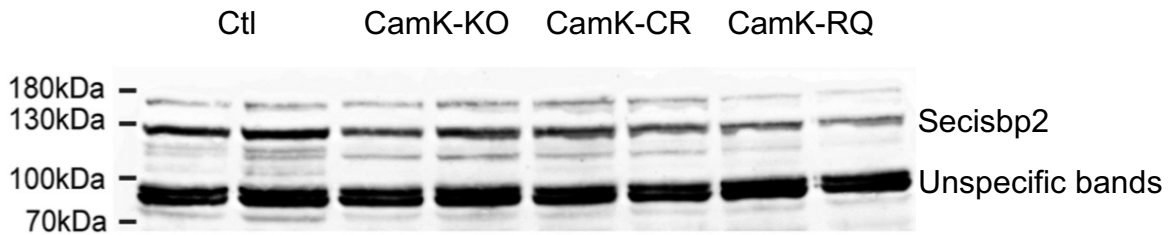
Fig 3.9 Secisbp2 expression in neuron-specific Secisbp2 mutant mice. Wildtype mice were compared with CamK-KO, CamK-CR, CamK-RQ. Western blot analysis for Secisbp2 protein expression. The non-specific bands indicate equal loading.

3.2.6 Generally reduced selenoprotein in CamK-RQ mouse cortex

Similar to the pattern of selenoprotein expression in CamK-CR, *Gpx4* mRNA was unaltered in CamK-RQ, while *Selenow* mRNA was reduced in CamK-RQ (Fig 3.10 A). With the exception of Txnrd1, all selected selenoprotein protein levels were reduced in CamK-RQ mouse cortex (Fig 3.10 B). However, the extent of the reduction of selenoprotein protein level in CamK-RQ is slightly lower than in CamK-CR, with the exception of Selenos. Moreover, a distinct pattern of individual selenoprotein mRNA and protein expression was observed. The above results of selenoprotein mRNA and protein expression were also verified by RNA-seq and Ribosome Profiling (Fig 3.10 C). The deep sequencing and evaluation of selenoprotein transcripts and ribosome protected fragments (RPF) can reflect selenoprotein mRNA abundance and selenoprotein translational state, respectively. Consistent with previous qPCR and western blot results, RNA-seq and ribosome profiling results also presented a general selenoprotein reduction in CamK-RQ mouse cortex (Fig 3.10 C). According to the distinct responses to mutant Secisbp2 RQ, selenoproteins can be categorized into three groups. 1: Selenoproteins (Gpx1, Selenow, Selenoh, Selenof, Selenom) were down-regulated in both mRNA and protein level in CamK-RQ mouse cortex. 2: Selenoprotein (Gpx4, Selenos, Sephs2) protein levels were reduced, while their mRNA levels were unaltered. 3: Selenoproteins (Txnrd family, Selenoo, Selenok, Selenoi) were unaltered on both mRNA and protein levels (Fig 3.10 C). Noticeably, Dio2 mRNA and protein level were unexpectedly upregulated in CamK-RQ

cortex. Therefore, a deeper insight on UGA recoding of individual selenoprotein was required.

A

Gpx4

y-axis: $2^{-\Delta\Delta CT}$ +/- SD (0.0, 1.0, 2.0, 3.0)
x-axis: Ctl, RQ

Selenow

y-axis: $2^{-\Delta\Delta CT}$ +/- SD (0.0, 0.5, 1.0, 1.5, 2.0)
x-axis: Ctl, RQ

B
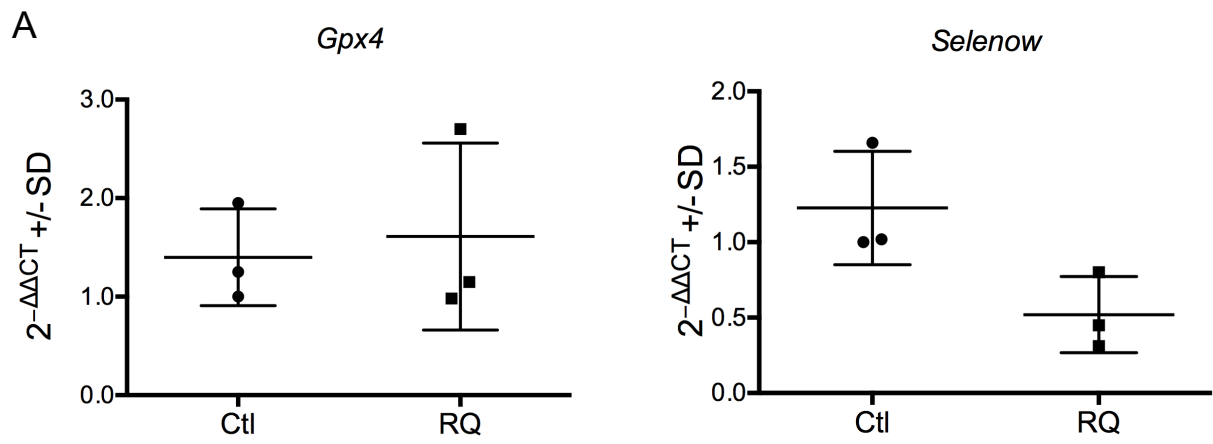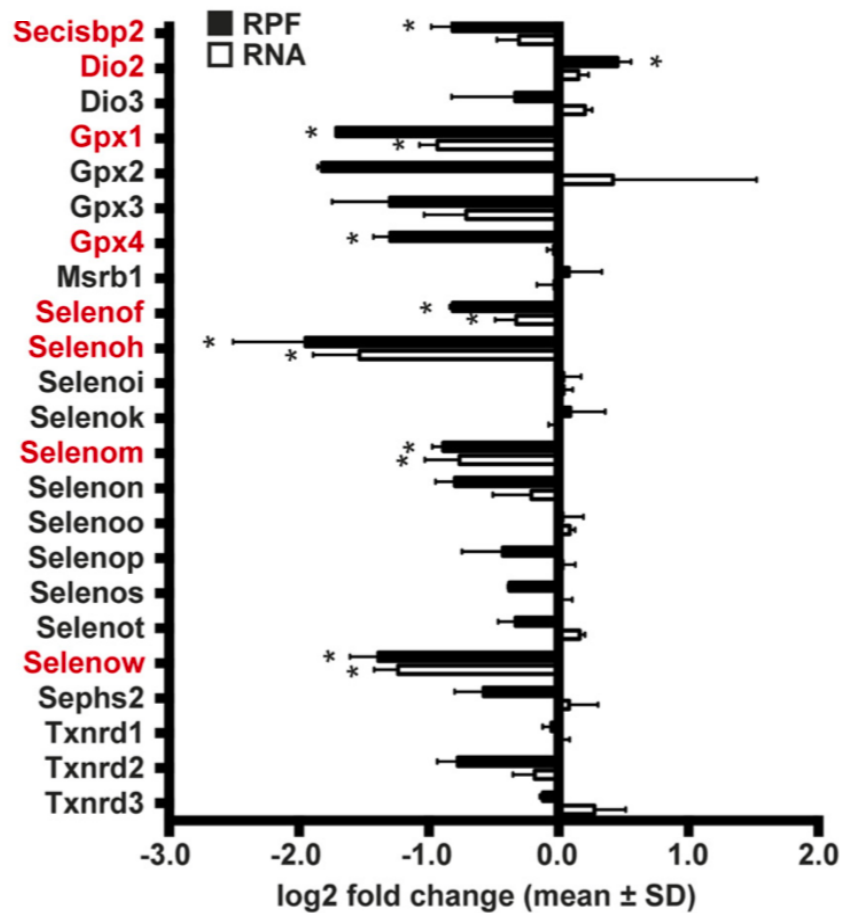
Fig 3.10 Global reduction of selenoprotein in CamK-RQ mouse cortex. A, RT-PCR analysis were applied for selected selenoprotein mRNA. Calculated ΔΔCT values are normalized to 18S rRNA as housekeeping gene. Means are given ± S.D. n=3 (per genotype). B, Selenoprotein protein level in neuron-specific Secisbp2 RQ and wild type mouse cortex. Two individual cortex extracts are analyzed for each group. Housekeeping protein β-actin indicates equal loading. C, Relative abundance of selenoprotein-related reads in Ribo-Seq (RPF) and RNA-Seq (mRNA) CamK-RQ mice were compared with wild types. n = 2, *, q < 0.05, BH correction. Significant changes are highlighted in red.

3.2.7 Mild immune response in CamK-RQ mouse cortex

Apart from reduced selenoproteins, a bunch of immune response related genes were up-regulated both on the transcriptional level (RNA-seq) and translational level (Ribosome Profiling). As in Fig 3.11 shown, red dots represented immune-related genes. Almost all the up-regulated immune-related genes were involved in the innate immune system. The pathway analysis also showed that the majority of regulated genes were involved inflammatory response and innate immune response (Fig 3.12 A). In details, upregulation of some immune cell (microglia, macrophage, neutrophil) markers (Cx3cr1, Mpeg1, Cd48, Cd180, Ly6e, Ly86, Lag3, Trem2) was observed. Accordingly, chemokines (Ccl3 and Ccl4), released by immune cells, was also up-regulated. Apart from activated immune cell markers, several up-regulated genes (C1qa, C4b, Itgax, Itgam) were involved in complement pathway, which plays an essential role in the innate immune system (Mayilyan et al., 2008). Interestingly, proteins associated with lysosomes (Lamp2, Lyz1, Lyz2, Laptm5, Hexb, Ctss, Ctsd, and Ctsz) were also observed in the up-regulated dataset. To be noticed, Gfap (astrocyte marker) mRNA level was increased in CamK-RQ mouse cortex, while Pvalb protein level was decreased.
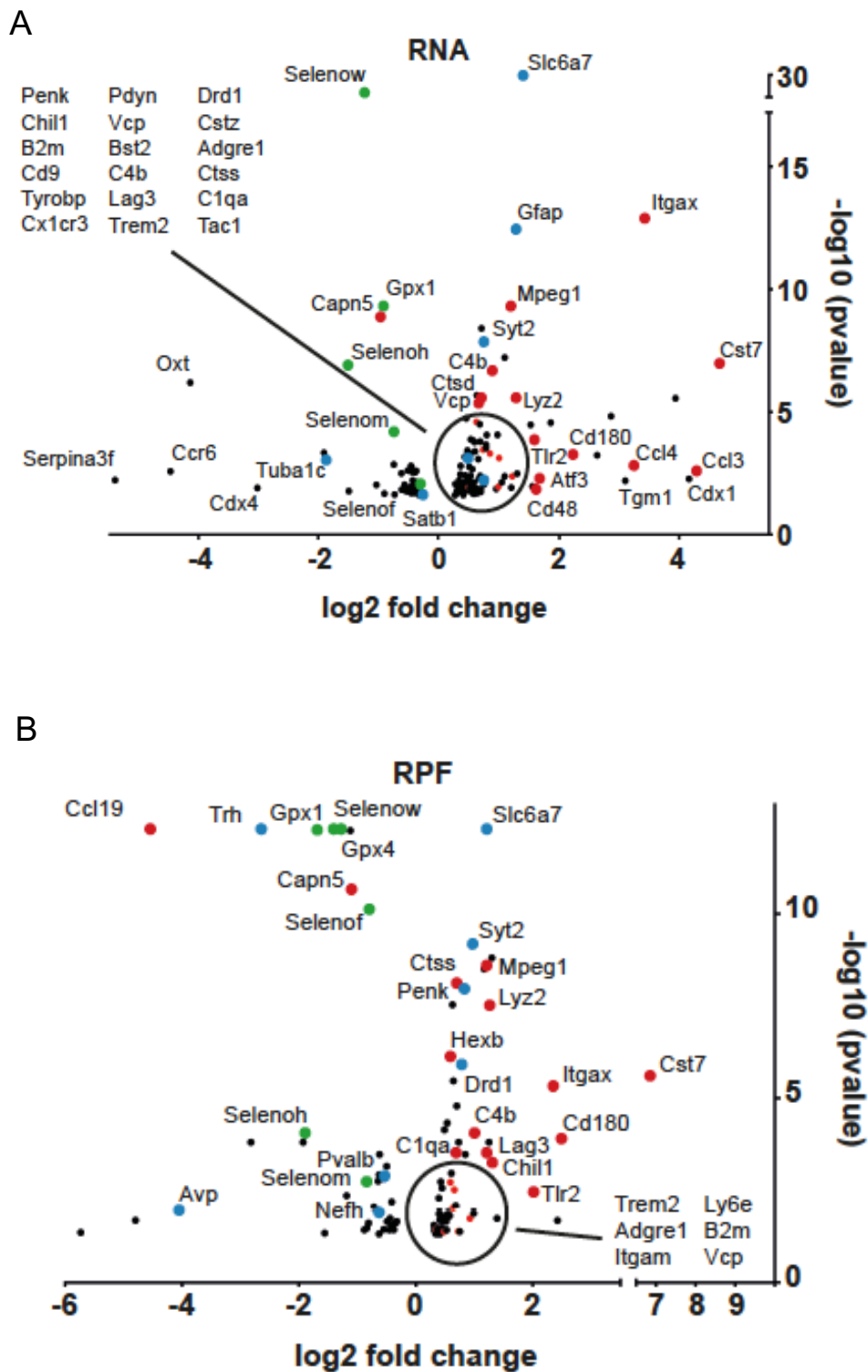
Fig 3.11 Transcriptional (mRNA) and translational (RPF) analysis by RNA-seq (A) and ribosome profiling (B). Selenoproteins are labeled in green and immune-related genes in red. Only significant regulated genes are shown. n = 2. *, q < 0.05, BH correction.

Since the expression of macrophage markers were upregulated in CamK-RQ mouse cortex, an immune infiltration (increased number of macrophages) and an activation of resident macrophage (microglia) has to be distinguished. Therefore, Iba-1 staining was performed on CamK-RQ and wild type mouse cortex (Fig 3.12 C). The mean amount of labelled cell density was 375 and 378 cells/mm^2 for control and CamK-RQ mice, respectively. No difference of cell density was observed, which indicated that microglia activation accounts for the up-regulation of macrophage markers. As mentioned before, pvalb protein level was slightly reduced in CamK-RQ, but previous parvalbumin staining did not show any difference between CamK-RQ and wild type. Additionally, *Gfap* mRNA was upregulated in CamK-RQ mouse cortex. Hence, Gfap immunohistology was performed for assessing the occurrence of astrogliosis. A widespread astrogliosis was observed in the lower cortical layers of CamK-RQ mouse cortex (Fig 3.12 B). Above all, a mild immune response associated with the dysregulation of selenoproteins was ongoing in the somatosensory cortex of CamK-RQ mice.

A

B

| Ctl | CamK-RQ |

Gfap

C

Iba-1
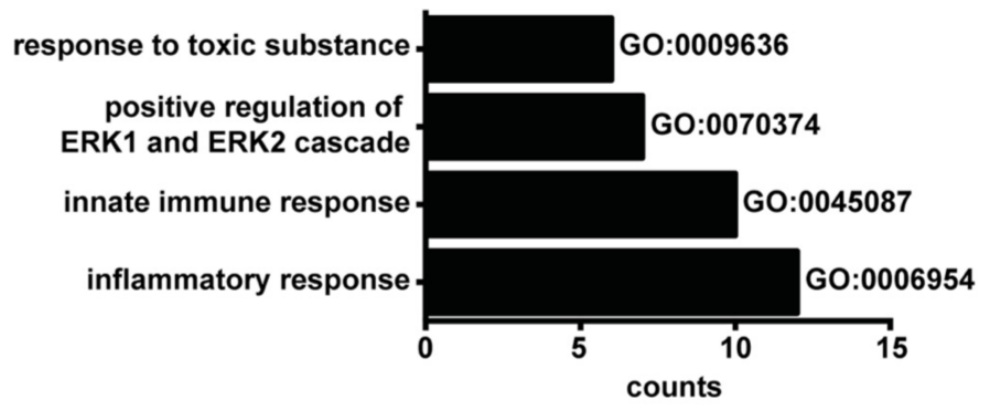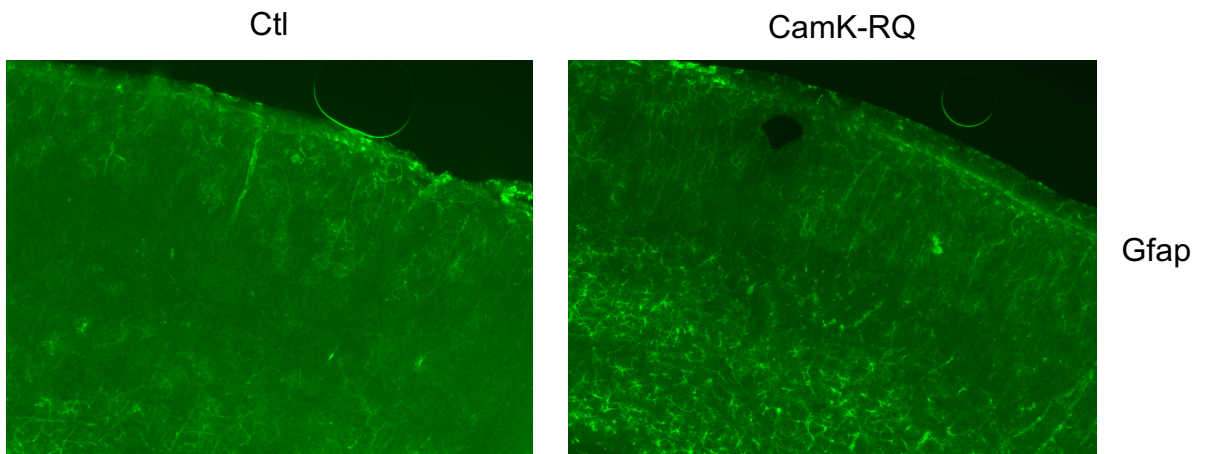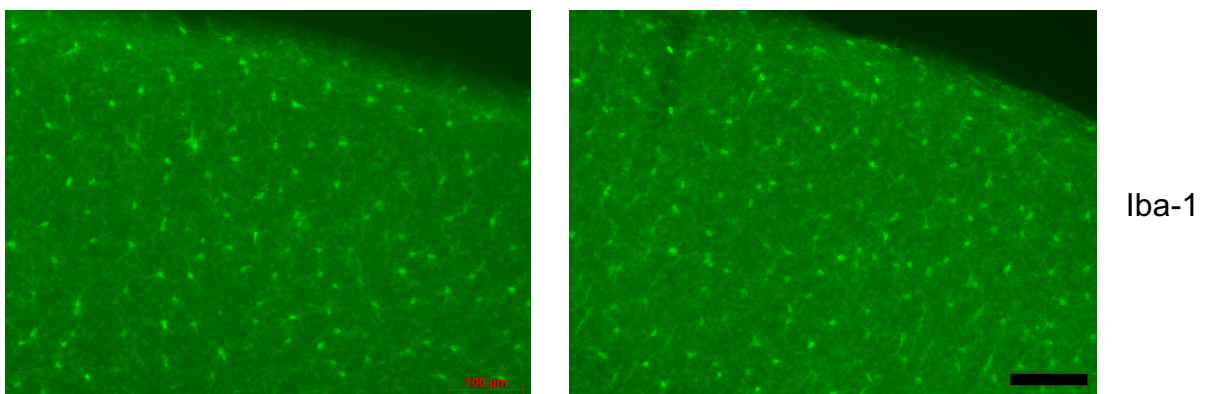
Fig 3.12 A mild immune response in CamK-RQ mouse cortex. A, Pathway analysis shows that immune-related pathways were induced on the transcriptional level. B, Astrogliosis assessed by GFAP staining in the somatosensory cortex. Gfap immunoreactivity was increased in the lower cortical layer of somatosensory cortex. The brain slices were sectioning for 70 µm by the vibratome. The images are the representative of results obtained from 2 animals per genotype. C, Iba1 staining in the somatosensory cortex. Mean cell density was 375 and 378 cells/mm^2 for control and CamK-RQ mice, respectively. Scale bar (black bar), 100 µm.

3.3 Analysis of selenoprotein translation in CamK-RQ mouse cortex by ribosome profiling

UGA recoding is the central event of selenoprotein biosynthesis. Secisbp2 is the central component of UGA recoding (Copeland et al., 2000). Therefore, evaluating UGA recoding efficiency of selenoproteins can reflect the functionality of Secisbp2. This can be achieved by deep sequencing of ribosome protected fragments (RPF) by performing ribosome profiling. 3' UGA/Sec RPFs on selenoprotein mRNAs can represent the occurrence of UGA recoding. Based on selenoprotein western blot results in CamK-RQ, a lower occurrence of UGA recoding event was expected.

3.3.1 RPF coverages on individual selenoprotein mRNA

By plotting the distribution of RPFs on individual selenoprotein mRNA, the translational state of selenoprotein can be visually presented. In a typical RPF coverage plot, the horizonal axis represents the open reading frame of selenoprotein mRNA, and the vertical axis represents the number of RPFs per million mapped reads (RPM). The red lines indicated the location of in-frame UGA/Sec codon. As shown in Fig 3.13, the RPF coverage plot of Gpx1 showed overall reduction of RPF reads along the open reading frame, which was consistent with previous qPCR and western blot results. The RPF coverage plot of Selenow showed a similar pattern to Gpx1, which was consistent with previous results. However, this overall RPF reduction on *Gpx1* and *Selenow* mRNA cannot reflect UGA coding efficiency accurately by only assessing 3' UGA/Sec RPFs. In contrast, the RPF coverage of 5' of the Gpx4 UGA codon was unaltered, but the RPF coverage of 3' of the Gpx4 UGA codon was impressively reduced. Therefore, a lower UGA recoding efficiency of Gpx4 was accordingly interpreted. A similar pattern as Gpx4 was also observed in Selenof. The RPF coverage plot of Selenom showed an overall reduction along the entire open reading frame, but the effect of Secisbp2 RQ on Selenom expression is not as remarkable as on Gpx1 expression.
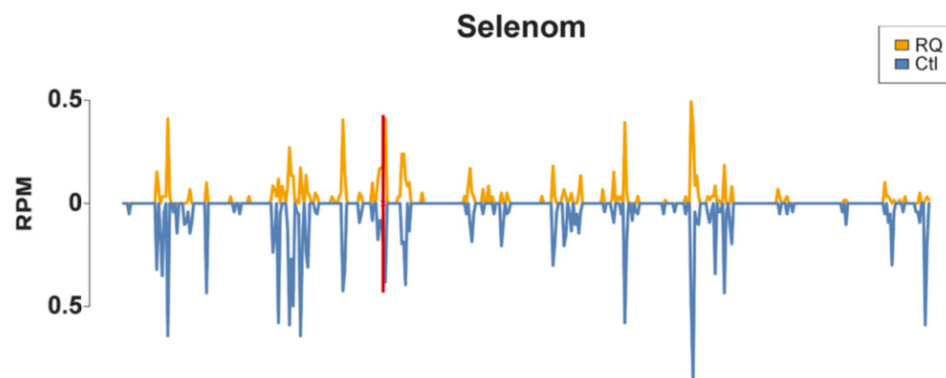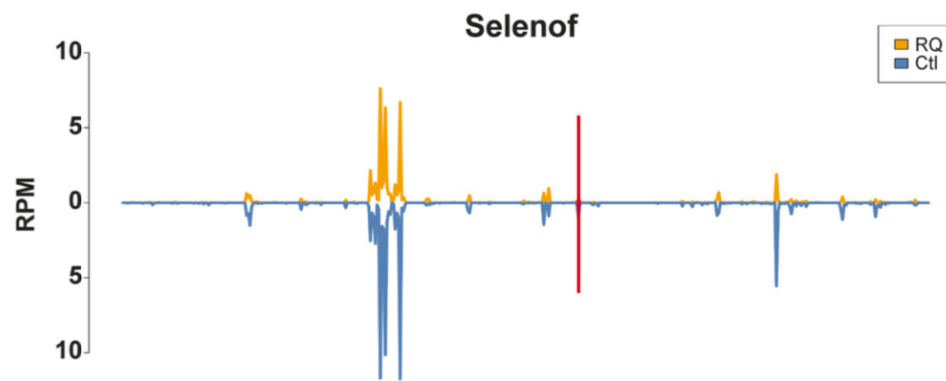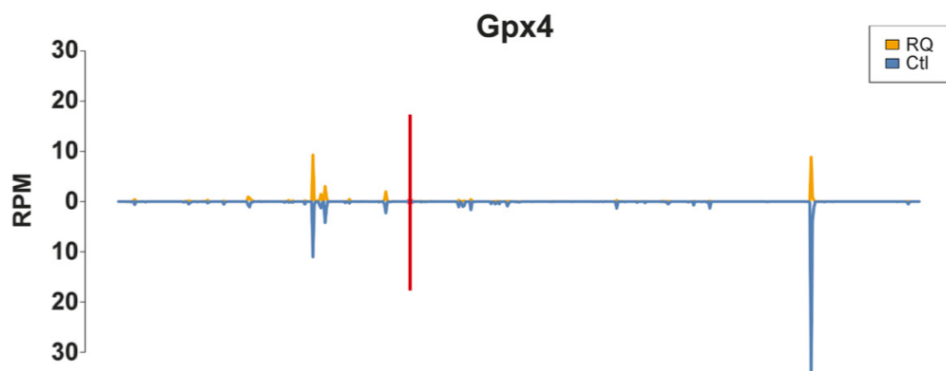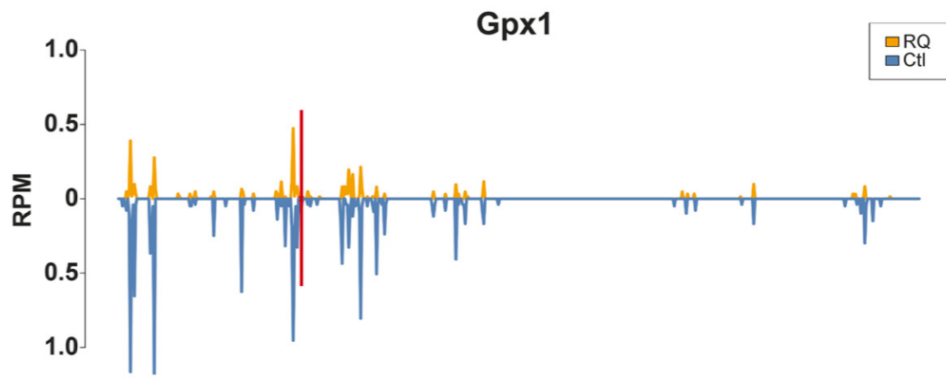
Fig 3.13 RPF coverage of selected selenoprotein mRNAs. The horizonal axis represents the open reading frame of selenoprotein mRNA, and the vertical axis represents the number of RPFs per million mapped reads (RPM). The position of the Sec/UGA codon is indicated by a red bar. Reads are plotted in blue for controls (Ctl) and in orange for CamK-RQ.

3.3.2 Lower UGA recoding efficiency of selenoproteins in CamK-RQ mouse cortex

Previous study from our group designed URE (UGA recoding efficiency) as a parameter for evaluating UGA recoding (Fradejas-Villar et al., 2017). URE is calculated as ribosomal density 3' of the Sec/UGA codon divided by ribosomal density 5' of the Sec/UGA codon. As shown in Fig 3.13 A, except for Gpx1 and Selenot, URE of the selected selenoproteins were reduced. Particularly, the URE of Gpx4 was strikingly decreased. However, URE does not account for the absolute number of RPFs on a single mRNA, if mRNA abundance has been changed significantly. For example, *Gpx1* mRNA was massively reduced. Consequently, its RPF reads were also accordingly reduced in CamK-RQ. Therefore, according to URE algorithm, URE of Gpx1 was unaltered in CamK-RQ compared to wild type. In contrast, *Gpx4* mRNA level was unchanged in CamK-RQ, while RPF reads were grossly reduced. Therefore, URE of Gpx4 were utmost decreased among the selected selenoprotein. Apparently, mRNA abundance should be considered as a normalization factor for evaluating UGA recoding. Hence, a new, accurate algorithm (3'RPM/mRNA) was introduced. The number of RPFs 3' of the Sec/UGA per million mapped reads (3'RPM) was calculated and further divided by mRNA abundance. By using 3'RPM/mRNA as a

new parameter of UGA recoding, a noticeable overall reduction of 3'RPM/mRNA of selected selenoproteins were observed in CamK-RQ, which means Secisbp2 RQ results in a lower UGA recoding efficiency of selenoprotein.
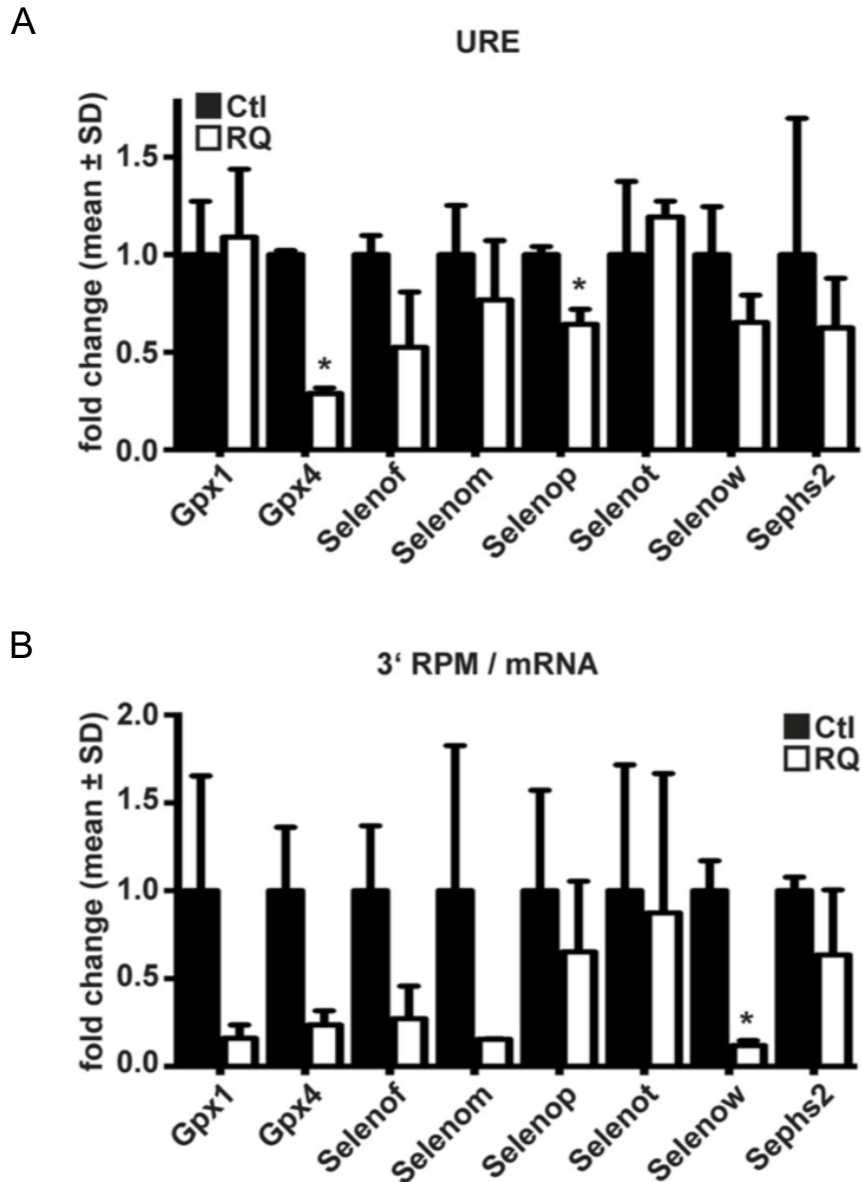
Fig 3.14 Lower UGA recoding efficiency in CamK-RQ assessed by ribosome profiling. A. URE calculated for selenoproteins. URE is calculated as (3'RPFmutant / 5'RPFmutant) / (3'RPFcontrol / 5'RPFcontrol). B.3'RPM (reads 3' of UGA/Sec per million mapped reads) calculated for selenoproteins and then normalized to mRNA abundance. *, p <0.05, Student's t test. Error bars, S.D.

3.4 The application of Translating Ribosome Affinity Purification (TRAP) on CamK-Cre Trit1 knockout mouse model

3.4.1 Validation of CamK-Cre L10-GFP mouse model

Initially, TRAP (L10-GFP) mice were interbred with CamK-Cre transgenic mice. In order to validate the activation of Cre-loxp recombination, GFP immunohistology was performed for CamK-Cre TRAP mice. As Fig 3.14 showed, GFP fluorescence was observed in several cerebral regions, like cortex, striatum and hippocampus, which was compatible with CamK (Ca^{2+}/CaM-activated protein kinase II) expression pattern (Wang et al., 2013). Taken together, our TRAP mouse model has been successfully generated. After the validation of Cre-loxp recombination, TRAP mice were interbred with CamK-Cre Trit1 KO mice. Consistent with the phenotype of CamK-Cre Trit1 KO mice, CamK-Cre Trit1 KO TRAP mice also presented smaller stature and microcephaly, indicating that TRAP mice cannot generate the negative effect on the original mouse model.

A

B

Cortex

Dentate gyrus

Stratium

Hippocampus (CA1)
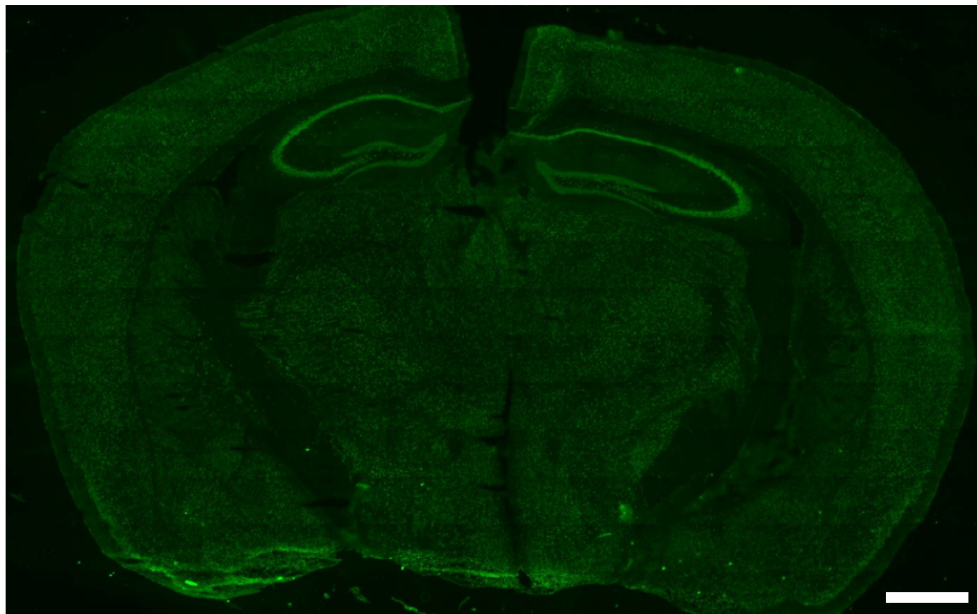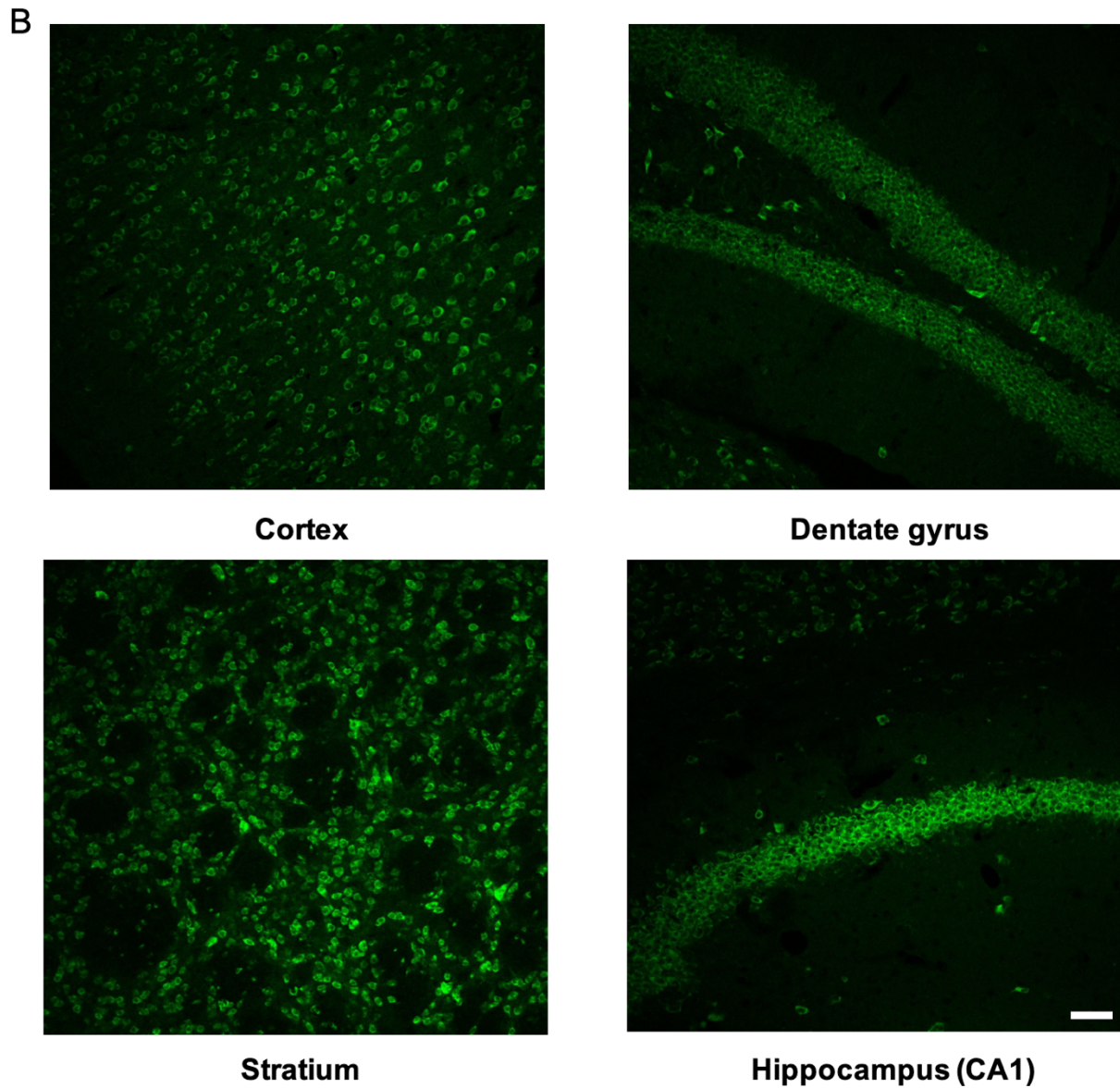
Fig 3.15 GFP fluorescence in CamK-Cre TRAP mouse brain slice. A. Overview of GFP expression (green) on the cerebral slice (coronal section) Scale bar (white bar), 2 mm. B. The confocal images display GFP expression in cortex, dentate gyrus, stratium, hippocampus (CA1). The brain slices were sectioning for 70 μm by the vibratome. Scale bar (white bar), 50 μm.

3.4.2 Amplified effect of the loss of Trit1 on the neurons in TRAP dataset

After the validation of TRAP mice, TRAP mice were interbred with CamK-Cre Trit1 KO mice, in order to test the feasibility of method. Consistent with the phenotype of CamK-Cre Trit1 KO mice, CamK-Cre Trit1 KO TRAP mice also presented smaller stature and microcephaly, which indicated that TRAP mice cannot generate the negative effect on exsiting mouse models. The 3'RNA-seq data of CamK-Cre Trit1 KO mouse cortex has been previously collected, and then differential analysis was performed by my colleague Dr. Simon Bohleber, which is further referred as non-TRAP dataset. Strikingly, several cytoskeleton-related genes (neurofilaments and tubulins) were down-regulated in CamK-Cre Trit1 KO, consistent with the phenotype of CamK-Trit1 KO mice – microcephaly. Moreover, the pathway analysis showed that integrated stress response (ISR) was induced by the loss of Trit1. Several genes involved in ISR were induced in CamK-Trit1 KO mouse cortex. The detailed dataset can be obtained from Dr. Simon Bohleber doctoral thesis.

In order to obtain neuron-specific information, TRAP was performed on CamK-Cre wildtype TRAP mouse cortex and CamK-Cre Trit1 KO TRAP mouse cortex. Subsequently, differential analysis of TRAP 3' RNA-seq dataset between two genotypes was performed by my colleague Dr. Simon Bohleber, which is further referred as TRAP dataset. A similar pattern of characterized gene clusters (cytoskeleton, ISR pathway) was observed in TRAP dataset and non-TRAP dataset. In the Table 3.2 and 3.3, a bunch of significant regulated genes existing in both non-TRAP and TRAP RNA-seq dataset were listed. Among the down-regulated genes in both datasets, cytoskeleton-related genes were most predominant. Importantly, the fold change of down-regulated neuronal cytoskeleton-related genes in TRAP dataset was generally higher than non-TRAP dataset. In the up-regulated gene list, ISR-related genes were most predominant. The fold change of up-regulated ISR-related genes in TRAP dataset was also generally higher than non-TRAP dataset. The effect of the loss of Trit1 on CamK-expressed neurons was amplified by performing TRAP. In another word, neuronal transcripts were enriched in TRAP samples.

Theoretically, only transcripts in CamK-expressed neurons were deep-sequencing in the TRAP dataset, while all neuronal and glial transcripts were deep-sequencing in the non-TRAP dataset. The differential analysis of non-TRAP dataset showed that astrocyte marker (Gfap) was significantly upregulated in CamK-Trit1 KO mouse cortex, which was also verified by Gfap immunohistology. However, this significant up-regulation of Gfap was not observed in TRAP dataset. This means that non-neuronal transcripts were largely excluded in the TRAP samples.

Table 3.2: List of downregulated cytoskeleton-related genes with their Log$_2$ fold change in both non-TRAP and TRAP RNA datasets. Differential analysis of 3' RNA sequencing datasets was performed. Only significant downregulated cytoskeleton-related genes were listed here. n = 2. q < 0.05, BH correction.

Gene	Non-TRAP (log$_2$ Fold Change)	TRAP (log$_2$ Fold Change)
Nefh	-0.9	-1.8
Nefl	-1.2	-1.5
Nefm	-1.3	-2.2
Tubb3	-1.0	-1.5
Tuba4a	-1.3	-1.4
Map1a	-0.5	-1.6
Myl4	-1.1	-1.8

Table 3.3: List of upregulated ISR-related genes with their Log$_2$ fold change in both non-TRAP and TRAP RNA datasets. Differential analysis of 3' RNA sequencing datasets was performed. Only significant upregulated ISR-related genes were listed here. n = 2. q < 0.05, BH correction.

Gene	Non-TRAP (log$_2$ Fold Change)	TRAP (log$_2$ Fold Change)
Slc7a11	1.2	2.6
Slc3a2	1.1	1.6
Slc1a4	1.1	1.7
Slc7a3	2.7	4.9
Sars	0.9	1.5
Yars	1.0	1.6
Lars	1.1	1.6
Aars	1.2	1.9
Nars	1.2	1.5
Cars	1.6	2.5
Atf5	2.4	3.7
Ddit3	1.9	3.5
Trib3	2.6	7.2
Shmt2	1.6	2.7
Mthfd2	2.1	4.0

4. Discussion

4.1 The choice of mouse models

Selenium is an essential trace element in many organisms. The studies on the physiological roles of Se revealed that selenocysteine (Sec), the 21st amino acid, is the major form of selenium in the cells. Sec is so unique among other amino acids that it is encoded by a canonical stop codon UGA and its biosynthesis occurs on its own tRNA (tRNA[Ser]Sec). Since the first discovery of Sec, 25 human selenoproteins, which contain Sec, were identified subsequently. Selenoproteins are indispensable for many essential biological processes, such as maintaining redox homeostasis, regulating thyroid hormone metabolism, involving in ferroptosis. (Labunskyy et al., 2014; Ingold et al., 2018). Given that the uniqueness and unconventionality of Sec and the importance of selenoproteins, Sec incorporation, the core event of selenoprotein biosynthesis, became an important issue to be elucidated in the selenium field. To date, this unique selenoprotein translation machinery has been uncovered progressively. In order to incorporate Sec at in-frame UGA codon, a unique RNA stem-loop structure in 3'UTR of selenoprotein mRNA (SECIS element) firstly interacts with SECIS-binding protein 2 (Secispb2). This interaction serves as a signal that dictates recoding of UGA as Sec, instead of a premature termination. Then tRNA[Ser]Sec is recruited by a unique elongation factor (eEFSec) and finally Sec is incorporated into the nascent polypeptide. Accumulating evidence indicated that Secisbp2 is the central component of selenoprotein translational machinery (Kinzy et al., 2005). One research group firstly demonstrated that Secisbp2 is the only limiting factor of selenoprotein translation in vitro (Copeland et al., 2000). Subsequently, total body Secisbp2 knockout mice were designed, but embryonic lethal (Seeher et al., 2014). Taken all together, the importance of Secisbp2 does not need further explanation.

Mutations in SECISBP2 are always related to human diseases (Schoenmakers and Chatterjee, 2020), since the disruption of SECISBP2 function lead to inappropriate Sec incorporation resulting the deficiency of selenoprotein expression. To date, 13 individuals carrying homozygous or compound heterozygous mutations in SECISBP2 have been identified, resulting in diverse clinical phenotypes. The identification of SECISBP2 patients

was based on two biochemical characteristics, lower circulating selenium (lower plasma GPX3 and SELENOP) and abnormal thyroid hormone function (lower activity of deiodinases) (Dumitrescu et al., 2005; Schoenmakers and Chatterjee, 2020). Among patient SECISBP2 mutations, most of them are non-sense mutations causing premature stop codon, which not surprisingly leads to produce non-fully functional, truncated SECISBP2 protein (Di Cosmo et al., 2009), while non-sense mutations located in C-terminal of SECISBP2 could completely abrogate SECISBP2 function. Before, *in vitro* protein truncation analysis has also revealed that the C-terminal domain of Secisbp2 (aa 399-846) accounts for the minimum fully functional protein (Fletcher et al., 2001). Subsequently, *in vitro* experiment uncovered that C-terminal domain of Secisbp2 is comprised of SID domain and RBD domain (Donovan et al., 2008). Based on *in vitro* studies of these two functional domains, SID domain is required for Sec incorporation but not directly binding with SECIS element, while RBD domain is indispensable for SECIS element binding (Allmang et al., 2002; Caban et al., 2007). In order to probe Secisbp2 functional domain (SID and RBD) *in vivo*, full-length Secisbp2 protein with disrupting two functional domains individually was required. Therefore, two human missense SECISBP2 mutations (R540Q, C691R) locating in the SID and RBD domain were our prior choices among all SECISBP2 mutations. Moreover, the patients carrying SECISBP2 homozygous R540Q and compound heterozygous C691R mutation showed distinct severities of phenotypes (Schoenmakers et al., 2010; Dumitrescu et al., 2005). Patients carrying R540Q mutation presented a relatively milder phenotype, while patients carrying C691R mutation had more severe phenotype. Therefore, to investigate genotype/phenotype correlation on a molecular basis was also necessary. Taken all together, both homozygous mutant Secisbp2 mice were the desired mouse models. However, both homozygous mutant Secisbp2 mice were embryonic lethal. Given that, conditional Secisbp2 mutant mouse models were generated.

Selenium organification, metabolism and distribution are organized by the liver. In addition, selenoprotein level in the liver can be substantially reduced by the depletion of Trsp, Secisbp2 or a selenium deficiency diet, but without disturbing normal liver function (Fradejas-Villar et al., 2017; Seeher et al., 2014). This indicates that the liver is tolerant to the loss of selenoproteins. Therefore, the liver is an ideal organ to study selenoprotein

deficiency. Brain is another essential targeted organ in the selenium research field, while patients with impaired selenoprotein expression displayed diverse neurological phenotypes (Fradejas-Villar, 2018). Global selenoprotein deficiency (Trsp, Secisbp2, Sepsecs) or single selenoprotein deficiency transgenic mouse models also presented distinct severities of neurological pathology (Renko et al., 2008; Wirth et al., 2010; Seiler et al., 2008). Taken all together, neuron and hepatocyte specific Secisbp2 mutant mouse models were the ideal materials for our study.

4.2 The assessment of four mouse models

4.2.1 Phenotypic discrepancy between human and mouse

Both homozygous Secisbp2 R543Q and C696R mice were embryonic lethal, while patients with these two mutations can survive. The case of Secisbp2 C696R mice was anticipated, while Secisbp2 R543Q mice not. The C696R mutation, locates in the conserved cysteine-rich L7Ae RBD domain of Secisbp2, was expected to disrupt protein structure and further protein function. This conserved RBD domain shared the similar sequence with U4 snRNA-binding protein 15.5 kD/Snu13p (Allmang et al., 2002). Based on the well-studied structural data of 15.5 kD/Snu13p, several amino acids in SECISBP2 were predicted to be directly involved in the interaction between SECISBP2 and SECIS element. Although C696 is not one of those predicted amino acids, it locates adjacent to two groups of interacting amino acids. Therefore, replacing a non-polar amino acid cysteine to a polar, bulky amino acid arginine might reconfigure the structure of this interacting domain, further disrupt SECIS element binding. *In vitro* translation assay also demonstrated that mutant Secisbp2 C696R abrogates the complete Secisbp2 function (Fig.S1). Moreover, patient carrying compound heterozygous SECISBP2 C691R mutation still harbor one allele (fs65X + fs76X), which can still synthesize truncated, but functional C-terminal SECISBP2 protein from downstream ATG codon, although the allele with C691R mutation synthesize non-functional SECISBP2 protein. Therefore, the embryonic lethality of homozygous Secisbp2 C696R mice mirrored like full body Secisbp2 knockout mice is rational.

The phenotype of patients carrying homozygous SECISBP2 R540Q is modest (Dumitrescu et al., 2005). However, homozygous Secisbp2 R543Q mice were unexpectedly embryonic lethal. Mouse study is extremely useful and necessary for studying a single gene function and human diseases when the desired organs are not accessible in human. However, despite of the similarities, the discrepancy between two species still has to be highly evaluated. Recently, a study revealed that mouse and human showed different tolerance towards the loss of selenoproteins. Mouse is more tolerant to the loss of deiodinases (DIOs) than human, while human is more tolerant to the loss of GPX4 and TXNRD2 than mouse (Santesmasses et al., 2020). The clinical phenotype of patients carrying pathological SECISBP2 mutations was mainly ascribed to abnormal thyroid hormone metabolism caused by the deficiency of deiodinases (Dumitrescu et al., 2005). Thyroid hormone test showed that patients carrying SECISBP2 mutations had elevated rT3 and T4 level and lower active T3 level, which resulted in a growth retardation (Schoenmakers and Chatterjee, 2020). However, the phenotype of double Dio1 and Dio2 knockout mice appears to be no different from the wild types (Shchedrina et al., 2010). Surprisingly, active T3 level was unaltered in double knockout mice, although Dio1 and Dio2 account for the conversion from T4 to active T3. The mouse was tolerant for the complete loss of Dio1 and Dio2, while human was even intolerant for reduced DIO2 activity. Another example is the differential tolerance between human and mouse towards the loss of Gpx4. The patient with a homozygous nonsense mutation in GPX4 could survive 4 months after birth, while Gpx4 knockout embryos died in utero (Smith et al., 2014; Yant et al., 2003). Both evidences imply the differences in the physiological importance of selenoproteins between human and mouse. This might explain that impaired selenoprotein expression caused by single Secisbp2 R543Q mutation can lead to the distinct phenotypes in two species.

4.2.2 Both mutant Secisbp2 R543Q and C696R resemble Secisbp2 knockout in the liver

To our knowledge of the phenotypic difference between patients carrying distinct SECISBP2 mutations and distinct functions of SID and RBD domain, a phenotypic difference in two mutant Secisbp2 mouse livers was expected. However, both mutant Secisbp2 R543Q and C696R resemble Secisbp2 knockout in the liver. Except Txnrd1, all the selected selenoprotein in Alb-CR and Alb-RQ were virtually undetectable as in Alb-KO. Paradoxically, *in vitro* translation assay showed that Secisbp2 C696R cannot facilitate Sec incorporation like several negative controls, while Secisbp2 R543Q appears no difference from wildtype Secisbp2 irrespective of the type of SECIS element (Fig.S1). Apparently, based on *in vitro* translation assay, selenoprotein expression in Alb-RQ was expected above in Alb-CR. Therefore, two questions were raised that why do both mutant Secisbp2 behave the same in the liver and what causes this paradoxical result *in vivo* and *in vitro*? Based on undetectable mutant Secisbp2 protein in the liver, the instability of mutant Secisbp2 protein *in vivo* was suspected. Further analysis of protein stability confirmed that Secisbp2 R543Q is thermally unstable with elevated temperature (Fig.S2). The distinct stability of mutant Secisbp2 *in vivo* and *in vitro* could explain the paradoxical results *in vivo* and *in vitro*. Secisbp2 C696R was not included in this experiment, since its Sec incorporation activity was as low as negative control which cannot be mediated by the temperature. However, Secisbp2 C696R might be also thermal unstable, based on its undetectable expression in the liver resembling Secisbp2 R543Q. Therefore, no phenotypic difference was observed between two mutant Secisbp2. And both Alb-CR and Alb-RQ behaved like Alb-KO.

Apart from mutant Secisbp2 instability in the liver, selenoproteins also had distinct responses to the loss of functional Secisbp2 in the liver. *Gpx1, Selenop, Selenow* and *Sephs2* mRNA were grossly reduced and almost undetectable, while *Gpx4* and *Selenot* mRNA were only 50% reduced. However, the protein levels of all the selected selenoproteins were reduced to a similar extent in Alb-CR and Alb-RQ due to the impaired selenoprotein translation machinery, except Txnrd1. These results point to a pre-translational regulation, which apparently only affecting selenoprotein mRNA levels. It seems like a selenoprotein hierarchy is existing when selenoprotein biosynthesis was

impaired. The concept of selenoprotein hierarchy was firstly initiated due to that selenoproteins have different responses to selenium deficiency (Hoffmann and Berry, 2005). While *Gpx1* and *Selenow* mRNA (referred to stress-related selenoproteins) were significantly decreased, mRNA expression of *Gpx4* and *Txnrd* family (referred to as housekeeping selenoproteins) is less regulated under Se-deficient dietary (Hill et al., 1992; Sunde and Raines, 2011). Since Secisbp2 is the limiting factor of selenoprotein biosynthesis, the loss of functional Secisbp2 might also establish a similar selenoprotein hierarchy. Moreover, previous study demonstrated that apart from the role in facilitating selenoprotein translation, Secisbp2 also plays a role in stabilizing selenoprotein mRNA by preventing non-sense mediated decay. The half-life of *Sephs2* mRNA was clearly reduced in Secisbp2-deficient hepatocytes (Fradejas-Villar et al., 2017), which is consistent with the gross reduction of *Sephs2* mRNA level in Alb-CR and Alb-RQ. Therefore, this pre-translational regulation (selenoprotein hierarchy) might be also mediated by mRNA surveillance pathways due to the loss of functional Secisbp2. However, other regulatory or compensatory mechanism of selenoprotein might be also contributed to selenoprotein hierarchy. For example, Selenot expression can be induced after injury in the liver which plays a cytoprotective role (Boukhzar et al., 2016). Therefore, it is not surprising that *Selenot* mRNA in mutant Secisbp2 mouse liver remained half level of wild types. In addition, Txnrd1 protein level was unaltered in all groups, because its in-frame UGA codon locates at the penultimate position close to the C terminus. One amino acid difference cannot be distinguished by western blot. Therefore, the failure of Sec incorporation in Txnrd1 was not able to be detected by assessing its protein expression. Overall, selenoprotein hierarchy is determined by multiple factors, which requires a more systematic research.

4.2.3 Secisbp2 C696R resembles Secisbp2 knockout in the brain, while Secisbp2 R543Q not

As mentioned above, Secisbp2 C696R is not functional irrespective of *in vivo* and *in vitro*. Therefore, it is not surprising that CamK-CR behaved mirroring like CamK-KO. CamK-CR presented all the clear-cut neurological phenotype of selenoprotein deficiency mouse models (i.e. the loss of parvalbumin positive interneurons) (Wirth et al., 2010; Seeher and

Schweizer, 2014; Pitts et al., 2014). Parvalbumin positive interneurons are a subpopulation of inhibitory GABAergic-interneurons, which supports critical developmental trajectories, sensory and cognitive processing, and social behavior (Steullet et al., 2017). Particularly, parvalbumin positive interneurons are vulnerable to oxidative stress (Behrens MM 2007). Therefore, the elevated oxidative stress can result in the loss of parvalbumin positive interneurons, which was caused by a single or global selenoprotein deficiency (Wirth et al., 2010; Seeher and Schweizer, 2014; Pitts et al., 2014). In details, 8-oxo-2'-deoxyguanosine (the marker of oxidative stress) was elevated in Selenop knockout mouse cortex, resulting the loss of parvalbumin positive interneurons. Nrf2-dependent genes (the regulators of an antioxidative responses) were induced in CamK-KO mouse cortex, also resulting the loss of parvalbumin positive interneurons. Although the oxidative stress has not been measured in CamK-CR yet, the loss of parvalbumin positive interneurons in CamK-CR mouse cortex can be also ascribe to the elevated oxidative stress resembling CamK-KO, causing by a global selenoprotein deficiency.

Interestingly, Alb-RQ mice behaved resembling Alb-CR and Alb-KO mice, while CamK-RQ mice did not present the obvious phenotype of CamK-CR and CamK-KO (Seeher et al, 2014). This indicates Secisbp2 R543Q retained partial Secisbp2 function above Secisbp2 C696R and KO in the brain, which rescued the severe phenotype of CamK-CR and CamK-KO mice. Unlike both undetectable mutant Secisbp2 expression in the liver samples, both mutant Secisbp2 remained partially in the brain samples assessing by western blot. Although the possibility of that the remaining mutant Secisbp2 was from other cell types in CNS cannot be excluded, it is still reasonable to deduce that the stability of Secisbp2 R543Q in the brain is completely different from unstable Secisbp2 R543Q in the liver. Therefore, the cellular environment might affect the stability of a mutant protein and thus its activity. This inspires to open up a new thought. The correlation between phenotype and genotype might not only depend on the location of single pathological mutation. The distinct stability of a mutant protein in different cellular environment can also result in a phenotypic difference. Therefore, it is also necessary to investigate the stability of mutant protein in different cell types for other missense point mutations in the future.

CamK-RQ mice presented only a mild inflammatory response in the brain. No loss of parvalbumin positive interneurons were observed, although Pvalb, a marker gene specific for parvalbumin positive interneuron (PV+ interneuron), was reduced in CamK-RQ ribosome profiling dataset. The reduction of Pvalb expression cannot lead to quantitative change of PV+ interneurons which indicated that the oxidative stress triggered in CamK-KO and CamK-CR was not induced in CamK-RQ. Additionally, the regulation of oxidative stress-related genes was also not observed in the RNA-seq data of CamK-RQ. Since oxidative stress was mainly caused by selenoprotein deficiency in CamK-KO and CamK-CR, global selenoprotein deficiency affected by Secisbp2 R543Q might be not as the same extent as in Secisbp2 C696R or Secisbp2 knockout.

4.3 The impact of Secisbp2 R543Q mutation on selenoprotein expression in the neurons

Unlike the unstable mutant Secisbp2 in the liver, both mutant Secisbp2 in the brain are detectable. In addition, Secisbp2 R543Q in the neurons remains partial function, while Secisbp2 C696R completely abrogates Secisbp2 function. Based on previous studies, selenoprotein function are mainly confined to the neurons in the CNS (Zhang et al., 2008). Taken all together, CamK-RQ is the desired model to study the impact of full-length Secisbp2 with single mutation on selenoprotein expression. Combined RNA-seq with ribosome profiling provides us a deeper insight on selenoprotein translation.

Highly consistent qPCR and RNA-seq results revealed a general selenoprotein mRNA reduction in CamK-RQ mouse cortex. Sec insertion (UGA recoding) is a relatively inefficient process compared to the insertion of other amino acids (Suppmann, 1999). It requires a unique translational machinery and has to compete with terminal signal. The interaction between Secisbp2 and SECIS element serves as a signal which could define in-frame UGA for Sec incorporation, instead of termination. Once the central component (Secisbp2) could not exert its function properly, this limited efficiency could be even lower. Then the terminal signal could overwhelm Sec insertion. Therefore, this in-frame UGA codon is identified as a pre-mature stop codon, which might lead to non-sense mediated decay (NMD). The current rule for NMD requires that the pre-mature stop codon is more than 50 nucleotides upstream of an exon–exon junction. For example, *Gpx1* and *Selenoh*

mRNA are subject to NMD rule, which could be the reason for the significant reduction of their mRNAs in CamK-RQ. But this is not a general role for all selenoproteins. *Gpx4* is also subject to canonical NMD rule, however, *Gpx4* mRNA level was unaltered. Moreover, *Selenow* is not subject to the NMD rule, but its mRNA level was still significantly reduced in CamK-RQ. This leads us to speculate that different extent of individual selenoprotein reduction caused by single mutant Secisbp2 is not simply only due to the NMD rules. Moreover, a consistence of selenoprotein reduction was observed in both liver and brain. Stress related selenoprotein mRNAs (*Gpx1, Selenow, Selenoh*) was grossly affected, while housekeeping selenoprotein mRNAs (*Txnrd family, Gpx4*) was relatively less affected. As mentioned before, selenoprotein hierarchy might be determined by multiple factors. However, at least this selenoprotein hierarchy is consistent between liver and brain.

In terms of selenoprotein protein level in CamK-RQ, most selenoproteins showed a remarkable reduction assessing by western blot and ribosome profiling. This indicated that selenoprotein translation was impaired by mutant Secisbp2 R543Q in the neurons. Noticeably, Txnrd1 is an exception, because its UGA/Sec codon locates at penultimate codon closed to C-terminal. Based on the robust method (Ribosome Profiling), ribosome coverage plot provided a deeper insight on selenoprotein translational state. In the case of Gpx4, 5' RPFs to in-frame UGA codon was unaltered (unchanged mRNA level), while only 3' RPFs to in-frame UGA codon was grossly reduced in CamK-RQ (less UGA recoding). This highly consistent result indicated that the UGA recoding of Gpx4 was largely impaired by Secisbp2 R543Q. While in the case of Gpx1, Selenom and Selenow, an overall reduced RPFs on selenoprotein mRNAs were observed in CamK-RQ due to less mRNA abundance. By interpreting the new parameter 3'RPM/RNA, Secisbp2 R543Q leads to a general lower UGA recoding efficiency of all selected selenoproteins. However, previous *in vitro* translation assay showed that Secisbp2 R543Q has no difference from non-mutant Secisbp2 in terms of the ability of Sec incorporation (Fig.S1). These paradoxical results lead to a hypothesis that the amount of recombinant Secisbp2 R543Q might be oversaturated in the assay. Subsequent titration experiment verified this hypothesis (Fig. S3). By adding less amount of recombinant Secisbp2 R543Q and titrated reporter mRNA into the assay, Secisbp2 R543Q results in less UGA recoding compared

to non-mutant Secisbp2, but still retains partial Secisbp2 function as *in vivo*. Although SID domain does not interact with SECIS element directly, it still plays a vital role in UGA recoding of selenoprotein irrespective of *in vivo* and *in vitro*. However, the effect of the loss of SID domain function on selenoprotein expression is not as same as the loss of RBD domain function. This indicates that SID domain is required for selenoprotein translation, but it is not indispensable.

4.4 Mild inflammatory response in CamK-RQ mouse cortex

The differential analysis of RNA-seq and ribosome profiling dataset are highly consistent. Apart from down-regulation of selenoproteins in CamK-RQ RNA-seq and ribosome profiling dataset, a group of up-regulated immune-related genes was observed in CamK-RQ mouse cortex dataset. Gfap is one of the most striking genes in this dataset, because the occurrence of astrogliosis is a typical phenotype in many neuron-specific single or global selenoprotein deficiency mouse models (Wirth et al., 2010; Seeher and Schweizer, 2014). Particularly, astrogliosis in these mouse models was often confined to occur in the lower cortical layers. This might be due to uneven CamK-Cre transgene expression and recombination patterns in the mouse cerebral cortex (Wang et al., 2013). The existence of astrogliosis commonly refers to a response to all forms of CNS injury and disease (Sofroniew, 2015). But astrogliosis does not occur independently, instead it coordinates with other glia cells in response to CNS insults, such as the resident immune cell in the CNS -- microglia. Therefore, it is not surprise that a bunch of microglia-related genes were also observed in up-regulated gene list. Although this can prove the activation of microglia on the molecular basis, the activation of microglia has to be further confirmed by determining its morphology via a higher resolution microscopy. Apart from reactive astrocytes and microglia, several macrophage and phagocytosis-related genes were also present in the up-regulated gene list. However, through Iba-1 staining (a marker for microglia and macrophage), no remarkable difference between wildtype and CamK-RQ was observe, indicating no considerable infiltrated macrophage penetrated into the brain through blood brain barrier under immune response. However, we could not exclude the possibility of that macrophage infiltration might be observed if the mice were killed later than 35 days. The interaction between microglia and astrocyte requires diverse molecular

signals, such as by releasing cytokines and chemokines (Sofroniew, 2015b). Hence, it is not hard to explain that several cytokines and chemokines were up-regulated in CamK-RQ mouse cortex. Additionally, complement genes were also increased in CamK-RQ, which are mostly involved in innate immune response. Pathway analysis also presented a bunch of differential genes enriched in innate immune response. Innate immune system provides a front line of host defense not only due to the engagement of pathogen or environmental insult, but also during brain injury and chronic disease (Rivest, 2009). Since the activation of innate immune system can be still observed in CamK-RQ, it is also a sign of "mild phenotype" of CamK-RQ mice.

By coincidence, a similarity between CamK-RQ and Niemann-Pick Type C (NPC) RNA-seq dataset has been discovered (Alam et al., 2012). Particularly, the genes involved innate immune system are highly overlapped. NPC disease is a lysosomal disorder with progressive neurodegeneration. Elevated lysozyme activity is one of diagnosis markers of NPC disease. Coincidently, a group of lysosomal genes (Lyz1, Lyz2, Lamp2, Laptm5) were upregulated in CamK-RQ RNA-seq dataset. This finding indicates mutant Secispb2 R543Q might also result in abnormal lysosomal function. But a severe neurodegeneration in NPC mouse model was not observed in CamK-RQ, and the induction of immune-related genes in NPC mouse model are much higher than in CamK-RQ mouse model. Since NPC mouse model presented "progressive" neurodegeneration, CamK-RQ mouse also has a possibility to develop neurodegeneration during the aging. The underlying correlation between lysosomal disorder NPC and CamK-RQ mouse model is fascinating to be uncovered in the future.

4.5 The validation of Translating ribosome affinity purification (TRAP) method

The cellular heterogeneity of central nerve system obstructs to elucidate the biological properties of distinct neuronal and non-neuronal types. Particularly, applying for differential analysis of gene expression in the brain is always not accurate and complete. The effect in a certain cell type in the CNS might not be observed or narrowed, while this effect can be diluted in the mixed and heterogeneous high-throughput dataset. Two possibilities of causing this situation are listed here. One is that the desired cell type is just

a small portion in the heterogeneous CNS. Any gene regulation in a small population of CNS might be so subtle that this regulation cannot be detected. Another possibility is that a compensatory regulation might be existing. Although different cell types in the CNS play distinct roles, the communication among these cell types is dynamic and helps maintain the CNS homeostasis. To overcome these difficulties, TRAP is an ideal method to be performed.

The GFP histology of our TRAP mice demonstrated that our interbreeding between CamK-Cre mouse and L10a-GFP mouse has been successfully settled down. This effective intercross and Cre-loxp recombination confirmed the feasibility of Zhou's Cre-driven TRAP method (Zhou et al., 2013). In order to establish and validate TRAP method in our lab, CamK-Cre Trit1 KO TRAP mouse line was generated. This new mouse line reproduced the neurological phenotype of CamK-Cre Trit1 KO mouse line, neither deterioration nor rescue. This indicates TRAP does not produce negative effect on original mouse line. Microcephaly is the characterized phenotype of CamK-Cre Trit1 KO mice. Based on immunohistology and RNA-seq data of CamK-Cre Trit1 KO mice, we inferred that microcephaly was caused by a bunch of down-regulated cytoskeleton-related genes instead of the loss of neurons. By the comparison of differential analysis between non-TRAP and TRAP dataset, all of differential cytoskeleton-related genes showed a greater reduction in the differential analysis of TRAP dataset than non-TRAP dataset. Apparently, the "dilution" effect of heterogeneous non-TRAP dataset was eliminated by the relatively "pure" TRAP dataset, since neuronal transcripts were enriched in TRAP samples. In a deeper sight, only the translating polysomes and monosomes in the neurons, which is the CamK-activated cell type in the cortex, were pulled down in TRAP sample.

Apart from reduced cytoskeleton-related genes in non-TRAP dataset, a bunch of up-regulated genes were involved in integrated stress response (ISR). Consistently, several ISR markers were also observed in the TRAP dataset. To be noticed, the induction of ISR in TRAP dataset was more remarkable than in non-TRAP dataset. This demonstrated that ISR was predominantly induced in the neurons rather than other cell types in the cortex. Again, the extent of ISR induction caused by the loss of Trit1 was diluted by heterogeneous non-TRAP dataset. Taken all together, neuron-specific transcripts were

obtained by performing TRAP method. However, the robustness of TRAP was not completely well presented, since CamK-driven neurons are a large cell population of the CNS. If a small subpopulation of neurons or other cell types in the CNS was the cell of interest, some subtle effects in these cell population can be remarkable amplified, which might be submerged in the heterogeneous non-TRAP datasets. Indeed, one of further goals is to investigate how the loss of Secisbp2 affect parvalbumin positive interneurons on the molecular basis.

As the shown selenoprotein mRNA and protein expression pattern, the discrepancy between the abundance of protein and mRNA molecules is frequently observed. TRAP dataset only reflects the abundance of translating transcripts, but not the translational state of transcripts. Therefore, a combination between TRAP and ribosome profiling (TRAP-RP) has been developed recently (Sapkota et al., 2019). The advantage of TRAP-RP is that the translational information of a certain cell type in a complex tissue is also accessible. Our preliminary trials also validated the feasibility of TRAP-RP (data not shown). Thus, a comprehensive and precise study of selenoprotein transcription and translation in the cell of interest in complex tissue will be conducted in the future.

Supplementary result
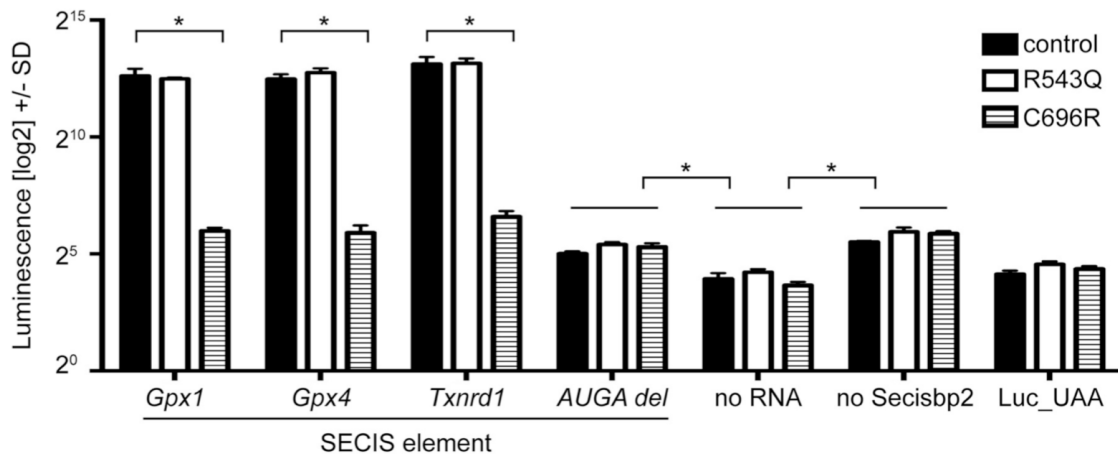
Fig.S1 Functional analysis (Sec incorporation) of recombinantly expressed mouse Secisbp2 R543Q and C696R assessed by *in vitro* translation assay. In vitro translation assay was adapted from Prof. Dr. Paul Copeland by my colleague Dr. Hendrik Schmidt (Mehta et al., 2004). Reporter constructs containing a Sec-dependent luciferase cDNA and SECIS elements cloned into the 3'UTR were in vitro translated, and the amount of luminescence produced by luciferase was measured by performing a luciferase assay. The reaction mix consists of 6.5 µl rabbit reticulocyte lysate (Promega), 13 nM of reporter mRNA, 0.02 mM amino acid mixture, 40 units of RiboLock (Thermo Fisher Scientific), and 160 nM recombinant C-terminal Secisbp2 in a total volume of 12.5 µl. After incubation at 30 °C for 1 h, 2 µl of the reaction mix were added to 50 µl of 1x PBS. Luminescence was measured after adding 50 µl of luciferase assay reagent (Promega) by using an Infinite M200 Pro plate reader (Tecan). The SECIS element of murine Gpx1, Gpx4 and Txnrd1 were cloned into the reporter constructs, respectively. The rat Gpx4 SECIS element lacking of the core kink-turn motif (AUGA) was cloned into reporter construct as a negative control. A substitution of UGA/Sec for UAA/Stop codon in reporter construct served as another negative control. Further negative controls were adding no reporter mRNA, no recombinant C-terminal Secisbp2 in the reaction mix. Secisbp2 R543Q and Secisbp2 C696R were compared to the positive control (non-mutant Secisbp2) and several negative controls. A log2 scale of luminescence is used to better illustrate the subtle experimental background (negative controls). Error bars, S.D. The assay was performed twice in triplicates. Overall, Secisbp2 R543Q is as functional as the positive control (non-mutant C-Secisbp2) irrespective of the types of SECIS element, while Secisbp2 C696R abrogates Secisbp2 function (Sec incorporation) completely as two negative controls (lacking of C-Secisbp2 in the reaction mix, deletion of the core of SECIS element) (Zhao et al., 2019).
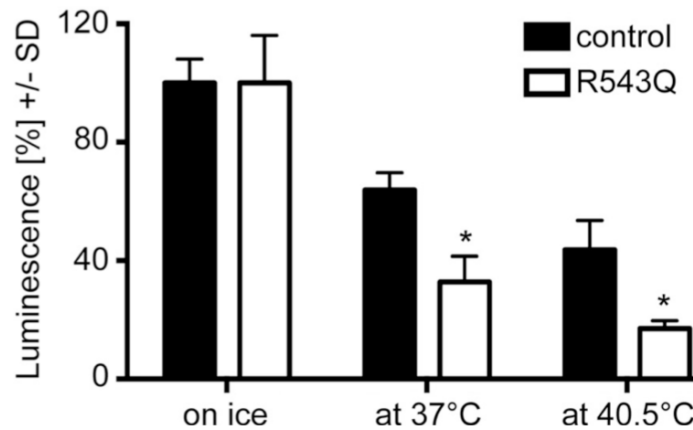
Fig.S2 Thermal instability of Secisbp2 R543Q *in vitro*. In order to test the thermal stability of Secisbp2, both control (non-mutant Secisbp2) and Secisbp2 R543Q was incubated for 30 minutes on ice or at 37 °C before in vitro translation assay (performed at 30 °C). (Error bar, S.D., $p < 0.05$, Student's t test). The assay was performed twice in triplicates. With the elevated temperature, Secisbp2 R543Q was more heat-labile than the control at the elevated temperatures. Secisbp2 C696R was not included, since the luminescence produced by Sec-dependent luciferase is not able to be mediated by the elevated temperature due to dysfunctionality of Secisbp2 C696R. (This assay was performed by Dr. Hendrik Schmidt.)

A
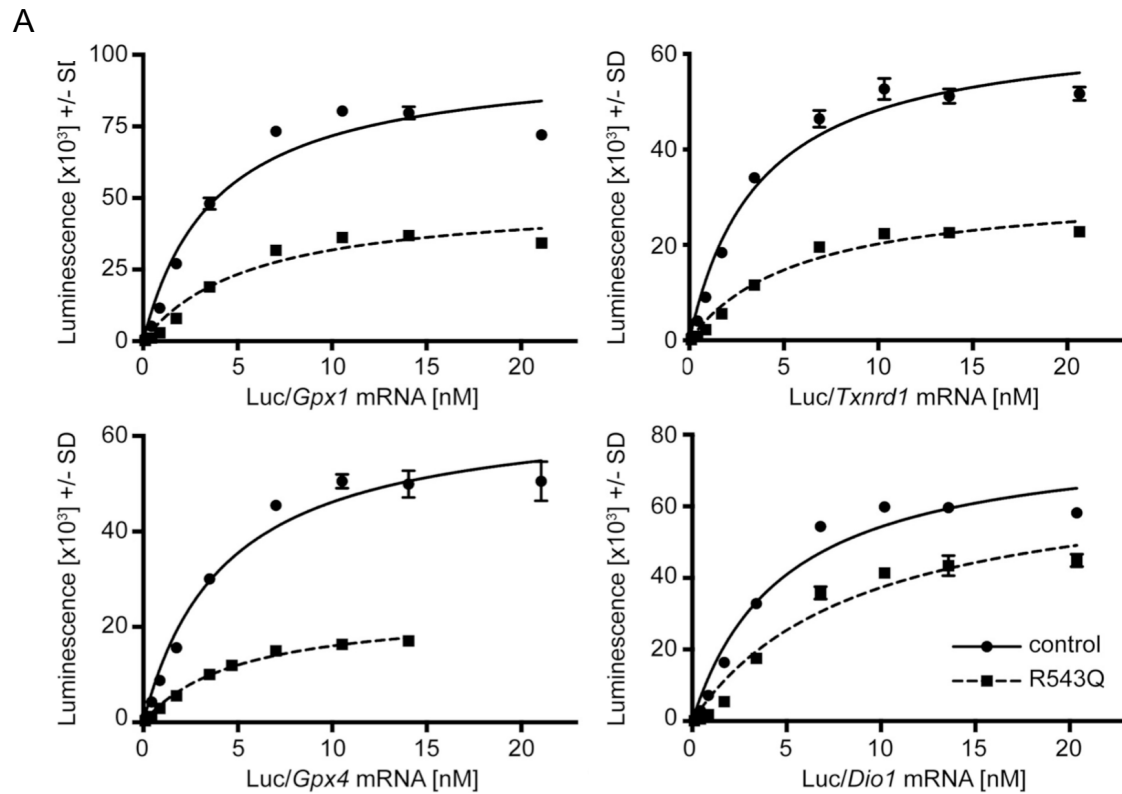
B

	EC$_{50}$ (control) [nM]	EC$_{50}$ (R543Q) [nM]	significance
Gpx1	3.8 +/- 0.6	5.8 +/- 1.1	NS
Gpx4	4.3 +/- 0.5	5.0 +/- 0.4	NS
Txnrd1	3.7 +/- 0.4	5.9 +/- 0.9	*
Dio1	4.8 +/- 0.8	8.9 +/- 2.0	*

Fig.S3 Secisbp2 R543Q affects Sec incorporation *in vitro*. In order to test the effect of Secisbp2 R543Q on Sec incorporation in vitro, titration experiments were performed twice in triplicates. (Error bar, S.D., $p < 0.05$, Student's t test) A. The luminescence produced by Secisbp2 R543Q group was consistently less than the control group irrespective of the types of SECIS element. The reporter mRNA was diluted into nine different concentrations in a range of 0.1-20 nM (shown in the figure) and 80 nM recombinant Secisbp2 was added into the reaction mix. B. The EC50 of Txnrd1 and Dio1 were significantly reduced in Secisbp2 R543Q, while the EC50 of Gpx4 was unaltered.The half maximal effective concentration (EC50) can be an indicator of the affinity of SECIS:Secisbp2 interaction. Although the EC of Gpx1 was reduced as expected, the reduction did not reach a statistic significance. Overall, Secisbp2 R543Q results in less UGA recoding and the affinity of SECIS; Secisbp2 in the case of Txnrd1 and Dio1. In the case of Gpx4, less UGA recoding was observed, although the affinity of SECIS:Secisbp2 was unaltered. This indicates Secisbp2 R543Q is less active than non-mutant Secisbp2.

5. Abstract

Recoding of in-frame UGA/Sec codon in selenoproteins requires a complex translational machinery. The core of this event is the interaction between selenocysteine insertion sequence (SECIS element) in the 3'UTR of eukaryotic selenoprotein mRNAs and SECIS-binding protein 2 (SECISBP2). SECISBP2 consists of three domains: N-terminal domain, Sec incorporation domain (SID) and RNA binding domain (RBD). N-terminal domain of Secisbp2 remains unclear, while the sum of SID and RBD domains (C-terminal domain) accounts for essential Secisbp2 function (facilitating selenoprotein translation). Patients carrying pathogenic SECISBP2 mutations displayed a spectrum of clinical phenotypes. The most common outcome is abnormal thyroid hormone level caused by the deficiency of deiodinase, a selenoprotein that regulates thyroid hormone. In order to investigate the correlation between genotype and phenotype on molecular basis, two pathogenic human SECSISBP2 missense mutations (R540Q and C691R) were selected and reproduced in mice (R543Q and C696R). Unexpectedly, both homozygous Secisbp2 mutant mice were embryonic lethal. Therefore, hepatocyte and neuron conditional Secisbp2 mutant mice were generated for further study. Regardless of in vivo or in vitro, the C696R substitution in the RBD domain abrogates SECIS binding function and does not support selenoprotein translation above the complete loss of Secisbp2. The R543Q missense substitution located in the SID domain leads to a residual activity in vitro and reduced selenoprotein expression in vivo. Further experiment showed that Secisbp2 R543Q is thermally unstable in vitro and undetectable in the liver, while being partial functional in the brain. Therefore, the interrogation of how this partial functional Secisbp2 R543Q in the brain impacts on selenoprotein expression is the priority. The R543Q mutation in the brain resulted in reduced selenoprotein translation evidenced by western blot and ribosome profiling. Combining with transcriptomic data, the expression of individual selenoproteins was affected by Secisbp2 R543Q in different ways. Selenoproteins like Gpx1 and Selenow were reduced both in transcriptional and translational level. Selenoprotein like Gpx4 was not changed in transcriptional level, but remarkable reduced in translational level due to the inefficient UGA/Sec recoding. The effect of Secisbp2 R543Q on selenoprotein expression is gene-specific. Apart from reduced selenoproteins, a mild immune response was observed in the neuron-specific Secisbp2 R543Q mouse cortex. Overall, differential

SECISBP2 protein stability in individual cell types may dictate clinical phenotypes to a much greater extent than molecular interactions involving a mutated amino acid in SECISBP2. Additionally, a single missense mutation can affect selenoprotein expression via different mechanisms which means that the hierarchy of selenoproteins is not simply a result of SECIS:SECISBP2 affinity.

The cellular diversity of heterogeneous tissue obstructs gene-function studies in a specific cell type, such as neurons in the mammalian central nervous system (CNS). A novel methodology, translating ribosome affinity purification (TRAP), is one way to address this limitation. In order to establish and validate this robust method, TRAP was performed on neuron-specific Trit1 knockout mouse model (CamK-Trit1 KO). The interbreeding between TRAP mice and CamK-Trit1 KO mice did not have side effects on original mouse model, while both presented similar phenotype. Differential analysis of TRAP dataset showed that the effect of the loss of Trit1 on neuronal transcripts was amplified compared to non-TRAP dataset, indicating the well-establishment and feasibility of TRAP method.

6. List of figures and tables

Figures

Tables

7. Bibliography

Alam, M.S., Getz, M., Safeukui, I., et al. (2012) Genomic Expression Analyses Reveal Lysosomal, Innate Immunity Proteins, as Disease Correlates in Murine Models of a Lysosomal Storage Disorder. *PLoS ONE*. doi:10.1371/journal.pone.0048273.

Allmang, C., Carbon, P. and Krol, A. (2002) The SBP2 and 15.5 kD/Snu13p proteins share the same RNA binding domain: Identification of SBP2 amino acids important to SECIS RNA binding. *RNA*. doi:10.1017/S1355838202020034.

Arbogast, S., Beuvin, M., Fraysse, B., et al. (2009) Oxidative stress in SEPN1-related myopathy: From pathophysiology to treatment. *Annals of Neurology*. doi:10.1002/ana.21644.

Arnér, E.S.J. (2009) Focus on mammalian thioredoxin reductases - Important selenoproteins with versatile functions. *Biochimica et Biophysica Acta - General Subjects*. doi:10.1016/j.bbagen.2009.01.014.

Berry, M.J., Banu, L., Harney, J.W., et al. (1993) Functional characterization of the eukaryotic SECIS elements which direct selenocysteine insertion at UGA codons. *The EMBO Journal*. doi:10.1002/j.1460-2075.1993.tb06001.x.

Bösl, M.R., Takaku, K., Oshima, M., et al. (1997) Early embryonic lethality caused by targeted disruption of the mouse selenocysteine tRNA gene (Trsp). *Proceedings of the National Academy of Sciences of the United States of America*. doi:10.1073/pnas.94.11.5531.

Boukhzar, L., Hamieh, A., Cartier, D., et al. (2016) Selenoprotein T Exerts an Essential Oxidoreductase Activity That Protects Dopaminergic Neurons in Mouse Models of Parkinson's Disease. *Antioxidants and Redox Signaling*. doi:10.1089/ars.2015.6478.

Caban, K., Kinzy, S.A. and Copeland, P.R. (2007) The L7Ae RNA Binding Motif Is a Multifunctional Domain Required for the Ribosome-Dependent Sec Incorporation Activity of Sec Insertion Sequence Binding Protein 2. *Molecular and Cellular Biology*. doi:10.1128/mcb.00632-07.

Carlson, B.A., Novoselov, S. V., Kumaraswamy, E., et al. (2004) Specific Excision of the Selenocysteine tRNA[Ser]Sec (T-rsp) Gene in Mouse Liver Demonstrates an Essential

Role of Selenoproteins in Liver Function. *Journal of Biological Chemistry*. doi:10.1074/jbc.M310470200.

Chapple, C.E., Guigó, R. and Krol, A. (2009) SECISaln, a web-based tool for the creation of structure-based alignments of eukaryotic SECIS elements. *Bioinformatics*. doi:10.1093/bioinformatics/btp020.

Chen, P.B., Kawaguchi, R., Blum, C., et al. (2017) Mapping gene expression in excitatory neurons during hippocampal late-phase long-term potentiation. *Frontiers in Molecular Neuroscience*. doi:10.3389/fnmol.2017.00039.

Chiu-Ugalde, J., Wirth, E.K., Klein, M.O., et al. (2012) Thyroid function is maintained despite increased oxidative stress in mice lacking selenoprotein biosynthesis in thyroid epithelial cells. *Antioxidants and Redox Signaling*. doi:10.1089/ars.2011.4055.

Chung, S., Weber, F., Zhong, P., et al. (2017) Identification of preoptic sleep neurons using retrograde labelling and gene profiling. *Nature*. doi:10.1038/nature22350.

Conrad, M., Bornkamm, G.W. and Brielmeier, M. (2006) "Mitochondrial and cytosolic thioredoxin reductase knockout mice." In *Selenium: Its Molecular Biology and Role in Human Health, Second Edition*. doi:10.1007/0-387-33827-6_18.

Conrad, M., Moreno, S.G., Sinowatz, F., et al. (2005) The Nuclear Form of Phospholipid Hydroperoxide Glutathione Peroxidase Is a Protein Thiol Peroxidase Contributing to Sperm Chromatin Stability. *Molecular and Cellular Biology*. doi:10.1128/mcb.25.17.7637-7644.2005.

Copeland, P.R. and Driscoll, D.M. (1999) Purification, redox sensitivity, and RNA binding properties of SECIS- binding protein 2, a protein involved in selenoprotein biosynthesis. *Journal of Biological Chemistry*. doi:10.1074/jbc.274.36.25447.

Copeland, P.R., Fletcher, J.E., Carlson, B.A., et al. (2000) A novel RNA binding protein, SBP2, is required for the translation of mammalian selenoprotein mRNAs. *EMBO Journal*. doi:10.1093/emboj/19.2.306.

Di Cosmo, C., McLellan, N., Liao, X.H., et al. (2009) Clinical and molecular characterization of a novel selenocysteine insertion sequence-binding protein 2 (SBP2) gene mutation (R128X). *Journal of Clinical Endocrinology and Metabolism*. doi:10.1210/jc.2009-0686.

Curran, J.E., Jowett, J.B.M., Elliott, K.S., et al. (2005) Genetic variation in selenoprotein S influences inflammatory response. *Nature Genetics*. doi:10.1038/ng1655.

Dobosz-Bartoszek, M., Pinkerton, M.H., Otwinowski, Z., et al. (2016) Crystal structures of the human elongation factor eEFSec suggest a non-canonical mechanism for selenocysteine incorporation. *Nature Communications*. doi:10.1038/ncomms12941.

Donovan, J., Caban, K., Ranaweera, R., et al. (2008) A novel protein domain induces high affinity selenocysteine insertion sequence binding and elongation factor recruitment. *Journal of Biological Chemistry*. doi:10.1074/jbc.M806008200.

Donovan, J. and Copeland, P.R. (2009) Evolutionary history of selenocysteine incorporation from the perspective of SECIS binding proteins. *BMC Evolutionary Biology*. doi:10.1186/1471-2148-9-229.

Downey, C.M., Horton, C.R., Carlson, B.A., et al. (2009) Osteo-chondroprogenitor-specific deletion of the selenocysteine tRNA gene, Trsp, leads to chondronecrosis and abnormal skeletal development: A putative model for Kashin-Beck disease. *PLoS Genetics*. doi:10.1371/journal.pgen.1000616.

Doyle, J.P., Dougherty, J.D., Heiman, M., et al. (2008) Application of a Translational Profiling Approach for the Comparative Analysis of CNS Cell Types. *Cell*. doi:10.1016/j.cell.2008.10.029.

Dubey, A. and Copeland, P.R. (2016) The selenocysteine-specific elongation factor contains unique sequences that are required for both nuclear export and selenocysteine incorporation. *PLoS ONE*. doi:10.1371/journal.pone.0165642.

Dumitrescu, A.M., Liao, X.H., Abdullah, M.S.Y., et al. (2005) Mutations in SECISBP2 result in abnormal thyroid hormone metabolism. *Nature Genetics*. doi:10.1038/ng1654.

Esworthy, R.S., Swiderek, K.M., Ho, Y.S., et al. (1998) Selenium-dependent glutathione peroxidase-GI is a major glutathione peroxidase activity in the mucosal epithelium of rodent intestine. *Biochimica et Biophysica Acta - General Subjects*. doi:10.1016/S0304-4165(98)00032-4.

Esworthy, R.S., Yang, L., Frankel, P.H., et al. (2005) Epithelium-Specific Glutathione Peroxidase, Gpx2, Is Involved in the Prevention of Intestinal Inflammation in Selenium-Deficient Mice. *The Journal of Nutrition*. doi:10.1093/jn/135.4.740.

Fletcher, J.E., Copeland, P.R., Driscoll, D.M., et al. (2001) The selenocysteine incorporation machinery: Interactions between the SECIS RNA and the SECIS-binding protein SBP2. *RNA*.

Florian, S., Krehl, S., Loewinger, M., et al. (2010) Loss of GPx2 increases apoptosis, mitosis, and GPx1 expression in the intestine of mice. *Free Radical Biology and Medicine*. doi:10.1016/j.freeradbiomed.2010.08.029.

Fradejas-Villar, N. (2018) Consequences of mutations and inborn errors of selenoprotein biosynthesis and functions. *Free Radical Biology and Medicine*. doi:10.1016/j.freeradbiomed.2018.04.572.

Fradejas-Villar, N., Seeher, S., Anderson, C.B., et al. (2017) The RNA-binding protein Secisbp2 differentially modulates UGA codon reassignment and RNA decay. *Nucleic Acids Research*. doi:10.1093/nar/gkw1255.

Fradejas, N., Carlson, B.A., Rijntjes, E., et al. (2013) Mammalian Trit1 is a tRNA[Ser]Sec-isopentenyl transferase required for full selenoprotein expression. *Biochemical Journal*. doi:10.1042/BJ20121713.

Friedmann Angeli, J.P., Schneider, M., Proneth, B., et al. (2014) Inactivation of the ferroptosis regulator Gpx4 triggers acute renal failure in mice. *Nature Cell Biology*. doi:10.1038/ncb3064.

Fu, J., Fujisawa, H., Follman, B., et al. (2017) Thyroid hormone metabolism defects in a mouse model of SBP2 deficiency. *Endocrinology*. doi:10.1210/en.2017-00618.

Galton, V.A., Schneider, M.J., Clark, A.S., et al. (2009) Life without thyroxine to 3,5,3′-triiodothyronine conversion: Studies in mice devoid of the 5′-deiodinases. *Endocrinology*. doi:10.1210/en.2008-1572.

Gladyshev, V.N. and Hatfield, D.L. (1999) Selenocysteine-containing proteins in mammals. *Journal of Biomedical Science*. doi:10.1007/BF02255899.

Grundner-Culemann, E., Martin, G.W., Harney, J.W., et al. (1999) Two distinct SECIS structures capable of directing selenocysteine incorporation in eukaryotes. *RNA*. doi:10.1017/S1355838299981542.

De Haan, J.B., Bladier, C., Griffiths, P., et al. (1998) Mice with a homozygous null mutation for the most abundant glutathione peroxidase, Gpx1, show increased susceptibility to the

oxidative stress- inducing agents paraquat and hydrogen peroxide. *Journal of Biological Chemistry*. doi:10.1074/jbc.273.35.22528.

Heiman, M., Kulicke, R., Fenster, R.J., et al. (2014) Cell type-specific mRNA purification by translating ribosome affinity purification (TRAP). *Nature Protocols*. doi:10.1038/nprot.2014.085.

Hernandez, A., Quignodon, L., Martinez, M.E., et al. (2010) Type 3 deiodinase deficiency causes spatial and temporal alterations in brain T3 signaling that are dissociated from serum thyroid hormone levels. *Endocrinology*. doi:10.1210/en.2010-0450.

Hill, K.E., Reid Lyons, P. and Burk, R.F. (1992) Differential regulation of rat liver selenoprotein mRNAs in selenium deficiency. *Biochemical and Biophysical Research Communications*. doi:10.1016/S0006-291X(05)80984-2.

Hill, K.E., Zhou, J., McMahan, W.J., et al. (2003) Deletion of selenoprotein P alters distribution of selenium in the mouse. *Journal of Biological Chemistry*. doi:10.1074/jbc.M300755200.

Hoffmann, P.R. and Berry, M.J. (2005) Selenoprotein synthesis: A unique translational mechanism used by a diverse family of proteins. *Thyroid*. doi:10.1089/thy.2005.15.769.

Holzerova, E., Danhauser, K., Haack, T.B., et al. (2016) Human thioredoxin 2 deficiency impairs mitochondrial redox homeostasis and causes early-onset neurodegeneration. *Brain*. doi:10.1093/brain/awv350.

Ingold, I., Berndt, C., Schmitt, S., et al. (2018) Selenium Utilization by GPX4 Is Required to Prevent Hydroperoxide-Induced Ferroptosis. *Cell*. doi:10.1016/j.cell.2017.11.048.

Ingolia NT (2014) Ribosome profiling: new views of translation, from single codons to genome scale. *Nature reviews. Genetics*.

Jakupoglu, C., Przemeck, G.K.H., Schneider, M., et al. (2005) Cytoplasmic Thioredoxin Reductase Is Essential for Embryogenesis but Dispensable for Cardiac Development. *Molecular and Cellular Biology*. doi:10.1128/mcb.25.5.1980-1988.2005.

Jin, R.C., Mahoney, C.E., Anderson, L., et al. (2011) Glutathione peroxidase-3 deficiency promotes platelet-dependent thrombosis in vivo. *Circulation*. doi:10.1161/CIRCULATIONAHA.110.000034.

Kasaikina, M. V., Hatfield, D.L. and Gladyshev, V.N. (2012) Understanding selenoprotein function and regulation through the use of rodent models. *Biochimica et Biophysica Acta - Molecular Cell Research*. doi:10.1016/j.bbamcr.2012.02.018.

Kiermayer, C., Northrup, E., Schrewe, A., et al. (2015) Heart-Specific Knockout of the Mitochondrial Thioredoxin Reductase (Txnrd2) Induces Metabolic and Contractile Dysfunction in the Aging Myocardium. *Journal of the American Heart Association*. doi:10.1161/JAHA.115.002153.

Kinzy, S.A., Caban, K. and Copeland, P.R. (2005) Characterization of the SECIS binding protein 2 complex required for the co-translational insertion of selenocysteine in mammals. *Nucleic Acids Research*. doi:10.1093/nar/gki826.

Kratz, A., Beguin, P., Kaneko, M., et al. (2014) Digital expression profiling of the compartmentalized translatome of Purkinje neurons. *Genome Research*. doi:10.1101/gr.164095.113.

Kryukov, G. V., Castellano, S., Novoselov, S. V., et al. (2003) Characterization of mammalian selenoproteomes. *Science*. doi:10.1126/science.1083516.

Kudin, A.P., Baron, G., Zsurka, G., et al. (2017) Homozygous mutation in TXNRD1 is associated with genetic generalized epilepsy. *Free Radical Biology and Medicine*. doi:10.1016/j.freeradbiomed.2017.02.040.

Labunskyy, V.M., Hatfield, D.L. and Gladyshev, V.N. (2014) Selenoproteins: Molecular pathways and physiological roles. *Physiological Reviews*. doi:10.1152/physrev.00039.2013.

Loh, K., Deng, H., Fukushima, A., et al. (2009) Reactive Oxygen Species Enhance Insulin Sensitivity. *Cell Metabolism*. doi:10.1016/j.cmet.2009.08.009.

Low, S.C., Grundner-Culemann, E., Harney, J.W., et al. (2000) SECIS-SBP2 interactions dictate selenocysteine incorporation efficiency and selenoprotein hierarchy. *EMBO Journal*. doi:10.1093/emboj/19.24.6882.

Lubos, E., Loscalzo, J. and Handy, D.E. (2011) Glutathione peroxidase-1 in health and disease: From molecular mechanisms to therapeutic opportunities. *Antioxidants and Redox Signaling*. doi:10.1089/ars.2010.3586.

Luchman, H.A., Villemaire, M.L., Bismar, T.A., et al. (2014) Prostate epithelium-specific

deletion of the selenocysteine tRNA gene Trsp leads to early onset intraepithelial neoplasia. *American Journal of Pathology*. doi:10.1016/j.ajpath.2013.11.025.

Luongo, C., Dentice, M. and Salvatore, D. (2019) Deiodinases and their intricate role in thyroid hormone homeostasis. *Nature Reviews Endocrinology*. doi:10.1038/s41574-019-0218-2.

Ma, F., Fuqua, B.K., Hasin, Y., et al. (2019) A comparison between whole transcript and 3' RNA sequencing methods using Kapa and Lexogen library preparation methods 06 Biological Sciences 0604 Genetics. *BMC Genomics*. doi:10.1186/s12864-018-5393-3.

Mariotti, M., Lobanov, A. V., Guigo, R., et al. (2013) SECISearch3 and Seblastian: New tools for prediction of SECIS elements and selenoproteins. *Nucleic Acids Research*. doi:10.1093/nar/gkt550.

Mayilyan, K.R., Kang, Y.H., Dodds, A.W., et al. (2008) *The Complement System in Innate Immunity*. doi:10.1007/978-3-540-73930-2_10.

McClung, J.P., Roneker, C.A., Mu, W., et al. (2004) Development of insulin resistance and obesity in mice overexpressing cellular glutathione peroxidase. *Proceedings of the National Academy of Sciences of the United States of America*. doi:10.1073/pnas.0308096101.

McKeever, P.M., Kim, T.H., Hesketh, A.R., et al. (2017) Cholinergic neuron gene expression differences captured by translational profiling in a mouse model of Alzheimer's disease. *Neurobiology of Aging*. doi:10.1016/j.neurobiolaging.2017.05.014.

Mehta, A., Rebsch, C.M., Kinzyi, S.A., et al. (2004) Efficiency of mammalian selenocysteine incorporation. *Journal of Biological Chemistry*. doi:10.1074/jbc.M404639200.

Moghadaszadeh, B., Petit, N., Jaillard, C., et al. (2001) Mutations in SEPN1 cause congenital muscular dystrophy with spinal rigidity and restrictive respiratory syndrome. *Nature Genetics*. doi:10.1038/ng713.

Moxon, A.L. and Franke, K.W. (1935) Effect of Certain Salts on Enzyme Activity: Effect of Sodium Selenate, Selenite, Selenide, Tellurite, Sulfate, Sulfite, Sulfide, Arsenite, and Vanadate on Rate of Carbon Dioxide Production during Yeast Fermentation. *Industrial and Engineering Chemistry*. doi:10.1021/ie50301a018.

Papp, L. V., Lu, J., Striebel, F., et al. (2006) The Redox State of SECIS Binding Protein 2 Controls Its Localization and Selenocysteine Incorporation Function. *Molecular and Cellular Biology*. doi:10.1128/mcb.02284-05.

Papp, L. V., Wang, J., Kennedy, D., et al. (2008) Functional characterization of alternatively spliced human SECISBP2 transcript variants. *Nucleic Acids Research*. doi:10.1093/nar/gkn829.

Pinsent, J. (1954) The need for selenite and molybdate in the formation of formic dehydrogenase by members of the Coli-aerogenes group of bacteria. *Biochemical Journal*. doi:10.1042/bj0570010.

Pitts, M.W., Byrns, C.N., Ogawa-Wong, A.N., et al. (2014) Selenoproteins in Nervous System Development and Function. *Biological Trace Element Research*. doi:10.1007/s12011-014-0060-2.

Pitts, M.W., Reeves, M.A., Hashimoto, A.C., et al. (2013) Deletion of selenoprotein M leads to obesity without cognitive deficits. *Journal of Biological Chemistry*. doi:10.1074/jbc.M113.471235.

Prabhakar, R., Morokuma, K. and Musaev, D.G. (2006) Peroxynitrite reductase activity of selenoprotein glutathione peroxidase: A computational study. *Biochemistry*. doi:10.1021/bi060456e.

Puglisi, R., Maccari, I., Pipolo, S., et al. (2012) The nuclear form of glutathione peroxidase 4 is associated with sperm nuclear matrix and is required for proper paternal chromatin decondensation at fertilization. *Journal of Cellular Physiology*. doi:10.1002/jcp.22857.

RAHMAN, M.M., DEYOE, C.W., DAVIES, R.E., et al. (1960) Selenium and exudative diathesis in chicks and poults. *The Journal of nutrition*. doi:10.1093/jn/72.1.71.

Reeves, M.A., Bellinger, F.P. and Berry, M.J. (2010) The neuroprotective functions of selenoprotein M and its role in cytosolic calcium regulation. *Antioxidants and Redox Signaling*. doi:10.1089/ars.2009.2883.

Renko, K., Werner, M., Renner-Müller, I., et al. (2008) Hepatic selenoprotein P (SePP) expression restores selenium transport and prevents infertility and motor-incoordination in Sepp-knockout mice. *Biochemical Journal*. doi:10.1042/BJ20071172.

Rivest, S. (2009) Regulation of innate immune responses in the brain. *Nature Reviews*

Immunology. doi:10.1038/nri2565.

Rotruck, J.T., Pope, A.L., Ganther, H.E., et al. (1973) Selenium: Biochemical role as a component of glatathione peroxidase. *Science*. doi:10.1126/science.179.4073.588.

Russell, D.W. (2003) Mechanism and regulation of selenoprotein synthesis. *Annual Review of Biochemistry*. doi:10.1146/annurev.biochem.72.121801.161712.

Santesmasses, D., Mariotti, M. and Gladyshev, V.N. (2020) Tolerance to Selenoprotein Loss Differs between Human and Mouse. *Molecular Biology and Evolution*. doi:10.1093/molbev/msz218.

Sapkota, D., Lake, A.M., Yang, W., et al. (2019) Cell-Type-Specific Profiling of Alternative Translation Identifies Regulated Protein Isoform Variation in the Mouse Brain. *Cell Reports*. doi:10.1016/j.celrep.2018.12.077.

Schneider, M., Forster, H., Boersma, A., et al. (2009) Mitochondrial glutathione peroxidase 4 disruption causes male infertility. *The FASEB Journal*. doi:10.1096/fj.09-132795.

Schneider, M.J., Fiering, S.N., Pallud, S.E., et al. (2001) Targeted disruption of the type 2 selenodeiodinase gene (Dio2) results in a phenotype of pituitary resistance to T4. *Molecular Endocrinology*. doi:10.1210/mend.15.12.0740.

Schneider, M.J., Fiering, S.N., Thai, B., et al. (2006) Targeted disruption of the type 1 selenodeiodinase gene (Dio1) results in marked changes in thyroid hormone economy in mice. *Endocrinology*. doi:10.1210/en.2005-0739.

Schoenmakers, E., Agostini, M., Mitchell, C., et al. (2010) Mutations in the selenocysteine insertion sequence-binding protein 2 gene lead to a multisystem selenoprotein deficiency disorder in humans. *Journal of Clinical Investigation*. doi:10.1172/JCI43653.

Schoenmakers, E., Carlson, B., Agostini, M., et al. (2016) Mutation in human selenocysteine transfer RNA selectively disrupts selenoprotein synthesis. *Journal of Clinical Investigation*. doi:10.1172/JCI84747.

Schoenmakers, E. and Chatterjee, K. (2020) Human Disorders Affecting the Selenocysteine Incorporation Pathway Cause Systemic Selenoprotein Deficiency. *Antioxidants & Redox Signaling*. doi:10.1089/ars.2020.8097.

Schomburg, L., Schweizer, U., Holtmann, B., et al. (2003) Gene disruption discloses role of selenoprotein P in selenium delivery to target tissues. *Biochemical Journal*. doi:10.1042/BJ20021853.

Schwarz, K. and Foltz, C.M. (1957) Selenium as an Integral Part of Factor 3 Against Dietary Necrotic Liver Degeneration. *Journal of the American Chemical Society*. doi:10.1021/ja01569a087.

Seeher, S., Atassi, T., Mahdi, Y., et al. (2014) Secisbp2 is essential for embryonic development and enhances selenoprotein expression. *Antioxidants and Redox Signaling*. doi:10.1089/ars.2013.5358.

Seeher, S. and Schweizer, U. (2014) Targeted deletion of Secisbp2 reduces, but does not abrogate, selenoprotein expression and leads to striatal interneuron loss. *Free Radical Biology and Medicine*. doi:10.1016/j.freeradbiomed.2014.10.849.

Seiler, A., Schneider, M., Förster, H., et al. (2008) Glutathione Peroxidase 4 Senses and Translates Oxidative Stress into 12/15-Lipoxygenase Dependent- and AIF-Mediated Cell Death. *Cell Metabolism*. doi:10.1016/j.cmet.2008.07.005.

Sengupta, A., Lichti, U.F., Carlson, B.A., et al. (2010) Selenoproteins are essential for proper keratinocyte function and skin development. *PLoS ONE*. doi:10.1371/journal.pone.0012249.

Shapiro, E., Biezuner, T. and Linnarsson, S. (2013) Single-cell sequencing-based technologies will revolutionize whole-organism science. *Nature Reviews Genetics*. doi:10.1038/nrg3542.

Shchedrina, V.A., Everley, R.A., Zhang, Y., et al. (2011) Selenoprotein K binds multiprotein complexes and is involved in the regulation of endoplasmic reticulum homeostasis. *Journal of Biological Chemistry*. doi:10.1074/jbc.M111.310920.

Shchedrina, V.A., Zhang, Y., Labunskyy, V.M., et al. (2010) Structure-function relations, physiological roles, and evolution of mammalian er-resident selenoproteins. *Antioxidants and Redox Signaling*. doi:10.1089/ars.2009.2865.

Shrimali, R.K., Weaver, J.A., Miller, G.F., et al. (2007) Selenoprotein expression is essential in endothelial cell development and cardiac muscle function. *Neuromuscular Disorders*. doi:10.1016/j.nmd.2006.10.006.

Sibbing, D., Pfeufer, A., Perisic, T., et al. (2011) Mutations in the mitochondrial thioredoxin reductase gene TXNRD2 cause dilated cardiomyopathy. *European Heart Journal*. doi:10.1093/eurheartj/ehq507.

Smith, A.C., Mears, A.J., Bunker, R., et al. (2014) Mutations in the enzyme glutathione peroxidase 4 cause Sedaghatian-type spondylometaphyseal dysplasia. *Journal of Medical Genetics*. doi:10.1136/jmedgenet-2013-102218.

Sofroniew, M. V. (2015a) Astrocyte barriers to neurotoxic inflammation. *Nature Reviews Neuroscience*. doi:10.1038/nrn3898.

Sofroniew, M. V. (2015b) Astrogliosis. *Cold Spring Harbor Perspectives in Biology*. doi:10.1101/cshperspect.a020420.

Steullet, P., Cabungcal, J.H., Coyle, J., et al. (2017) Oxidative stress-driven parvalbumin interneuron impairment as a common mechanism in models of schizophrenia. *Molecular Psychiatry*. doi:10.1038/mp.2017.47.

Streckfuß, F., Hamann, I., Schomburg, L., et al. (2005) Hepatic deiodinase activity is dispensable for the maintenance of normal circulating thyroid hormone levels in mice. *Biochemical and Biophysical Research Communications*. doi:10.1016/j.bbrc.2005.09.102.

Su, D., Novoselov, S. V., Sun, Q.A., et al. (2005) Mammalian selenoprotein thioredoxin-glutathione reductase: Roles in bisulfide bond formation and sperm maturation. *Journal of Biological Chemistry*. doi:10.1074/jbc.M503638200.

Sun, Q.A., Su, D., Novoselov, S. V., et al. (2005) Reaction mechanism and regulation of mammalian thioredoxin/glutathione reductase. *Biochemistry*. doi:10.1021/bi051321w.

Sunde, R.A. and Raines, A.M. (2011) Selenium Regulation of the Selenoprotein and Nonselenoprotein Transcriptomes in Rodents. *Advances in Nutrition*. doi:10.3945/an.110.000240.

Sunde, R.A., Raines, A.M., Barnes, K.M., et al. (2009) Selenium status highly regulates selenoprotein mRNA levels for only a subset of the selenoproteins in the selenoproteome. *Bioscience Reports*. doi:10.1042/BSR20080146.

Suppmann, S. (1999) Dynamics and efficiency invivo of UGA-directed selenocysteine insertion at the ribosome. *The EMBO Journal*. doi:10.1093/emboj/18.8.2284.

Takahashi, K., Avissar, N., Whitin, J., et al. (1987) Purification and characterization of human plasma glutathione peroxidase: A selenoglycoprotein distinct from the known cellular enzyme. *Archives of Biochemistry and Biophysics*. doi:10.1016/0003-9861(87)90624-2.

Tujebajeva, R.M., Copeland, P.R., Xu, X.M., et al. (2000) Decoding apparatus for eukaryotic selenocysteine insertion. *EMBO Reports*. doi:10.1093/embo-reports/kvd033.

Ursini, F., Maiorino, M. and Gregolin, C. (1985) The selenoenzyme phospholipid hydroperoxide glutathione peroxidase. *BBA - General Subjects*. doi:10.1016/0304-4165(85)90182-5.

Verma, S., Hoffmann, F.W., Kumar, M., et al. (2011) Selenoprotein K Knockout Mice Exhibit Deficient Calcium Flux in Immune Cells and Impaired Immune Responses. *The Journal of Immunology*. doi:10.4049/jimmunol.1002878.

Voetsch, B., Jin, R.C., Bierl, C., et al. (2007) Promoter polymorphisms in the plasma glutathione peroxidase (GPx-3) gene: A novel risk factor for arterial ischemic stroke among young adults and children. *Stroke*. doi:10.1161/01.STR.0000252027.53766.2b.

Wang, X., Zhang, C., Szábo, G., et al. (2013) Distribution of CaMKIIα expression in the brain in vivo, studied by CaMKIIα-GFP mice. *Brain Research*. doi:10.1016/j.brainres.2013.04.042.

Whanger, P.D., Muth, O.H., Oldfield, J.E., et al. (1969) Influence of Sulfur on Incidence of White Muscle Disease in Lambs. *The Journal of Nutrition*. doi:10.1093/jn/97.4.553.

Wirth, E.K., Conrad, M., Winterer, J., et al. (2010) Neuronal selenoprotein expression is required for interneuron development and prevents seizures and neurodegeneration. *The FASEB Journal*. doi:10.1096/fj.09-143974.

Xu, X.M., Carlson, B.A., Irons, R., et al. (2007a) Selenophosphate synthetase 2 is essential for selenoprotein biosynthesis. *Biochemical Journal*. doi:10.1042/BJ20070165.

Xu, X.M., Carlson, B.A., Mix, H., et al. (2007b) Biosynthesis of selenocysteine on its tRNA in eukaryotes. *PLoS Biology*. doi:10.1371/journal.pbio.0050004.

Yant, L.J., Ran, Q., Rao, L., et al. (2003) The selenoprotein GPX4 is essential for mouse development and protects from radiation and oxidative damage insults. *Free Radical Biology and Medicine*. doi:10.1016/S0891-5849(02)01360-6.

Yoo, M.H., Xu, X.M., Carlson, B.A., et al. (2006) Thioredoxin reductase 1 deficiency reverses tumor phenotype and tumorigenicity of lung carcinoma cells. *Journal of Biological Chemistry*. doi:10.1074/jbc.C600012200.

Zhang, Y., Zhou, Y., Schweizer, U., et al. (2008) Comparative analysis of selenocysteine machinery and selenoproteome gene expression in mouse brain identifies neurons as key functional sites of selenium in mammals. *Journal of Biological Chemistry*. doi:10.1074/jbc.M707951200.

Zhao, W., Bohleber, S., Schmidt, H., et al. (2019) Ribosome profiling of selenoproteins in vivo reveals consequences of pathogenic Secisbp2 missense mutations. *Journal of Biological Chemistry*. doi:10.1074/jbc.RA119.009369.

Zhou, P., Zhang, Y., Ma, Q., et al. (2013) Interrogating translational efficiency and lineage-specific transcriptomes using ribosome affinity purification. *Proceedings of the National Academy of Sciences of the United States of America*. doi:10.1073/pnas.1304124110.

8. Acknowledgement

First of all, I would like to express my sincere gratitude to my supervisor, Prof. Ulrich Schweizer, for selecting me through many applications and constantly supporting me in the past three years. Prof.Schweizer is the best advisor and one of smartest people I know. He is so erudite that often generates some creative ideas. Most importantly, he is always willing to share and discuss his creative ideas with me. Moreover, whenever I encounter the difficulties in the projects, he is always patient to guide me to find a solution instead of telling me the right answer directly. I am very grateful to Prof.Schweizer for his scientific advices and many insightful discussions. This endless support is not only from the academic work, but also the daily life from the first day I arrived at Bonn. Before I came to Germany, finding an apartment was the first big issue for me. Prof.Schweizer kindly offered me one room in his apartment for a month transition. I have to say this was a bold decision for him because we never met before. But for me, this was the greatest welcome for a helpless foreigner in an unfamiliar country. Here, I also would like to express my gratitude to Prof.Schweizer and his family for having me like a real family member.

I sincerely want to express my gratitude to my second supervisor, Prof. Walter Witke. I still remember the first day we met in BFB meeting. He was so friendly to me. He asked me several inspiring and thoughtful questions about my project. I appreciate that he made it possible for me to pursue a PhD title in the medical faculty. I also appreciate for his extraordinary professional commitment.

I would like to express my sincere gratitude to Prof. Regina Betz and Prof. Martin Schlee. I am so grateful to all the effort they made during my PhD promotion. I appreciate for their extraordinary professional commitment.

I am so lucky to have my colleagues during my PhD life. Without their supports, I may not survive not only in the academic life, but also in the daily life. First, I want to say thanks to Dr. Noelia Fradejas Villar. I could not finish the project without her generous help. She was always patient whenever I had endless questions. She set up a good example to me to be a competent researcher. Apart from the laboratory work, she always worried about

Seeher. I am so lucky to be a member of AG Schweizer with all of them. I enjoy my PhD life so much also because of them. I only want to say "Thank you so much" to all of them.

In the end, I would like to sincerely thank my parents and my girlfriend. Without their endless supports, I would never go further.